Fall 2004

Ocean color modeling: Parameterization and interpretation

Hui Feng
University of New Hampshire, Durham

OCEAN COLOR MODELING: PARAMETERIZATION AND INTERPRETATION

By

Hui Feng

B.Sc., East China Normal University, Shanghai, China, 1983

M.Sc., University of New Hampshire, Durham, NH, 1996

DISSERTATION

Submitted to the University of New Hampshire
In Partial Fulfillment of
the Requirements for the Degree of

Doctor of Philosophy

In

Earth Sciences: Oceanography

September, 2004

This dissertation has been examined and approved.

Dissertation Director, Dr. Janet W. Campbell
Research Professor of Earth Sciences
Ocean Process Analysis Lab., EOS, University of New Hampshire

Dr. Mark D. Dowell
Research Scientist
Inland and Marine Waters Unit,
Joint Research Center of the European Commission, Ispra, Italy

Dr. Patrick McCormick
Professor of Physics, Center for Atmospheric Sciences
Hampton University

Dr. David Meeker
Professor Emeritus of Mathematics, Dept. of Mathematics
University of New Hampshire

Dr. Jonathan Pennock
Associate professor of Marine Science, Dept. of Natural Resources
University of New Hampshire

Dr. James Yoder
Professor of Oceanography
University of Rhode Island

Date _____

Acknowledgements

I had the good fortune to have Professor Janet W. Campbell as my principal advisor in this doctoral program. I deeply appreciate Janet for guiding me at both academic and personal levels. She taught me a great part of ocean color modeling, data analysis and statistics, and fully supported all my initiatives for this dissertation project. She expressed an understanding when I took off almost 3 years from March 2000 to November 2002 during which I worked as a full-time software engineer, and was still considered as part of her research group. Without her constant encouragement and understanding, I simply would not have finished the dissertation.

I am greatly indebted to Dr. Mark Dowell. I thank Mark for his creative and innovative inputs to this thesis research. With his exceptional knowledge and experience in ocean color modeling, he has given me invaluable guidance and suggestions on the thesis after I came back to UNH in November 2002.

My heartfelt appreciation is also extended to the other members of my thesis committee: Dr. Patrick McCormick, Dr. David Meeker, Dr. Jonathan Pennock and Dr. James Yoder. I have been greatly honored that they agreed to serve on my committee. Their comments and suggestions are invaluable for this thesis.

I would also like to express my thanks to Tim Moore for his support in the observational data collection and image processing, and many productive discussions when we shared an office for years. A special thanks goes to Doug Vandemark, a NASA/GSFC scientist, who has given me the actual opportunity to come back to UNH to finish this thesis, and what I have learned from him in a broader spectrum of ocean

remote sensing has benefited this study and will benefit my career.

I also need to thank many of the "old" OPAL colleagues and members, Wendell Brown, Frank Bub, Yanlin Fan, Karen Garrison, Sam Miller, Frank Smith, Greg Weiss, and Zhitao Yu, and the current OPALites, Seung-Hyun Son and Joe Salisbury for their help, friendship and companionship.

Finally, I would like to thank my wife Yan and my son Kevin for all of their love, patience and understanding during my "long term" graduate study in UNH.

This thesis work was sponsored originally through a graduate research assistantship from June 1996 to February 2000 under a MODIS Instrument Team Investigation (NASA Contract NAS5-96063) granted to Janet W. Campbell, and since November 2002 my work has been funded through a GEST (Goddard Earth Sciences and Technology Center) post-doctorial fund granted to Doug Vandemark in NASA/GSFC and Patrick McCormick in Hampton University.

Contents

List of Figures

List of Tables

ABSTRACT

OCEAN COLOR MODELING: PARAMETERIZATION AND INTERPRETATION

by

Hui Feng

University of New Hampshire, September, 2004

The ocean color as observed near the water surface is determined mainly by dissolved and particulate substances, known as "optically-active constituents," in the upper water column. The goal of ocean color modeling is to interpret an ocean color spectrum quantitatively to estimate the suite of optically-active constituents near the surface. In recent years, ocean color modeling efforts have been centering upon three major optically-active constituents: chlorophyll concentration, colored dissolved organic matter, and scattering particulates. Many challenges are still being faced in this arena. This thesis generally addresses and deals with some critical issues in ocean color modeling.

In chapter one, an extensive literature survey on ocean color modeling is given. A general ocean color model is presented to identify critical candidate uncertainty sources in modeling the ocean color. The goal for this thesis study is then defined as well as some specific objectives. Finally, a general overview of the dissertation is portrayed, defining each of the follow-up chapters to target some relevant objectives.

In chapter two, a general approach is presented to quantify constituent concentration retrieval errors induced by uncertainties in inherent optical property (IOP) submodels of a semi-analytical forward model. Chlorophyll concentrations are retrieved by inverting a forward model with nonlinear IOPs. The study demonstrates how uncertainties in individual IOP submodels influence the accuracy of the chlorophyll concentration retrieval at different chlorophyll concentration levels. The important finding for this study shows that precise knowledge of spectral shapes of IOP submodels is critical for accurate chlorophyll retrieval, suggesting an improvement in retrieval accuracy requires precise spectral IOP measurements.

In chapter three, three distinct inversion techniques, namely, nonlinear optimization (NLO), principal component analysis (PCA) and artificial neural network (ANN) are compared to assess their inversion performances to retrieve optically-active constituents for a complex non-linear bio-optical system simulated by a semi-analytical ocean color model. A well-designed simulation scheme was implemented to simulate waters of different bio-optical complexity, and then the three inversion methods were applied to these simulated datasets for performance evaluation.

In chapter four, an approach is presented for optimally parameterizing an irradiance reflectance model on the basis of a bio-optical dataset made at 45 stations in the Tokyo Bay and nearby regions between 1982 and 1984. The measured reflectance spectra exhibit high variability in their spectral shapes and defy precise modeling with a single forward model. Thus, we proposed a parameterization scheme by which an unsupervised classification is first applied to the irradiance reflectance spectra, leading to three spectrally-distinct optical water types, and a reflectance model is then

parameterized for the individual optical water types. The model validation exhibits that the accuracy was significantly improved in parameterizing the reflectance model for classified waters as compared to non classified waters in the forward problem, but the improvement in the inverse problem (retrieval accuracy) was not significant.

In the last chapter, a concise thesis summary is given to conclude the major findings from chapters 2-4. A discussion focuses upon the significance of this thesis research and suggests the continuation of this research afterwards. We believe that the parameterization scheme demonstrated in chapter 4 is very promising because it possesses its observational evidence and theoretical basis. It adapts to an objective requirement for retrieval algorithm switching in the global inversion application. However, more work is necessary for a solid validation to this new parameterization scheme. In particular, we need a large bio-optical database for rigorous ocean color model parameterization.

Chapter 1 Introduction

Abstract

In this chapter, an extensive literature survey on ocean color modeling is given. A general ocean color model is presented to identify critical candidate uncertainty sources in modeling the ocean color, and then the goal as well as some specific objectives for this thesis study are defined. Finally, a general overview of the dissertation is portrayed, defining the relevant objectives of each of the following chapters.

1.1 Background

Ocean color observed just above the water surface depends greatly upon the interactions of incident light with optically active constituents in the upper water column. Optical processes (i.e. absorption and scattering) within the water column vary with constituents, and thus affect observed ocean color. As a result, there exists an implicit relationship of an ocean color signal to in-water constituents, a potential avenue to the remote detection of constituent concentrations by ocean color measurements. How do we interpret an ocean color quantitatively to derive a suite of in-water constituent concentrations that affect the color? This is the primary and direct objective of ocean color remote sensing.

Modeling techniques for optically-active constituent retrievals from ocean color data have evolved from empirical (data-based) towards analytical (model-based) algorithms for the last few decades. During the early days of ocean color remote sensing, empirical algorithms were adopted to retrieve constituent concentrations from remotely-

sensed ocean color data. A classically successful case was the Coastal Zone Color Scanner (CZCS) chlorophyll algorithm (Gordon and Morel, 1983). The CZCS algorithm worked well for optically simple oceanic waters whose optical properties are determined predominantly by phytoplankton and their associated substances in the surface water column. The optical properties of water influenced only by phytoplankton are defined as Case 1 waters (Morel *et al.* 1977). All other waters are considered Case 2 waters, including coastal, estuarine and inland waters whose optical properties are influenced by substances such as suspended sediments and colored dissolved organic matter (CDOM, also called yellow substance or gelbstoff) in addition to phytoplankton (IOCCG Report 3, 2000).

In studies of coastal and estuarine waters, phytoplankton are not the only substance of interest. Suspended sediment and CDOM concentrations are important measures of water quality to be detected. Scientists in different fields tend to be interested in different variables for their own studies. For example, the distribution and transportation of suspended sediment are primary concerns of coastal engineers and geologists (Stumpf and Pennock, 1989). The spatial distribution of CDOM or suspended sediment in estuarine and coastal regions may be used as a potential tracer for the spatial variation of river plumes (Vodack *et al.* 1997; Salisbury *et al.* 2004).

Even though empirical CZCS-like chlorophyll algorithms do not work well for Case 2 waters, empirical retrieval algorithms for Case 2 waters of interest have been developed on the basis of concurrent measurements of the remotely-sensed signals and constituent concentrations (Klemas *et al.*1974). For such empirical Case-2 algorithms, a statistical regression between some constituent concentration and measured ocean color

signal(s) is usually established as a prediction model for this concentration. As known, such empirical algorithms are not based on physical principles, and can not be applied universally. Moreover, an empirical retrieval algorithm usually focuses on retrieving one single constituent concentration by using a few channels of spectral information.

In Case 2 waters, variations in water color are controlled by more than one optically active constituent which vary in a complex way. Suspended matter affects both backscattering and absorption over a wide spectral range from the blue to near infrared bands, and their effect depends on their physical properties such as size distribution and composition (Bricaud and Morel, 1986). CDOM changes water color by absorbing light primarily in the blue-green spectral region (Bricaud *et al.* 1981). Of course, phytoplankton are also a significant constituent affecting water color by both absorption and backscattering. To establish a physically-based model relating the ocean color signal to individual constituent concentrations, the absorption and backscattering from all the optically active constituents must be considered simultaneously. Due to the spectral complexity of Case 2 waters, more spectral bands may be necessary for identifying these constituents. With the appearance of the new generation of satellite ocean color sensors, such as SeaWiFS (Sea-viewing Wide Field-of-View Sensor) and MODIS (Moderate Resolution Imaging Spectroradiometer) with more spectral bands and better radiometric sensitivity than CZCS, ocean color remote sensing has become more capable of monitoring coastal and estuarine waters quantitatively.

In recent years, attention has been turned to studies of both the optical properties and retrieval algorithms of constituents in estuarine and coastal (Case 2) waters. Many efforts have been made to develop model-based analytical inversion algorithms for

retrieving properties of more than one constituent for either Case 1 or Case 2 waters (Lee *et al.* 1994; Roesler and Perry, 1995; Hoge *et al.* 1996; Garver and Siegel, 1997; Krawczyk *et al.*1995 and 1997; Doerffer and Schiller, 1999; Schiller and Doerffer, 1999). A class of models, called *semi-analytical*, has evolved essentially based upon both a physical model and *in situ* bio-optical data used to parameterize the physical model.

Robust physically-based relationships were developed from precise radiative transfer simulations during the 1970s and 1980s (Gordon *et al.* 1975, 1988; Kirk, 1981; Jerome *et al.* 1988). These relationships relate apparent optical properties (AOPs) to inherent optical properties (IOPs) and lay a physical foundation for interpreting ocean color signals quantitatively.[1] Developing a semi-analytical inversion algorithm generally involves two primary steps: 1) parameterize a forward ocean color model with *in situ* bio-optical measurements, and 2) invert the model given an observed ocean color spectrum to retrieve a set of optically-active constituent concentrations.

For the parameterization, a suite of IOP submodels, which may be termed *bio-optical models*, is established to account for how optically active constituents affect IOPs. Forward model parameters are a quantitative linkage between IOPs and optically active constituent concentrations. An extensive dataset of *in situ* bio-optical measurements is usually necessary for a model parameterization procedure. A parameterized forward ocean color model can be used to describe the light environment in terms of constituent concentrations (the so-called forward problem) or inverted to retrieve optically-active constituent concentrations in terms of the ocean color signal (the inverse problem). Next, an ocean color model is presented in a general way in order to address some essential issues related to the goal and specific objectives of this thesis work.

[1] Detailed definitions of AOPs and IOPs are provided in the Appendix.

1.2 General Considerations

Without losing generality, a *forward* ocean color model may be simplified as

$$L(\lambda) = f(\boldsymbol{C},\Theta(\lambda)) \tag{1.1}$$

where $L(\lambda)$ is an ocean color measurement at wavelength λ (e.g. water-leaving radiance, remote sensing reflectance, or a quantity derived from them), remotely sensed either at the sensor altitude or just above the sea surface. Throughout this thesis work, $L(\lambda)$ refers to an ocean color signal observed at the sea surface, or as derived from a remotely sensed signal after atmospheric correction. The symbol f denotes a forward semi-analytical ocean color model (or a function) relating $L(\lambda)$ to the constituent concentration vector $\boldsymbol{C}$ to be retrieved, and $\Theta(\lambda)$ is a model parameter vector. The vector $\boldsymbol{C}$ commonly consists of three optically-active constituents, representing the concentration of chlorophyll, CDOM, and suspended matter concentrations.

For a purely empirical model, the model parameter vector $\Theta(\lambda)$ provides a direct linkage between the ocean color signal $L(\lambda)$ and the concentrations $\boldsymbol{C}$ in terms of a statistically derived relationship. There is usually no physical meaning behind such a parameter vector $\Theta(\lambda)$. For a semi-analytical model, $\Theta(\lambda)$ not only is a mathematical bridge between $L(\lambda)$ and $\boldsymbol{C}$, but also describes the physical relationships between the IOPs (i.e. absorption and backscattering) and constituent concentrations. The corresponding *inverse* model may be generalized by

$$\boldsymbol{C} = f^{-1}(L(\lambda),\Theta(\lambda)) \tag{1.2}$$

Note that the symbol f^{-1} indicates an inversion, which might either be an explicit expression, as in the case of a model that is linear with respect to constituent

concentrations (e.g., Hoge and Lyon, 1996), or denote an inversion technique for the case in which a direct inversion of Eq. (1.1) does not exist. Figure 1.1 generally shows the main elements for ocean color modeling in both the forward and inverse directions.

For the inverse problem represented in Eq.(1.2), there are generally four potential candidate sources of error in retrieving the constituent concentration vector $\boldsymbol{C}$. The *first* is the model f itself which links an apparent optical property, $L(\lambda)$, to inherent optical properties. Exact analytical solutions to radiative transfer equations are highly complex (Zaneveld, 1995), and are not amenable to inverse solutions. Almost all forward models are approximations to more complex equations. The *second* source of error is the inherent variability in constituent-specific IOPs. The IOP submodels defined by the model parameter vector $\Theta(\lambda)$ only approximate the real constituent-specific IOPs, and thus the inherent uncertainties of forward model parameterization may influence the model-based inversion for retrieving $\boldsymbol{C}$. The *third* source of error is from errors in the measurements of $L(\lambda)$ caused by sensor calibration, atmospheric correction, etc., which affect accuracy of the concentration retrievals. The *fourth* source of error may be the inversion scheme itself. In many cases, f^{-1} can not be written explicitly, but can be approximated using some advanced statistical techniques, such as nonlinear optimization, principal component analysis or artificial neural network techniques. In this thesis work, the effect of the second and third error sources on concentration retrievals has been characterized quantitatively (Chapter 2). The fourth source is addressed and discussed in detail in Chapter 3.

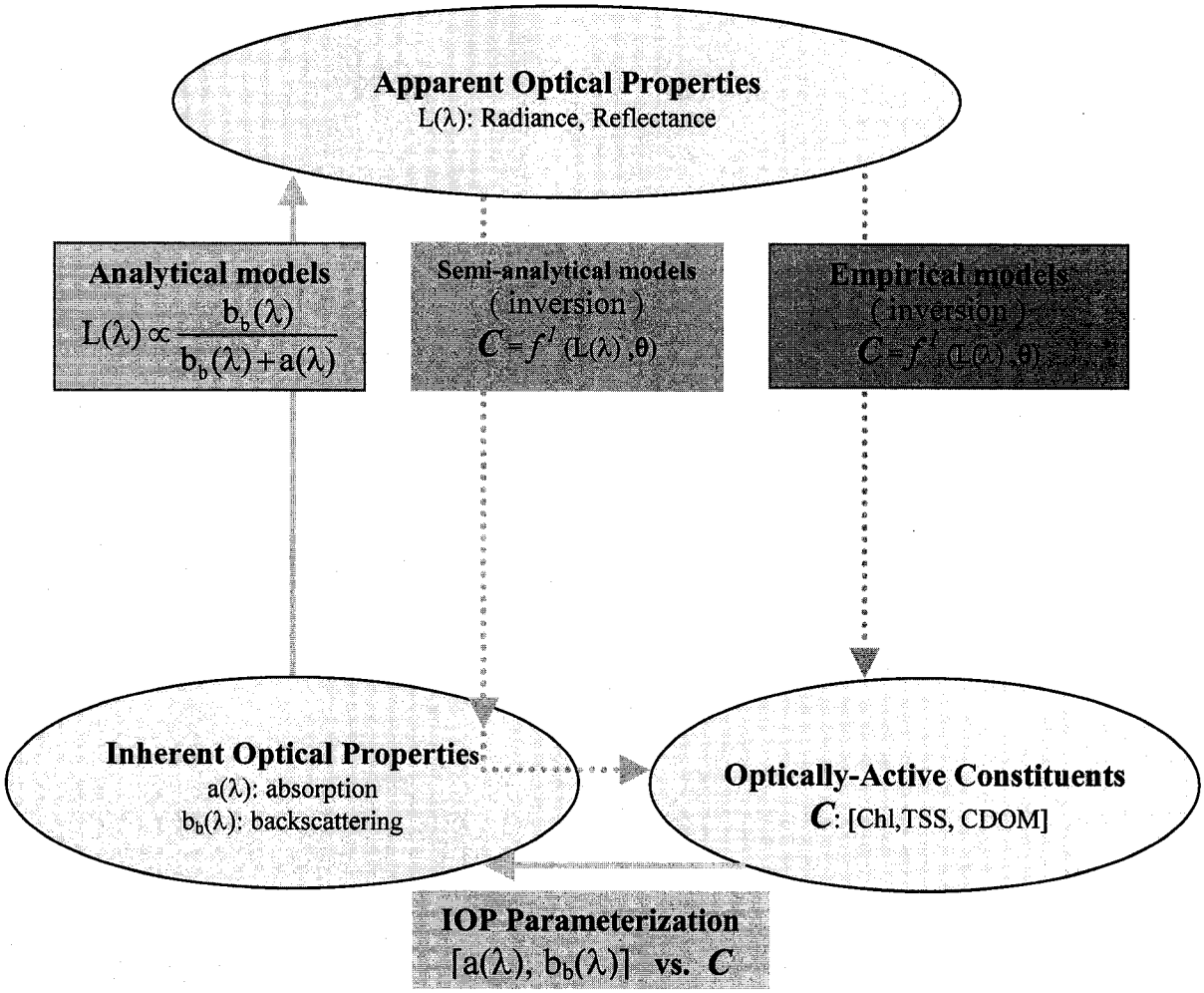

Figure 1.1. Main elements and their relationships among these elements in ocean color modeling.

Modeling Keys:

- Modeling Entities
- Modeling Procedures
- Forward modeling
- Inverse modeling

1.3 Forward ocean color model

1.3.1 Reflectance model: the relationship between AOPs and IOPs

Given the radiance distribution incident on the sea surface, the exact solution of the radiative transfer equation (RTE, see Appendix) is the best description of a forward model for a given set of IOPs. However, there is no exact analytical forward solution to the RTE for real oceanic waters, and hence one has to depend on numerical solutions (Gordon, 1994). There are various advanced numerical solutions to the RTE such as Monte Carlo (Gordon,1994), Invariant Imbedding (Mobley, 1994), and Discrete Ordinates (Jin and Stamnes, 1994) techniques. The results from Monte Carlo simulations by many studies (Gordon *et al.* 1975, 1988; Kirk, 1981, 1984; Jerome *et al.* 1988) have shown that remote sensing reflectance $R_{rs}(\lambda)$ or irradiance reflectance $R(\lambda)$, near the surface can be expressed as a function of absorption and backscattering coefficients, $a(\lambda)$ and $b_b(\lambda)$. In the arena of ocean color remote sensing, a well-accepted analytical reflectance model by Gordon *et al.* (1975, 1988) is

$$R(\lambda) = \sum_n r_n \left[\frac{b_b(\lambda)}{a(\lambda) + b_b(\lambda)} \right]^n \tag{1.3}$$

and a similar model exists for the remote-sensing reflectance, $R_{rs}(\lambda)$. The corresponding expansion coefficients can be found in their papers.

The additivity principle (Gordon, 1994) can be applicable to all associated optically-active constituent IOPs so that $a(\lambda)$ and $b_b(\lambda)$ become

$$a(\lambda) = a_w(\lambda) + \sum_i a_i(\lambda). \tag{1.4}$$

$$b_b(\lambda) = b_{bw}(\lambda) + \sum_i b_{bi}(\lambda). \tag{1.5}$$

where $a_w(\lambda)$ and $b_{bw}(\lambda)$ are the absorption and backscattering coefficients of pure sea water, and $a_i(\lambda)$ and $b_{bi}(\lambda)$ are the absorption and backscattering coefficients of the i^{th} optically-active constituent in the sea water, respectively.

1.3.2 Constituent IOP parameterization: bio-optical models

The reflectance model presented in Eqs. (1.3-1.5) is related to the i^{th} optically-active constituent concentration C_i through a subset of the model parameters in $\Theta(\lambda)$ defining the constituent-associated IOP submodels of $a_i(\lambda)$ and $b_{bi}(\lambda)$. In fact, a model parameterization is an attempt to estimate these parameters in $\Theta(\lambda)$ using *in situ* bio-optical measurements.

Conventionally, IOP submodels were usually expressed in terms of *constant* constituent-specific IOP coefficients. For example, the absorption coefficient for the i^{th} constituent could be written as $a_i(\lambda) = a_i^*(\lambda)\, C_i$ where the specific absorption coefficient for the i^{th} constituent $a_i^*(\lambda)$ was considered constant. Relatively recently, some IOP submodels have been modeled as nonlinear relationships between the constituent concentration C_i and its IOPs. In effect, $a_i^*(\lambda)$ varies with constituent concentration C_i.

It is also well accepted that some model parameters may not be applied universally. Parameters in the IOP submodels may vary in space and time due to intrinsic variations in optically active constituents. Therefore, IOP submodels may need parameterizing where regional *in situ* bio-optical measurements are available. Some published and well-accepted constituent IOP submodels are reviewed briefly in the following sections.

Constituent absorption parameterization

Previous studies have shown that the primary absorbing constituents in sea water include the sea water itself, phytoplankton pigments, particulates (detritus and inorganic matter) and CDOM. Their contributions are described as follows:

$$a(\lambda) = a_w(\lambda) + a_p(\lambda) + a_g(\lambda) \tag{1.6}$$

and the absorption of particulates, $a_p(\lambda)$, can be partitioned further as

$$a_p(\lambda) = a_\varphi(\lambda) + a_d(\lambda) \tag{1.7}$$

where the subscripts refer to water (w), particles (p), CDOM (g), phytoplankton (φ), and detritus (d). The absorption of pure sea water, $a_w(\lambda)$, is known and constant (Pope and Fry, 1997).

Based on the models by Bricaud *et al.* (1995, 1998), $a_\varphi(\lambda)$ and $a_p(\lambda)$ can be parameterized as functions of chlorophyll concentration Chl:

$$a_\varphi(\lambda) = a^*_\varphi(\lambda)\mathrm{Chl} = A_c(\lambda)\mathrm{Chl}^{Bc(\lambda)} \tag{1.8}$$

and

$$a_p(\lambda) = a^*_p(\lambda)\mathrm{Chl} = A_p(\lambda)\mathrm{Chl}^{Bp(\lambda)} \tag{1.9}$$

The models of $a_\varphi(\lambda)$ and $a_p(\lambda)$ are both nonlinear with respect to Chl, and were developed on the basis on a large data set of 1166 samples (Bricaud *et al.* 1998). Note that total particulate absorption, $a_p(\lambda)$, includes the contributions from both phytoplankton pigments and detritus. Bricaud *et al.* (1998) pointed out the following limitations: 1) Both models are applicable to Case 1 waters only and may be not valid outside the range of chlorophyll concentration from 0.02 to 25 mg/m^3; 2) In spite of the large data set, the models are not universal because some special oceanic waters were not explored (e.g. polar waters); 3) The specific coefficients $a^*_\varphi(\lambda)$ and $a^*_p(\lambda)$ vary by more than one order

of magnitude whereas Chl varies by three orders of magnitudes (0.02 to 25 mg/m^3). Such variations may have an impact on both the forward and inverse problems once they are implemented in a semi-analytical reflectance model.

The absorption coefficients of detrital particles and CDOM are $a_d(\lambda)$ and $a_g(\lambda)$, respectively. Their spectral shapes are very similar, exponentially decreasing with increasing wavelength (Roesler *et al.* 1989; Carder *et al.* 1991), and thus they are often modeled together as one term $a_{gd}(\lambda)$, with a spectral slope S_{gd}:

$$a_{gd}(\lambda) = a_{gd}(\lambda_0)\exp(-S_{gd}(\lambda - \lambda_0)) \tag{1.10}$$

The factor S_{gd} has a mean value of 0.0145 nm^{-1} (Roesler *et al.* 1989). The value of the absorption coefficient at a reference wavelength λ_0, $a_{gd}(\lambda_0)$, is often used as a surrogate variable for CDOM concentration.

Constituent Backscattering Parameterization:

The backscattering coefficient, $b_b(\lambda)$, another key IOP in modeling ocean color, is generally modeled by

$$b_b(\lambda) = b_{bw}(\lambda) + b_{bp}(\lambda) \tag{1.11}$$

where the backscattering coefficient of the sea water, $b_{bw}(\lambda)$ is well known. The total particle backscattering coefficient, $b_{bp}(\lambda)$, can be partitioned further into two components associated with organic (φ) and inorganic (s) particles (Sathyendranath *et al.* 1989).

$$b_{bp}(\lambda) = b_{b\varphi}(\lambda) + b_{bs}(\lambda) \tag{1.12}$$

Theory (Bricaud and Morel, 1986; Morel and Prieur, 1977) predicts that $b_{bp}(\lambda)$ can be represented by a spectral power-law model:

$$b_{bp}(\lambda) = b_{bp}(\lambda_0)\left(\frac{\lambda_0}{\lambda}\right)^{n_p} \tag{1.13}$$

where the exponent n_p has a range from 0 to 2 according to Mie theory and varies with the size distribution and composition (i.e. refraction index) of the particulate matter (Bricaud and Morel,1986). *In situ* measurements show that the exponent n_p varies in the range of 0.7-1.1 for surface waters (Maffione and Dana, 1996, 1997).

A specific parameterization scheme of $b_{bp}(\lambda)$ by Chl was proposed by Gordon *et al.* (1988) in the form of

$$b_{bp}(\lambda) = b_0 A_b(\lambda) \mathrm{Chl}^{B_b(\lambda)} \tag{1.14}$$

This expression involves two variables, b_0 and Chl, being used to describe variations in the total particle backscattering. The variable b_0 is associated with variability in total particle scattering which was found empirically to be a function of chlorophyll given by $b_p(550) = b_0 \mathrm{Chl}^{0.62}$ where b_0 ranges from 0.12 to 0.45 with a mean of 0.32 (Gordon *et al.*, 1988). The particle backscattering probability $b_{bp}(\lambda)/b_p(\lambda)$ is dependent on both wavelength and Chl, and is parameterized as a power-law function of chlorophyll with assumptions regarding the spectral dependence at low and high Chl levels. $A_b(\lambda)$ and $B_b(\lambda)$ were obtained by linear fits on log-log plots.

If a one-component model (Eq. 1.11) does not represent the total backscattering $b_{bp}(\lambda)$ well for more optically-complex waters, a two-component backscattering model (Eq. 1.12) may be necessary. Sathyendranath *et al.* (1989) proposed a two-component particle backscattering model in which $b_{bp}(\lambda)$ was partitioned into two independent components $b_{b\varphi}(\lambda)$ and $b_{bs}(\lambda)$. The contribution by phytoplankton, $b_{b\varphi}(\lambda)$, is modeled in the same form as that in Eq. (1.14). The other component, $b_{bs}(\lambda)$, contributed from non-chlorophyllous particles, is expressed as

$$b_{bs}(\lambda) = b_{bs}(550)(\frac{550}{\lambda})^n \quad (1.15)$$

Theoretical studies (Morel and Bricaud, 1981) suggested that $b_{bs}(550)$ is proportional to non-chlorophyllous particle concentration (mineral suspended sediment concentration SSC). Some other studies (Tassan, 1994; Krawczyk *et al.* 1995, 1997) parameterized $b_{bs}(550)$ in the form of

$$b_{bs}(550) = b^*_{bs}(550)[SSC] \quad (1.16)$$

where the specific backscattering coefficient, $b^*_{bs}(550)$ for non-chlorophyllous particles, was assumed to be constant.

1.4 Quantitative interpretation of ocean color: the inverse problem

Interpreting an ocean color spectrum quantitatively is an inverse problem. How do we use the ocean color observation to obtain a set of constituent concentrations? The essential problem to be solved is: given a measured ocean color spectrum $L(\lambda)$ along with a parameterized ocean color model, estimate constituent concentrations that result in the particular color spectrum. If Eq.(1.1) is nonlinear, its inversion denoted by f^{-1} in Eq.(1.2) is an approach or a technique rather than an exact analytical formula. To date, there exist three main types of model-based inversion techniques being applied widely to ocean color interpretation using all spectral signals. They are non-linear optimization (NLO), principal component analysis (PCA), and artificial neural network (ANN) inversions.

1.5 Overview of the dissertation

In this dissertation, the goal is to have an overall understanding in developing a semi-analytical ocean color model for solving the inverse problem. Several aspects in quantitatively modeling an ocean color spectrum are explored by means of both *in situ*

data analysis and model simulation. The dissertation is presented in the context of three self-contained papers, chapters 2-4, with each chapter having one or two specific objectives associated with the overall goal stated above. Thus, each chapter contains its own abstract, methods, results, discussion, and conclusions sections, and references. Some overlap and redundancy among the chapters is expected because of this format of the dissertation.

In chapter 2, a simulation approach was used to quantify retrieval errors in chlorophyll concentrations induced by uncertainties in IOP submodel parameterizations. A radiance model configured with a three-component IOP system is inverted using a non-linear optimization inversion technique. I demonstrate quantitatively how uncertainty in the individual IOP submodel parameterization influences the accuracy of the chlorophyll concentration retrieval at different chlorophyll concentration levels. In general, this approach is applicable for any semi-analytical ocean color model to quantify retrieval errors caused by uncertainties from IOP model parameterization. The results in this chapter were presented at the 4th Pacific Ocean Remote sensing Conference in Qingdao, China in 1998, and later published in the *Journal of Advanced Marine Science and Technology Society* (Feng *et al.* 1998).

In Chapter 3, an objective comparison of the three widely-used inversion algorithms (i.e. NLO, PCA and NN) is presented. The objective for that research is to assess their strength and weakness for different optical water types. Based on a compiled dataset of bio-optical measurements from various sources, reflectance spectra were classified to identify optically different water types using a classification scheme (Moore *et al.* 2001). For each of the identified water types, forward radiance models configured

with three-component IOP submodels were parameterized and used to generate simulated datasets. The reflectance signals were inverted with the three inversion algorithms. The PCA and ANN techniques, unlike NLO, usually depend on a model-simulated ocean color dataset to find a statistical inversion function, a relation that is used to derive optically-active concentrations from ocean color. The results in this chapter were originally presented at the Ocean Optics XV conference in Monaco, France in 2000. It is going to be submitted to the Journal of Applied Optics.

In Chapter 4, an optimal scheme to parameterize a spectral reflectance model in terms of bio-optical measurements is demonstrated. This parameterization scheme was realized first by a comprehensive bio-optical data set obtained at 45 stations in Tokyo Bay and nearby region between 1982 and 1984 (Kishino *et al.* 1984). Specifically, a forward model was parameterized using the whole dataset, and then parameterized using three subsets of the data. The subsets were determined by applying a classification routine (Moore *et al.* 2001) to the reflectance spectra to identify optically-distinct water types. The results have shown that this approach could significantly improve the performance of the forward model. In comparing inversion results, we found that this approach was not significantly different from that of the single parameterized model. The results in this chapter were originally presented at the AGU/ASLO meeting in San Diego, USA, in 1988. It is going to be submitted to the Journal of Remote Sensing of Environment.

In Chapter 5, a brief summary of the thesis is given with the focus on the significance of the thesis, and further work is proposed.

Appendix: Definitions of optical properties of water

Preisendorfer (1961) first proposed that the optical properties of seawater can be divided into two classes: the inherent optical properties (IOPs) and apparent optical properties (AOPs). This Appendix presents the fundamental terms used in this thesis with some discussions. The context is based mainly on the papers by Morel and Smith (1982) and Jerlov (1976). Note that all the physical terms presented in the following are spectral quantities, meaning they are functions of wavelengths (with the dimension of a derivative with respect to wavelength). The water depth (z) dependence of optical properties in the water is often there, but is ignored in any mathematical expression throughout this thesis under the assumption that we are considering surface water unless explicitly specified

Basic Radiative Quantities

Radiant Energy Q: in units of J (joule)

Radiant Flux Φ: the rate of transport of radiant energy in units of watt (W=J/sec)

$$\Phi = \frac{dQ}{dt} \tag{A1}$$

Radiant Intensity I: the radiant flux emitted by a point source in a small cone containing a given direction, divided by that element of solid angle $d\Omega$, in units of W sr^{-1}

$$I = \frac{d\Phi}{d\Omega} \tag{A2}$$

Radiance $L(\theta,\varphi)$: the radiant flux per solid angle per unit projected area incident in a given direction (θ,φ), in units of W $sr^{-1}m^{-2}$.

$$L(\theta,\varphi) = \frac{d^2\Phi}{dA\,d\Omega} \tag{A3}$$

where $d\Omega$ is a solid angle in units of steradian (sr); dA is area (m^2) subtending the solid angle $d\Omega$; and angles θ and φ are the zenith angle and the azimuthal angle, respectively. A radiance distribution, the complete set of radiance values in all directions at a point, gives a complete geometrical structure of the light field. The radiance is the fundamental measure relevant to ocean color remote sensing since a sensor measuring the radiative energy from the sea is viewing the sea surface as a "light" source.

Apparent Optical Properties

Apparent optical properties are those properties that depend both on the medium (the IOPs) and on the structure of the incident light field. Obviously, radiance is the most fundamental apparent optical property since all the other AOPs can be derived essentially from it.

Irradiance E: the radiant flux from all directions incident on a small element of a surface containing the point under consideration, divided by the area of that element, in units of W m^{-2}.

$$E = \frac{d\Phi}{dA} \tag{A4}$$

Downwelling Irradiance E_d: the radiant flux incident on a small element of the upper face (i.e. facing zenith) of a horizontal surface containing the point under consideration, divided by the area of that element, in units of W m^{-2}. E_d can be defined as an integral of the radiance in a spherical coordinate system by

$$E_d = \int_{\varphi=0}^{2\pi} \int_{\theta=0}^{\pi/2} L(\theta, \varphi) \cos\theta \sin\theta \, d\theta \, d\varphi \tag{A5}$$

Upwelling Irradiance E_u: the radiant flux incident on a small element of the lower face (i.e. facing nadir) of a horizontal surface containing the point under consideration,

divided by the area of that element, in units of W m^{-2}. Similarly, E_u can be defined as an integral of the radiance by

$$E_u = \int_{\varphi=0}^{2\pi} \int_{\theta=\pi/2}^{\pi} L(\theta, \varphi) \cos\theta \sin\theta \, d\theta \, d\varphi \tag{A6}$$

Vertical Attenuation Coefficients K_x (m^{-1}): vertical gradient of the natural logarithm of a radiative quantity X.

$$K_x = -\frac{d \ln(X(z))}{dz} = -\frac{1}{X(z)} \frac{dX(z)}{dz} \tag{A7}$$

where z is depth; X(z) stands for E_d, E_u, or any other radiative quantity, which varies with depth z. X(z) can be written as :

$$X(z) = X(z_0) \cdot e^{-\int_{z_0}^{z} K_x dz} \tag{A8}$$

Irradiance Reflectance R: the ratio of the upwelling to the downwelling irradiance (dimensionless)

$$R = \frac{E_u}{E_d} \tag{A9}$$

Downwelling and upwelling irradiance have been the most commonly measured quantities in optical oceanography. R is usually estimated by directly measuring E_d and E_u.

Remote Sensing Reflectance R_{rs}: the ratio of the upwelling radiance (simulating the geometric acceptance of a sensor) to the downwelling irradiance (sr^{-1})

$$R_{rs} = \frac{L_u}{E_d} = \frac{R}{Q} \tag{A10}$$

The Radiative Transfer Equation (RTE)

The inherent and apparent optical properties of water are related by RTE that may be written by

$$\frac{dL(z,\theta,\varphi)}{dz}\cos\theta = -cL(z,\theta,\varphi) + L^{*} \qquad (A11)$$

where z is the vertical coordinate, positive downward, and $L=L(z,\theta,\varphi)$ is the radiance at depth z from the direction (θ,φ).θ and φ are the zenith and azimuth angle, respectively. L^{*} is the so-called source function or path function defined by

$$L^{*} = \int_{4\pi} \beta(\theta,\varphi,\theta',\varphi') \cdot L(z,\theta',\varphi') d\Omega' \qquad (A12)$$

where $d\Omega'$ is a small solid angle in the direction (θ',φ'), and $\beta(\theta,\varphi,\theta',\varphi')$ is the volume scattering function for light scattered with the direction (θ,φ) from the direction (θ',φ').

Exact analytical solutions to the RTE are impossible for most oceanic waters (Gordon,1994). Therefore, one must rely on numerical solutions as approximation. There are many numerical methods for solving the RTE, such as invariant imbedding (Mobley,1994), discrete ordinates (Jin and Stamnes, 1994), and Monte Carlo (Gordon, 1975,1988). Mobley *et al.* (1993) gave a comparison of those numerical solutions to the RTE.

References

Bricaud, A., Morel, A. and Prieur, L., 1981. Absorption by dissolved organic matter of the sea (yellow substance) in the UV and visible domains, Limnol. And Oceanogr. 26,1, 43-53.

Bricaud, A. and. Morel, A., 1986. Light attenuation and scattering by phytoplanktonic cells: A theoretical modeling, Applied Optics, 25, 571-580.

Bricaud, A., Babin, M., Morel, A. and Claustre, H., 1995. Variability in the chlorophyll-specific coefficients of natural phytoplankton: analysis and parameterization, J. Geophys. Res. 100, C7, 13,321-13,332.

Bricaud, A., Babin, M., Morel, A. and Claustre, H., 1998. Variations of light absorption by suspended particles with chlorophyll concentration in oceanic (case 1) waters: analysis and implications for bio-optical models, J.Geophys. Res. **103**, C13, 31,033-31,044.

Carder, K.L., Hawes, S.K., Baker, K.A., Smith, R.C., Steward, R.G. and Mitchell, B.G., 1991. Reflectance model for quantifying chlorophyll a in the presence of productivity degradation products, J.Geophys. Res., 96, 20,599-20,611.

Doerffer, R. and Fischer, J., 1994. Concentrations of Chlorophyll, suspended matter, and gelbstoff in Case II waters derived from satellite coastal zone color scanner data with inverse modeling methods, J. of Geophys. Res., 99,7457-7466.

Doerffer, R. and Schiller, H., 1999. First test of a two-step neural network inverse modeling technique using MOS data. The 2nd International Workshop on MOS-IRS and Ocean Colour, Berlin, June 1—12, 1999.

Dowell, M.D. and Hoepffner, H., 1997. Reflectance model in Case II waters: contamination of the elastic signal by CDOM fluorescence, The 1st International Workshop on MOS-IRS and Ocean Colour, Berlin, April 28-30.

Feng, H., Campbell, J. W. and Moore, T.S., 1998. Uncertainty analysis for retrieval of chlorophyll concentration from ocean color: a simulation study, Journal of Advanced Marine Science and Technology Society, 4, 2, 265-274.

Garver, S.A. and Siegel, D.A., 1997. Inherent optical property inversion of ocean color spectra and its biogeochemical interpretation 1. Time series from the Sargasso Sea, J.Geophys. Res., 102, C8, 18,607-18,625.

Gordon, H.R., Brown, O. B . and Jacobs, M.M., 1975. Computed relationship between the inherent and apparent optical properties of a flat homogeneous ocean, Appl.Opt., 14,417-427.

Gordon, H.R. and Morel, A., 1983. Remote assessment of ocean color for interpretation of satellite visible imagery, A review. New York,: Springer.

Gordon, H.R., Brown, O.B., Evans, R.H., Brown, J.W., Smith, R.C. , Baker, K.S. and Clark, D.K., 1988. A semi-analytical radiance model of ocean color, J. Geophys. Res., 93, 10,909-10,924.

Gordon, H.R., 1994. Modeling and simulating radiative transfer in the ocean. Ocean Optics, R.W. Spinard, K.L. Carder and M.J. Perry (ed.), Oxford University Press.

Hoge, F. E. and Lyon, P.E., 1996. Satellite retrieval of inherent optical properties by linear matrix inversion of oceanic radiance model: an analysis of model and radiance measurement error, J. Geoohys. Res., 100(C7), 16631-16648.

IOCCG Report Number 3: Remote Sensing of Ocean Colour in Coastal, and Other Optically-Complex, Waters 2000. in S. Sathyendranath (Ed.), Dartmouth, Canada.

Jerome, J.H., Bukata, R. P. and Bruton, J.E., 1988. Utilizing the components of vector irradiance to estimate the scalar irradiance in natural waters, Appl. Optics, 27, 4012-4018.

Jin, Z. and Stamnes, K., 1994. Radiative transfer in nonuniformly refracting layered media: atmosphere-ocean system, *Appl. Opt.*, 33, 431-442.

Kirk, J.T.O., 1981. A Monte Carlo study of the nature of the underwater light field in, and the relationships between optical properties of turbid yellow waters, Aust. J. Mar. Freshwater Res., 32, 157-32.

Kirk, J.T.O., 1984. Dependence of relationship between inherent and apparent optical properties of water on solar altitudes, Limnology and Oceanography, 29: 350-356.

Klemas, V., Bartlett, D., Philpot, W., Rogers, R. and Reed, L., 1974. Coastal and estuarine studies with ERTS-1 and Skylab, Remote Sens. Env., 3,153-74.

Krawczyk, H., Neumann, A. and Walzel, T., 1995. A Complex approach to quantitative interpretation of spectral high resolution imagery, The Third Thematic Conference on Remote Sensing for Marine and Coastal Environments, September, Seattle, USA, pp. II-57-68.

Krawczyk, H. and Hetscher, M., 1997. Principal Component inversion algorithm for the retrieval of water constituents and its application, Proceedings of the 1st International Workshop on MOS-IRS and Ocean Color.

Lee, Z.P., Carder, K.L, Hawes, S.K., Steward, R.G., Peacock, T.G. and Davis, C.O., 1994. Model for the interpretation of hyperspectral remote-sensing reflectance, Applied Optics, **33**, 5721-5732.

Maffione, R.A and Dana, D.R., 1996. Recent measurements of the spectral backward-scattering coefficient in coastal waters, Ocean Optics XIII, SPIE 2963, Halifax, Canada.

Maffione, R.A and Dana, D.R., 1997. Instruments and methods for measuring the backward-scattering coefficient of ocean waters, Applied Optics, 36, 6057-6067.

Mobley, C.D., Gentili, B., Gordon, H.R., Jin, Z., Kattawar, G.W ., Morel, A., Reinersman, P., Stamnes, K. and Stavn, R.H., 1993. Comparison of Numerical Models for Computing Underwater Light Fields, Applied Optics, 32, 7484-7504.

Mobley, C. D., 1994. Light in water; Radiative transfer in natural waters. San Diego, Academic Press, Inc.

Morel, A. and Prieur, L., 1977. Analysis of variations in ocean color, Limnology and Oceanography, 22, 709-722.

Morel, A. and Bricaud, A.,1981. Some theoretical results concerning optics of phytoplankton with spectral reference to remote sensing, In Oceanography from Space, edited by J.F.R. Gower (New York:Plenum Press), 313-317.

Moore, T.S., Campbell, J.W. and Feng, H., 2001. A fuzzy logic classification scheme for selecting and bending satellite ocean color algorithms, IEEE Trans.Geosci. Remote Sens., 39(8), 1764-1776.

Pope, R.M. and Fry, E.S., 1997. Absorption spectrum (380-700nm) of pure water: II. Integrating cavity measurements, Applied Optics, 6, 8710-8723.

Preisendorfer, R.W., 1961. Application of radiative transfer theory to light measurements in the sea, Internataional Union of Geodesy and Geophysics Monograph (Symposium on Radiant energy in the Sea) no.10, pp11-30.

Roesler, C.S., Perry, M.J. and Carder, K.L., 1989. Modeling in situ phytoplankton absorption from total absorption spectra in productive inland marine waters, Limnol. Oceanogr. 34, 1510-1523.

Roesler, C.S. and Perry, M.J., 1995. In situ phytoplankton absorption, fluorescence emission, and particular backscattering spectra determined from reflectance, Journal of Geophysical Research,100, 13279-13294.

Salisbury, J.E., Campbell, J.W., Linder, L.D., Meeker, D., Muller-Karger, F.E. and Vörösmarty, C.J., 2004. Spatio-temporal studies of the Mississippi Plume using satellite ocean color and wind discharge data, Deep Sea Research (in press).

Sathyendranath, S., Prieur, L. and Morel, A., 1989. A three-component model of ocean

color and its application of phytoplankton pigments in coastal waters, Int. J. of Remote Sensing, 10,8,1373-1794.

Schiller, H. and Doerffer, R., 1999. Neural network for emulatin of an inverse model---operational derivation of Case II water properties from MERIS data, Int. J. of Remote Sensing, 20,9, 1735-1746.

Stumpf, R. P. and Pennock, J.R., 1989. Calibration of a general optical equation from remote sensing of suspended sediments in a moderately turbid estuary, J. Geophys Res., 94,C10, 14,363-14,371.

Tassan, S., 1994. Local algorithms using SeaWiFS data for the retrieval of phytoplankton, pigments, suspended sediments, and yellow substance in coastal waters, Applied Optics, 33,12, 2369-2378.

Vodacek, A., Blough, N.V., DeGrandpre, M.D., Peltzer, E.T. and Nelson, R.K., 1997. Seasonal variation of CDOM and DOC in the Middle Atlantic Bight: Terrestrial inputs and photooxidation, Limnology and Oceanography, 42 (4): 674-686.

Zaneveld, R.,1995. A theoretical derivation of the dependence of the remotely sensed reflectance of the ocean on the inherent optical properties, J.Geophys. Res., 100, C7, 13,135-13,142.

Chapter 2 The Effect of Uncertainty in Inherent Optical Property Parameterization on Chlorophyll Retrieval from Ocean Color Spectra: A Simulation Study

(Published in Journal of Advanced Marine Science and Technology Society, 4(2), 265-274, 1998 by Hui Feng, Janet W. Campbell, and Timothy S. Moore)

Abstract

A general approach is presented to quantify retrieval errors in in-water constituent concentrations induced by uncertainty in inherent optical property (IOP) submodel parameterization. Chlorophyll concentrations are retrieved by inverting a radiance model with nonlinear IOP submodels. We demonstrate quantitatively how uncertainty in the IOP submodel parameterization influences the accuracy of the chlorophyll concentration retrieval at different chlorophyll concentration levels. Two complete sets of simulations were designed and conducted. These represent two extreme cases between which "real" cases are expected to occur. The simulations show that precise knowledge of spectral shapes of IOP submodels is important in chlorophyll retrieval.

2. 1 Background

One of the primary objectives in ocean color remote sensing is to determine in-water constituent concentrations. Oceanic constituents of interest include phytoplankton chlorophyll, colored dissolved organic matter (CDOM), and suspended sediments. Techniques for constituent retrieval have evolved from empirical (data-based) towards

analytical (model-based) algorithms for the last two decades. Analytical algorithms usually resort to an inversion technique applied to a parameterized ocean color model. Currently, several such inversion techniques have been proposed for ocean color applications. Hoge and Lyon (1996) applied a semi-analytical radiance model (Gordon *et al.* 1988) with IOP submodels to the retrieval of three in-water variables using three CZCS spectral bands. For each constituent under consideration, its IOP was modeled as the product of the IOP at a reference wavelength multiplied by a spectral shape function. The spectral shape functions were fixed and independent of in-water constituent concentrations. Thus, the IOPs at reference wavelengths could be retrieved by a linear system inversion. Garver and Siegel (1997) presented an inverse model to retrieve chlorophyll concentrations using six SeaWiFS spectral bands. In their model, the chlorophyll-specific absorption coefficient was a nonlinear function of the chlorophyll concentration, and thus a non-linear optimization technique was needed to invert their model. Campbell *et al.* (1997) used a radiance model configured with nonlinear IOPs to retrieve chlorophyll concentration, CDOM absorption, and a variable associated with total particle backscattering. Their model can be inverted using a nonlinear inversion method. The model configurations and inversion techniques essentially differ in the three models mentioned above. For any inverse model, it is necessary to quantify the potential sources of uncertainty in an inverse solution. Hoge and Lyon (1996) showed that their inverse solution is very sensitive to variability in model parameters. The goal of this work is to quantitatively characterize retrieval errors resulting from IOP parameterization uncertainties for the model of Campbell *et al.* (1997) using normalized water-leaving radiances in the first five SeaWiFS bands (412, 443, 490, 510, and 550 nm). We focus

strictly on chlorophyll retrieval errors in this paper.

2.2 Methodology

General Consideration

Without losing generality, a forward ocean color model may be expressed as

$$L(\lambda) = f(\boldsymbol{C},\Theta(\lambda)) \tag{2.1}$$

where $L(\lambda)$ is an ocean color measurement at wavelength λ (e.g. water-leaving radiance or remote sensing reflectance), and f is a model configuration (or function) relating $L(\lambda)$ to the in-water concentration vector $\boldsymbol{C}$ to be retrieved through a model parameter vector $\Theta(\lambda)$. Parameters in the vector $\Theta(\lambda)$ related to IOPs depend on the constituent-specific IOP submodels being used. In the case of the chlorophyll-specific absorption coefficient, for example, the models of Carder *et al.* (1991) and Bricaud *et al.* (1995) had different parameters. Carder *et al.* (1991) used a hyperbolic tangent function with four model parameters to describe chlorophyll-specific absorption, while Bricaud *et al.* (1995) used a power function of chlorophyll concentration with two parameters to describe variation in chlorophyll-specific absorption.

The retrieval of vector $\boldsymbol{C}$ based on Eq. (2.1) can be written by

$$\boldsymbol{C} = f^{-1}(L(\lambda),\Theta(\lambda)) \tag{2.2}$$

where f^{-1} represents an inversion of the model f. The symbol f^{-1} might either be an explicit expression, as in the case of a model that is linear with respect to the in-water concentrations (e.g., Hoge and Lyon, 1996), or denote an inversion technique if the inversion of equation (2.1) does not yield an explicit solution.

Generally speaking, there exist four potential candidate sources of error in retrieving the concentration vector $\boldsymbol{C}$. The first is the model f itself which links an apparent optical property, $L(\lambda)$, to inherent optical properties. Exact solutions to radiative transfer equations are highly complex (Zaneveld, 1995), and are not amenable to inverse solutions. Almost all forward models are approximations to more complex equations. The second source of error is the inherent variability in constituent-specific IOPs. The IOP submodels and their associated model parameter vector $\Theta(\lambda)$ only approximate the actual constituent-specific IOPs. This work mainly attempts to quantify the retrieval errors caused by IOP model uncertainty. A third source of error might be the inversion scheme itself although this can generally be controlled by setting convergence criteria. Finally, errors in the measurements of $L(\lambda)$ caused by sensor calibration, atmospheric correction, etc., can affect accuracy of the retrievals. In this paper, we consider only the errors resulting from the parameterization of constituent-specific IOP submodels. Analysis of other error sources will be the subject of future work.

Radiance Model

Normalized water-leaving radiance is related to remote sensing reflectance $R_{rs}(\lambda)$ by the relationship based on (Gordon *et al.* 1988)

$$nL_w(\lambda) = \frac{MF_0R_{rs}(\lambda)}{1-rQR_{rs}(\lambda)} \tag{2.3}$$

Where F_0 is the extraterresstrial solar irradiance (Gregg and Carder, 1990); and the term $M=(1-\rho)(1-\rho')/n^2$ where ρ (~0.021) is the Fresnel reflectivity of the sea surface at normal incidence, ρ' (~0.043) is the Fresnel reflection albedo of the sea surface for irradiance from the sun and sky; n (~1.32) is the index of refraction of water; r (~0.48) is the water-

air reflectance for totally diffuse upwelling irradiance; Q is the ratio of the upwelling irradiance to upwelling radiance. Q ranges between 3.14 and 5, and is taken as 4. The values of M, F_o and rQ are listed in Table 2.1.

Based on Monte Carlo simulations of Gordon el al. (1975), $R_{rs}(\lambda)$ is directly related to IOPs by

$$R_{rs}(\lambda) = 0.0949\, X(\lambda) + 0.0794\, X(\lambda)^2 \tag{2.4}$$

where

$$X(\lambda) = \frac{b_b(\lambda)}{a(\lambda) + b_b(\lambda)} \tag{2.5}$$

The absorption coefficient is modeled by $a(\lambda) = a_w(\lambda) + a_\phi(\lambda) + a_{gd}(\lambda)$ and the backscattering coefficient as $b_b(\lambda) = b_{bw}(\lambda) + b_{bp}(\lambda)$, where subscripts w, ϕ, g, d, and p refer to pure seawater, phytoplankton, CDOM ("gelbstoff"), detritus, and particles, respectively. The absorption of detritus decreases exponentially with increasing wavelength in a manner similar to that of CDOM (Carder *et al.* 1991). For simplification, we combine these into one single term, $a_{gd}(\lambda) = a_{gd}(375)\exp[-S(\lambda-375)]$. The absorption coefficient of CDOM and detritus at 375 nm, $a_{gd}(375)$, is used as a measure of the CDOM and detritus concentration. The spectral shape parameter for CDOM and detritus absorption, S, usually varies between 0.011 and 0.021 with a mean of 0.0145 (Bukata *et al.* 1995).

The phytoplankton absorption coefficient $a_\phi(\lambda) = A_c(\lambda)\cdot \mathrm{Chl}^{B_c(\lambda)}$ is based on the model by Bricaud *et al.* (1995). This model gives the chlorophyll-specific absorption coefficient, $a_\phi^*(\lambda)$, as a function of the chlorophyll concentration, Chl, and is based on

about 800 globally distributed observations of absorption spectra and chlorophyll concentration. The model used for our analysis involves two spectral parameters, $A_c(\lambda)$ and $B_c(\lambda) = B_c^*(\lambda) + 1$, where $A_c(l)$ and $B_c^*(\lambda)$ are tabulated in Bricaud *et al.* (1995).

The particle backscattering submodel is $b_{bp}(\lambda) = b_0 \cdot A_b(\lambda) \cdot Chl^{B_b(\lambda)}$ and is based on the parameterization scheme of Gordon *et al.* (1988). This expression involves two independent variables, b_0 and Chl, being used to describe variations in particle backscattering. The variable b_0 is associated with variability in total particle scattering which was found empirically to vary with chlorophyll concentration such that $b_p(550) = b_0 \cdot Chl^{0.62}$. All spectral dependence was assigned to the particle backscattering probability, $b_{bp}(\lambda)/b_p(\lambda)$, parameterized as a power-law function of chlorophyll (Gordon *et al.* 1988), and its parameters, $A_b(\lambda)$ and $B_b^*(\lambda)$ were obtained by linear fits on log-log plots. The exponent in the particle backscattering coefficient submodel was, thus, $B_b(\lambda) = B_b^*(\lambda) + 0.62$. Variation in particle backscattering is associated with the properties of particles, such as their size distribution and composition (i.e. refraction index).

The model parameter vector, $\Theta(\lambda) = [S, A_c(\lambda), B_c(\lambda), A_b(\lambda), B_b(\lambda)]$, fully defines the IOP submodels for each wavelength. Constant model parameters used in the inversion algorithm are given in Table 2.1. The in-water constituent concentration vector defined in this model is $\boldsymbol{C} = [a_{gd}(375), Chl, b_0]$.

Inversion method

Given a measured radiance, $L_w(\lambda)$, and assumed values for r, M, F_o and Q (Table 2.1), Eq. 2.3 can be solved for $R_{rs}(\lambda)$, and given $R_{rs}(\lambda)$, equation (2.4) can then be solved for $X(\lambda)$. Thus, a value of $X(\lambda)$ is derived from the measured radiance, $L_w(\lambda)$. A non-

linear optimization technique is then required to solve equation 2.5 for the constituent vector, ***C***. The Gauss-Newton algorithm was selected for this purpose. This algorithm is now widely used in ocean color inversion models (Bukata *et al.* 1995; Roesler and Perry, 1995; Garver and Siegel, 1997; Feng *et al.* 1998). Its theoretical basis is documented in detail by Press *et al.* (1992). Bukata *et al.* (1995) gave an excellent review of its potential applications in ocean color interpretation.

Simulations

Uncertainties in the three constituent-specific IOP parameterizations (i.e. $a_{gd}(\lambda)$, $a_{\phi}(\lambda)$ and $b_{bp}(\lambda)$ were simulated as follows:

$$S' = S + \delta_S \tag{2.6a}$$

$$\log(a_{\phi}'(\lambda)) = \log(a_{\phi}(\lambda)) + \delta_{\phi}(\lambda) \tag{2.6b}$$

$$\log(b_{bp}'(\lambda)) = \log(b_{bp}(\lambda)) + \delta_{bp}(\lambda) \tag{2.6c}$$

where δ_S, $\delta_{\phi}(\lambda)$, and $\delta_{bp}(\lambda)$ were normally distributed pseudo-random errors with zero means, and standard deviations equal to 0.0015, 0.04, and 0.04, respectively. These values represent 10% RMS errors in the corresponding IOP submodels. Two complete sets of simulations were designed and carried out: one in which IOP errors were spectrally uncorrelated (i.e. $\delta_{\phi}(\lambda_1)$ ... $\delta_{\phi}(\lambda_5)$, and $\delta_{bp}(\lambda_1)$ ... $\delta_{bp}(\lambda_5)$ were all statistically independent) , and the other in which $\delta_{\phi}(\lambda_1) = ... = \delta_{\phi}(\lambda_5)$, and $\delta_{bp}(\lambda_1) = ... = \delta_{bp}(\lambda_5)$, but where $\delta_{\phi}(\lambda_i)$ and $\delta_{bp}(\lambda_i)$ were uncorrelated. We refer to these as "Independent Error" and "Correlated Error" simulations, respectively. Figure 2.1 demonstrates the distinction between the two simulations. Although neither assumption is realistic, clearly real cases are bounded between these two extremes. Later, we discuss the implication of this.

To determine whether retrieval accuracy is dependent on the chlorophyll concentration, simulations were conducted for three cases representing low (0.1 mg m^{-3}), medium (1.0 mg m^{-3}) and high (10.0 mg m^{-3}) chlorophyll levels. For each chlorophyll level, we simulated a random sample of 200 $a_{gd}(375)$ and b_0 values. The distribution of $a_{gd}(375)$ depended on Chl as follows

$$\log a_{gd}(375) = 0.47909 \log(Chl) - 0.75657 + \delta_{ag} \qquad (2.7)$$

where δ_{ag} was normally distributed with a zero mean and a standard deviation of 0.1649. This relationship was derived from *in situ* measurements of Chl and $a_{gd}(375)$. The distribution of b_0 was assumed to be normal with a mean of 0.3 and a standard deviation of 0.07, and b_0 was independent of $a_{gd}(375)$.

For each chlorophyll level, the following steps were taken:

Step One: The radiance model was run in the forward direction and forced by the ensemble of 200 in-water concentration vectors, $\boldsymbol{C}=[a_{gd}(375), Chl, b_0]$, using IOP models with the constant parameter vector shown in Table II.1 to generate a set of 200 $L_w(\lambda)$ vectors. Each $L_w(\lambda)$ spectrum was then inverted to obtain the concentration vector $\boldsymbol{C'}$ which was then compared with $\boldsymbol{C}$. The purpose of this step was to estimate errors due to the inversion method itself, since the IOPs were assumed to be exact (i.e. with no errors).

Step Two: The radiance model was run forward again with a perturbed IOP model (or models) as defined by equations (2.6-2.7) to produce another simulated data set of 200 $L'_W(\lambda)$ spectra, and these spectra were then inverted to obtain $\boldsymbol{C'}$ as in Step One. Strategically, each IOP was perturbed separately to isolate the impact of individual IOP

models on concentration retrievals, and then errors were added to all three IOP models to determine their combined effect.

Step Three: Differences between vectors $\boldsymbol{C'}$ and $\boldsymbol{C}$ were used to define retrieval errors caused by uncertainties in IOP model parameterization. The RMS errors in both Chl and log(Chl) were used as measures of error. Specifically, from the sample of 200 retrievals, we calculated simple difference errors: Δ = Chl' – Chl, and log difference errors Δ_{log} = log Chl' – log Chl, which are related to relative errors. For each type of errors, two statistics were obtained: the mean error, **M** and $\mathbf{M_{log}}$, and the mean-square error, **MSE** and $\mathbf{MSE_{log}}$.

Steps Two and Three were repeated 100 times, each time with a new random set of IOP perturbations applied individually and then simultaneously. The statistics on **M**, $\mathbf{M_{log}}$, **MSE** and $\mathbf{MSE_{log}}$ were accumulated. The root-mean-square errors, **RMSE** and $\mathbf{RMSE_{log}}$ were then computed as the square roots of **MSE** and $\mathbf{MSE_{log}}$. Thus, resulting statistics were actually based on N = 20,000 random retrieval errors (100 simulations, each with an ensemble of 200 $\boldsymbol{C}$ vectors).

2.3 Results and Discussion

Effect of Inversion Scheme (Step One)

We found no errors resulting from the inversion scheme in Step One. That is, the inversion algorithm was able to retrieve each of the 200 $\boldsymbol{C}$ vectors to an arbitrary level of accuracy controlled by the convergence criteria.

Effect of IOP Uncertainties (Steps Two and Three)

Results from all the simulations are shown in Table 2.2, and percent RMS errors are compared in Figure 2.2. In all simulations, the "Correlated Error" retrievals had much less error than the "Independent Error" retrievals. This was not surprising since "Correlated Error" perturbations result in shifts of the IOP spectra upward or downward without changing their spectral shapes. The resulting radiance spectra also tend to vary with minimal changes in spectral shape, and thus band ratios, for example, remain stable. In the "Independent Error" case, however, spectral shapes were altered significantly, and this resulted in much larger errors in the chlorophyll retrievals.

"Correlated Error" perturbations applied only to $b_{bp}(\lambda)$ produced no errors in chlorophyll retrievals. In examining the corresponding retrievals of $a_{gd}(375)$ and b_0 (not shown here), we found that only the b_0 retrievals had errors, and in fact its errors were precisely equal to the perturbation $\delta_{bp}(\lambda)$. The effect of a nonspectrally varying (i.e., correlated error) perturbation in $b_{bp}(\lambda)$ is equivalent to a perturbation in b_0. In Step One we found that perturbations in $a_{gd}(375)$ and b_0 did not affect our ability to retrieve Chl, in the absence of other IOP perturbations. This result is quite significant, because in the case of "Independent Errors" the $b_{bp}(\lambda)$ uncertainty was the largest source of error among the three IOP submodels when they were perturbed separately (Figure 2.2, Table2.2). *This suggests that the accuracy in chlorophyll retrievals can be improved significantly if the spectral shape of the particle backscattering coefficient is known, whereas the absolute level of $b_{bp}(\lambda)$ (whether shifted upward or downward) does not affect chlorophyll retrievals.*

The effect of uncertainty in $a_{gd}(\lambda)$ and $a_{\phi}(\lambda)$ depended on the chlorophyll level, with a general tendency that $a_{\phi}(\lambda)$ became more critical as Chl increased. Comparing low-chlorophyll (Table 2.2a) and medium-chlorophyll results (Table 2.2b), we see that errors tended to be proportional to the chlorophyll level. For example, in the "Independent Error" case, the combined **M** ranged from 10% to 12%, and the **RMSE** was between 63% and 70% of the chlorophyll level. The tendency for errors to be proportional to Chl is also indicated by the consistency in $\mathbf{M_{log}}$ and $\mathbf{RMSE_{log}}$ between Tables 2.2a and 2.2b, since the log-difference Δ_{log} reflects a "relative" error.

In the high-chlorophyll "Independent Error" case (Table 2.2c), the combined **RMSE** represented only a 48% error, but the $\mathbf{RMSE_{log}}$ increased from 0.30 to 0.42 between medium and high chlorophyll cases. Further examination of the retrievals revealed a number of anomalously low chlorophll retrievals (< 1 mg m^{-3}) when the true chlorophyll was high (10 mg m^{-3}).

IOP model errors from *in situ* measurements

As mentioned earlier, neither of the two extreme cases we have simulated is realistic. However, we believe that highly correlated errors in individual IOP spectral models are closer to reality than independent errors. To test our speculation, we computed error correlation matrices for the two IOP submodels (i.e., $a_{\phi}(\lambda)$ and $b_{bp}(\lambda)$). In the case of the phytoplankton absorption model, we were able to use the *in situ* data which Bricaud *et al.* (1995) used to parameterize their model. We do not have *in situ* backscattering coefficient measurements to test backscattering IOP parameterization. Instead, we assumed that the model (equations 2.3-2.5) is precise, and thus we were able

to calculate $b_{bp}(\lambda)$ from measured reflectance and total absorption spectra. From these, we estimated the spectral correlation matrix of $b_{bp}(\lambda)$ errors.

- *Phytoplankton absorption model*

Using the original measurements of Bricaud *et al.*(1995), $a_\phi^{meas}(\lambda)$, we found that spectral errors, defined $\delta_\phi(\lambda)=\log(a_\phi^{meas}(\lambda)) - \log(A_c(\lambda)Chl^{B_c(\lambda)})$ is highly correlated. The spectral correlation matrix of the $\delta_\phi(\lambda)$ errors is shown in Table 2.3a. Correlation coefficients are >0.8 for the first four SeaWiFS bands, but relatively low (around 0.5) for the last band.

- *Particle backscattering model*

Using the $b_{bp}(\lambda)$ spectra calculated from measured reflectance and total absorption spectra, we modeled particle backscattering as $b_{bp}(\lambda) = A(\lambda)Chl^{B(\lambda)}$, where Chl is chlorophyll concentration, and $A(\lambda)$ and $B(\lambda)$ are spectral parameters. Based on about 100 *in situ* measurements of reflectance and absorption spectra as well as chlorophyll concentrations from Tokyo Bay (Kishino *et al.* 1985) and the Gulf of Maine regions, the spectral errors $\delta_{bp}(\lambda)= \log(b_{bp}^{meas}(\lambda)) - \log(A(\lambda)Chl^{B(\lambda)})$ were estimated. The spectral correlation matrix of the $\delta_{bp}(\lambda)$ errors is shown in Table 2.3b. Correlation coefficients ranged between 0.79 and 0.99 among all the first five SeaWiFS bands.

2.4 Summary

A general approach is presented for assessing retrieval errors of in-water concentrations. The simulations focus on demonstrating how retrieval errors in chlorophyll concentration are affected by uncertainties of inherent optical property (IOP)

submodels in an underlying radiance model. Two complete sets of simulations conducted represent two extreme cases between which "real" cases are expected to occur. The results from "Correlated Errors" and "Independent Errors" are significantly different. The most significant finding in this work is the improvement in retrieval accuracy that resulted from "Correlated Errors" compared with "Independent Errors." The analyses of spectral correlations among IOP submodel errors from *in situ* measurements suggest that the "Correlated Errors" case is more realistic. Although the inherent variability in IOPs cannot be controlled, we believe it is important to model their spectral shape as accurately as possible. Knowledge of the spectral shape is critical, particularly in the case of the particle backscattering coefficient. Shifts in the IOP spectra upward or downward had little effect on chlorophyll retrieval accuracy, whereas random independent perturbations to the spectral IOP values resulted in very large errors (RMSE values as high as 70%).

Acknowledgements for Chapter 2

This work was supported by a MODIS Instrument Team Investigation (NASA Contract NAS5-96063).

References

Bukata, R.P., Jerome, J.H., Kindratyev, K.Y. and Pozdnyakov, D.V., 1995. Optical properties and remote sensing of inland and coastal water, CRC Press, 362pp.

Bricaud, A., Babin, M., Morel, A. and Claustre, H., 1995. Variability in the chlorophyll-specific coefficients of natural phytoplankton: analysis and parameterization, J.Geophys. Res.,100, C7, 13,321-13,332.

Campbell, J.W., Moore, S.T. and Feng, H., 1997. Phytoplankton backscattering properties derived from satellite ocean color data, Abstract, ASLO97, Santa Fe, NM.

Carder, K.L., Hawes, S.K., Baker, K.A., Smith, R.C., Steward, R.G. and Mitchell, B.G., 1991. Reflectance model for quantifying chlorophyll a in the presence of productivity degradation products, J.Geophys. Res., 96, 20,599-20,611.

Feng, H., Campbell, J.W. and Moore, T. S., 1998. Parameterization of water color model from *in situ* measurements from Tokyo Bay, EOS Trans. AGU, 79(3).

Garver, S.A. and Siegel, D.A., 1997. Inherent optical property inversion of ocean color spectra and its biogeochemical interpretation 1, Time series from the Sargasso Sea,. J.Geophys. Res., 102, C8, 18,607-18,625.

Gordon, H.R., Brown, O.B. and Jacobs, M.M., 1975. Computed relationship between the inherent and apparent optical properties of a flat homogeneous ocean, Appl.Opt., 14,417-427.

Gordon, H.R., Brown,O.B., Evans, R.H., Brown,J.W., Smith, R.C., Baker, K.S. and Clark, D.K., 1988. A semianalytical radiance model of ocean color, J. Geophys. Res., 93, 10,909-10,924.

Gregg, W.W. and Carder, K.L., 1990. A simple spectral solar irradiance model for cloudless maritime atmospheres, Limnol. Oceanogr., 35, 1657-1675.

Hoge, F. E. and Lyon, P.E., 1996. Satellite retrieval of inherent optical properties by linear matrix inversion of oceanic radiance model: an analysis of model and radiance measurement error, J. Geoohys. Res., 100(C7), 16631-16648.

Kishino, K.M., Okami, N. and Ichimura, S., 1985. Estimation of the spectral absorption coefficients of phytoplankton in the sea, Bull. Mar.Sci., 37, 634-642.

Press, W.H. and Tuekolsy,S.A., Vettering, W.T. and Flannery, B.P., 1992. Numerical Recipes in C: The Art of Scientific Computing. Cambridge Press, 2nd edition, 994pp.

Zaneveld, R., 1995. A theoretical derivation of the dependence of the remotely sensed reflectance of the ocean on the inherent optical properties, J.Geophys. Res., 100, C7, 13,135-13,142.

Table 2.1. Model parameters assumed to be constant in inverting the radiance model. Parameters are listed in column 1, units in column 2, and values for each spectral band in columns 3-7.

Parameter	Units	412nm	443nm	490nm	510nm	555nm
$rQ(\lambda)$	None	1.92	1.92	1.92	1.92	1.92
$M(\lambda)$	None	0.5375	0.5373	0.5398	0.5390	0.5390
$F_o(\lambda)$	$Mw/cm^2/\mu m$	171.7	189.2	194.4	187.5	185.9
$A_c(\lambda)$	m^{-1}	0.0313	0.0393	0.0274	0.0180	0.0071
$B_c(\lambda)$	None	0.7270	0.6600	0.6390	0.7400	0.9660
$A_b(\lambda)$	m^{-1}	0.0111	0.0100	0.0104	0.0108	0.0109
$B_b(\lambda)$	None	0.2390	0.2250	0.2850	0.3190	0.3620
S	nm^{-1}	0.0145	0.0145	0.0145	0.0145	0.0145

Table 2.2. Error statistics: **M, RMSE, M_{log}, and $RMSE_{log}$** after perturbing each IOP submodel separately, and after perturbing all three IOP submodels simultaneously ("Combined") for spectrally-Independent Error case (flat font) and spectrally-Correlated Error case (bold font). The units of **M** and **RMSE** are mg Chl m^{-3} and the units of $\mathbf{M_{log}}$ and $\mathbf{RMSE_{log}}$ are decades of log base 10. These statistics are based on 20,000 simulations.

Table 2.2a. Case of low chlorophyll (Chl = 0.1 mg m^{-3}).

Submodel	M	RMSE	M_{log}	$RMSE_{log}$
$a_{gd}(\lambda)$	0.0029/**0.0029**	0.0276/**0.0276**	-0.0022/ **-0.0022**	0.1137/**0.1137**
$a_{\phi}(\lambda)$	0.0014/**0.0009**	0.0206/**0.0119**	-0.0027/ **0.0011**	0.0887/**0.0505**
$b_{bp}(\lambda)$	0.0059/**0.0000**	0.0500/**0.0000**	-0.0273/ **0.0000**	0.2317/**0.0000**
Combined	0.0102/**0.0039**	0.0629/**0.0301**	-0.0330/**-0.0011**	0.2817/**0.1250**

Table 2.2b. Case of medium chlorophyll (Chl = 1.0 mg m^{-3}).

Submodel	M	RMSE	M_{log}	$RMSE_{log}$
$a_{gd}(\lambda)$	0.0239/**0.0239**	0.2581/**0.2581**	-0.0032/**-0.0032**	0.1094/**0.1094**
$a_{\phi}(\lambda)$	0.0128/**0.0118**	0.2081/**0.1387**	-0.0038/ **0.0011**	0.0906/ **0.0589**
$b_{bp}(\lambda)$	0.0828/**0.0000**	0.5768/**0.0000**	-0.0273/**0.0000**	0.2543/ **0.0000**
Combined	0.1207/**0.0356**	0.6991/**0.2938**	-0.0352/-**0.0022**	0.3022/ **0.1254**

Table 2.2c. Case of high chlorophyll (Chl = 10 mg m^{-3}).

Submodel	M	RMSE	M_{log}	$RMSE_{log}$
$a_{gd}(\lambda)$	-0.1680/**-0.1680**	0.7008/**0.7008**	-0.0087/**-0.0087**	0.0378/**0.0378**
$a_{\phi}(\lambda)$	-0.4090/**-0.1744**	2.5222/**0.8445**	-0.0384/**-0.0094**	0.1552/**0.0414**
$b_{bp}(\lambda)$	-1.0078/ **0.0108**	4.0424/**0.0158**	-0.1208/**0.0005**	0.3474/**0.0007**
Combined	-1.0772/**-0.2949**	4.7737/**1.2029**	-0.1549/**-0.0174**	0.4244/**0.0697**

Table 2.3a. Correlation matrix of error, $\delta_\phi(\lambda)=\log(a_\phi^{meas}(\lambda)) - \log(A_c(\lambda)Chl^{B_c(\lambda)})$. (based on the data from Bricaud *et al.* 1995). The matrix is symmetric so the left lower is ignored.

	412nm	443nm	490nm	510nm	550nm
412nm	1.00	0.90	0.81	0.86	0.51
443nm		1.00	0.93	0.89	0.46
490nm			1.00	0.91	0.57
510nm				1.00	0.75
550nm					1.00

Table 2.3b. Correlation matrix of error, $\delta_{bp}(\lambda)=\log(b_{bp}^{meas}(\lambda)) - \log(A(\lambda)Chl^{B(\lambda)})$ (based on 101 observations). The matrix is symmetric so the left lower is ignored.

	412nm	443nm	490nm	510nm	550nm
412nm	1.00	0.93	0.87	0.84	0.79
443nm		1.00	0.97	0.96	0.92
490nm			1.00	0.99	0.96
510nm				1.00	0.98
550nm					1.00

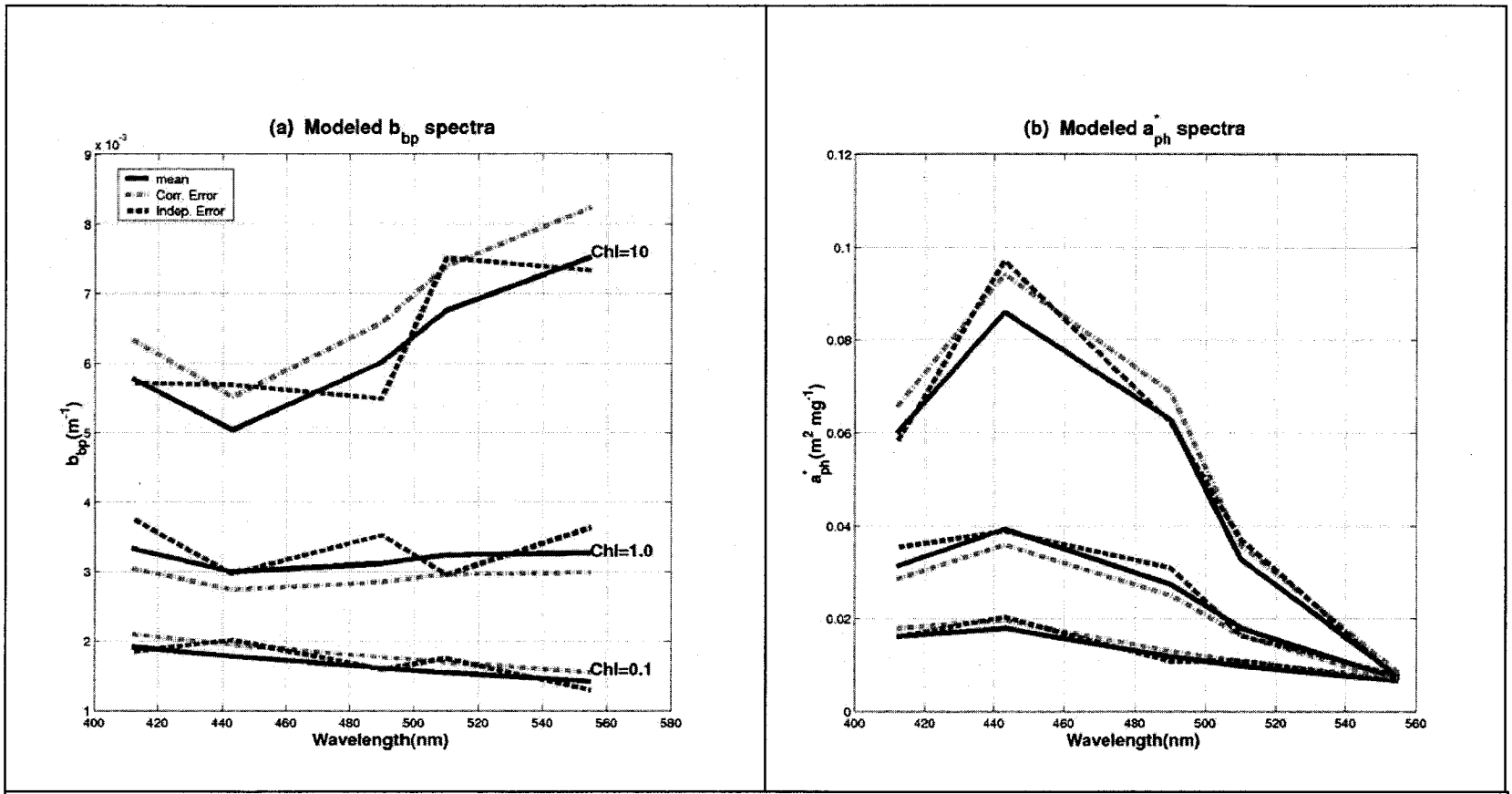

Figure 2.1. Plots of IOP spectra demonstrating the distinction between two assumptions: the Independent Error (IE) case assumes that random errors among 5 spectral values are statistically independent, whereas the Correlated Errors (CE) case assumes that the random errors among 5 spectral values are equal. (a) is for $b_{bp}(\lambda)$ model, and (b) is for $a_{\phi}(\lambda)$.

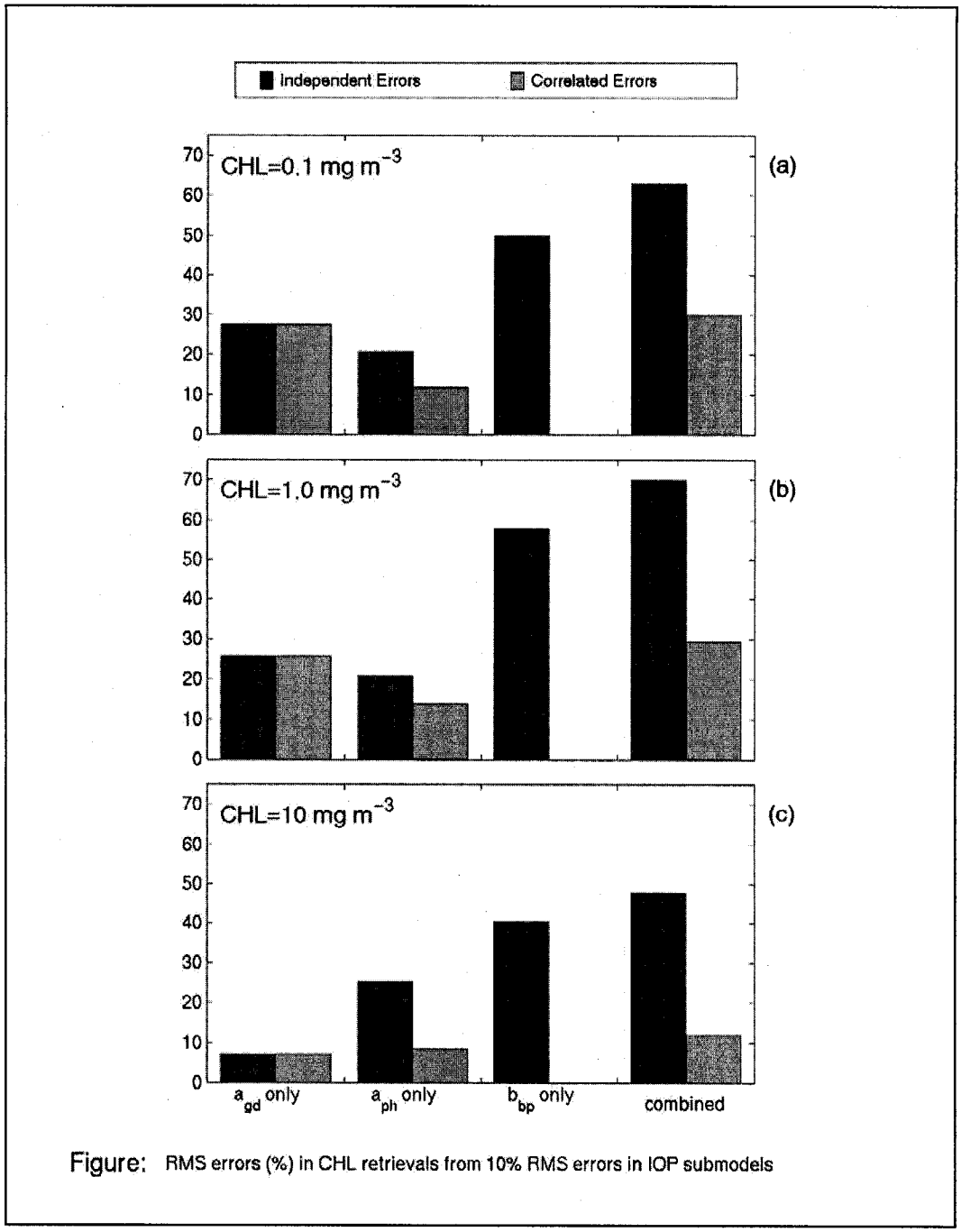

Figure: RMS errors (%) in CHL retrievals from 10% RMS errors in IOP submodels

Figure 2.2. RMS errors (%) in chlorophyll retrievals resulting from 10% RMS errors in IOP submodels.

Chapter 3 A comparison of inversion techniques for semi-analytical ocean color models (to be submitted to *Applied Optics* by Hui Feng, Mark D. Dowel, Janet W. Campbell, and Timothy S. Moore)

Abstract

Three fundamentally different inversion techniques, nonlinear optimization (NLO), principal component analysis (PCA) and artificial neural network (ANN), are compared to test their skills to retrieve optically-active constituents given spectral radiance data simulated by a commonly used, semi-analytical ocean color model. A simulation scheme was implemented to simulate spectral radiances from ocean waters of different bio-optical complexities. The three inversion methods were applied to these simulated datasets, with and without noise, and their performance evaluated.

The NLO inversion method has the advantage that it is directly related to a forward ocean color model, but its inverse solution is highly sensitive to noise, faces non-convergence issues, and its computational load is substantially high. The PCA inversion algorithm assumes a linear relationship between optically-active constituents (logarithm-transformed) and ocean color spectral signals. Within limited ranges and with low values of optically-active constituents, our simulations show that such a linear assumption is an excellent approximation to the nonlinear problem, giving it comparable inversion performance with the other two methods. The ANN inversion method exhibits its powerfulness in solving a complex nonlinear ocean color inverse problem. ANN overcomes most of the weaknesses and disadvantages of the other two methods. The

ANN method trained with realistic input data retrieves the constituents from noise-free data with nearly the same accuracy as the NLO method, and yet is less sensitive to noise.

3.1 Introduction

Quantitative detection of ocean surface bio-optical properties from ocean color observations is critical for various marine environmental studies. Thus, for years, attention has been paid to interpreting an ocean color spectrum to retrieve optically-active constituents in the upper water column. Inversion techniques have evolved from empirical (data-based) towards semi-analytical (model-based) bio-optical algorithms. The inverse problem to be solved can be stated in general as follows: Given an observed ocean color spectrum $L(\lambda)$ and bio-optical model f

$$L(\lambda)=f(\boldsymbol{C},\Theta(\lambda)) \tag{3.1}$$

estimate a set of optically-active constituent concentrations that lead to the observed spectrum. In Eq. (3.1), f denotes a semi-analytical forward bio-optical model relating $L(\lambda)$ to the optically active constituent vector $\boldsymbol{C}$ to be retrieved through a model parameter vector $\Theta(\lambda)$. The inversion of Eq. (3.1) may be generalized by

$$\boldsymbol{C} = f^{-1}(L(\lambda),\Theta(\lambda)) \tag{3.2}$$

Due to the non-linearity of the forward model f, it is generally not possible to find an analytical inverse solution, and thus, in this paper, f^{-1} indicates an inversion method. Parameters in $\Theta(\lambda)$ are related to constituent-specific inherent optical properties (IOPs, absorption and backscattering properties). The determination of $\Theta(\lambda)$ (model parameterization) requires *in situ* measurements of constituent-specific IOPs along with the relevant constituent concentrations and the radiance spectrum $L(\lambda)$. It is generally

well recognized that no bio-optical model will be capable of being applied universally to all optical water types, because constituent-specific IOPs are often distinct from one water type to another. Specifically, the model parameter vector $\Theta(\lambda)$ is not applicable universally. The best-known example is the difference between so-called Case 1 and Case 2 water types (Morel et al. 1977).

In general, there exist four sources of error in retrieving the concentrations in the vector $\boldsymbol{C}$. The first is the forward model f itself because almost all forward models are approximations to more complex radiative transfer equations. The second is the inherent variability in constituent-specific IOPs. Parameterized IOP submodels described by the vector $\Theta(\lambda)$ only approximate realistic constituent-specific IOPs. Feng et al. (1998) presented a general approach to characterize the effect of such uncertainty on the retrieval of chlorophyll concentration. The third is the inversion methods themselves, and fourth are errors in the measurement of $L(\lambda)$ induced by errors in the sensor calibration, atmospheric correction, and other environmental effects. In this paper, we assess the inversion errors induced by the last two sources mentioned.

To date, three major inversion techniques have been applied to retrieve optically-active constituents from ocean color data. They are non-linear optimization (NLO), principal component analysis (PCA), and artificial neural network (ANN) methods. The approach of NLO inversion algorithms, such as the Gauss-Newton and Levenberg-Marquart, is to iteratively adjust the optically-active constituent vector $\boldsymbol{C}$ being retrieved to a convergent value at which a forward-modeled ocean color spectrum matches a measured spectrum with an overall minimum error for a given criterion. The application of NLO techniques to ocean color inverse problem began in the middle 1970s. Jain and

Miller (1976) first applied a NLO algorithm to airborne ocean color data to estimate two bio-optical in-water variables, chlorophyll concentration and the scattering coefficient at a reference wavelength under a simple two-flow radiative transfer model. During the 1980s and 1990s, Bukada and his coworkers (1985, 1991, 1995) did some pioneering studies in applying the NLO technique to quantitatively interpret *in situ* spectral measurements for retrieving optically-active constituents in Lake Ontario. Since the 1990s, NLO inversion methods have become more widely applied to both surface-based *in situ* (Roesler and Perry, 1995; Garver and Siegel, 1997) and satellite-based (Doerffer and Fischer, 1994; Frette et al. 1998; Moore et al. 2001) ocean color data to retrieve constituent concentrations.

PCA is a statistical method for signature extraction. For multi-spectral or hyper-spectral ocean color data, PCA is capable of extracting a small number of principal components (PCs) that account for most of the variance in the original ocean color data. A few variance-dominant PCs are retained, rather than the original ocean color spectra, so as to keep all significant information and filter out noise. In the 1970s, attempts were made to apply PCA directly to *in situ* ocean color data to extract a few dominant PCs, and then those extracted PCs were interpreted (Mueller 1976; Grew, 1977; Gower et al, 1984). These early efforts focused upon finding empirical inversion models of f^{-1} between PCs' loadings and measured optically-active constituent concentrations. Later on, scientists (Fischer et al. 1986; Satheyendranath et al. 1989) realized that *in situ* measured data were usually too limited to cover a wide range of constituent concentrations and applications were also limited. Thus, they turned to forward model-simulated bio-optical datasets over a wider range of constituents of interest to find such empirical inverse

models. More recently, Krawczyk et al. (1995, 1999) developed a well-formulated PCA inversion algorithm to establish an approximated inverse relationship directly relating the ocean color spectrum $L(\lambda)$ to constituent concentrations $\boldsymbol{C}$. This PCA inversion algorithm has been applied to MOS (the Modular Optoelectronic Scanner) ocean color data to retrieve in-water constituents (Hetscher et al. 2004).

The artificial neural network (ANN) technique is a powerful tool for estimating an inverse transfer function, f^{-1}, particularly for the case where the forward function f is highly nonlinear. The application of ANN techniques to constituent retrievals from ocean color data began quite recently. Keiner and Brown (1999) successfully developed a simply-constructed ANN to retrieve chlorophyll concentrations using the SeaWiFS Bio-optical Algorithm MiniWorkshop (SeaBAM) spectral reflectance data for training. They have shown that the ANN inversion for chlorophyll retrieval is more accurate than traditional spectral ratio algorithms. In recent years, the ANN inversion technique has been applied to model-simulated ocean color data to train ANNs for retrieving constituent concentrations (Schiller and Doerffer, 1999; Doerffer and Schiller, 1999; Gross et al. 2000; Zhang et al. 2003) for both Case 1 and Case 2 waters.

It has recently been proposed (IOCCG Report 3, 2000) that there be an objective comparison of different inversion techniques to identify the strengths and weaknesses of the individual techniques. In this paper, the three inversion techniques listed above have been applied to several model-simulated ocean color data sets generated by a set of parameterized forward models representing different optical water types with distinct bio-optical properties. The model simulation focuses on the first 5 SeaWiFS wavelengths (412, 443, 490, 510, and 550nm). The goal is to explore the fundamental distinctions

among the three inversion techniques, to assess their sensitivity to noise contained in ocean color data, and to determine how the optical complexity of the water affects the algorithm performance.

We first describe a semi-analytical bio-optical model and its parameterization briefly. Next, the simulation strategy is described showing how the forward model is run to generate simulated datasets, and then follows the comparison results of inversion performance. Finally, discussion and conclusion are presented. In Appendix A, the fundamental framework for each inversion method is given in more detail.

3.2 Methods

Forward bio-optical model

Normalized water-leaving radiance (Gordon et al. 1988) is related to remote sensing reflectance $R_{rs}(\lambda)$ just beneath the water surface by the relationship

$$L_{wn}(\lambda) = \frac{MF_0 R_{rs}(\lambda)}{1 - rQR_{rs}(\lambda)} \tag{3.3}$$

where M is a factor accounting for losses at the air-sea interface; F_0 is the downwelling solar irradiance; r is the diffuse reflectance of the water-air interface (from beneath), and Q is the ratio of upwelling irradiance to upwelling radiance. These parameters are considered spectral constants and listed in Table 3.1

Following Gordon et al. (1988), the remote-sensing reflectance $R_{rs}(\lambda)$ is related to the IOPs by

$$R_{rs}(\lambda) = 0.0949\, X(\lambda) + 0.0794\, X(\lambda)^2 \tag{3.4}$$

where

$$X(\lambda) = \frac{b_b(\lambda)}{b_b(\lambda) + a(\lambda)} \tag{3.5}$$

The total absorption $a(\lambda)$ and backscattering $b_b(\lambda)$ coefficients are decomposed as a three-component IOP system by $a(\lambda) = a_w(\lambda) + a_\phi(\lambda) + a_{gd}(\lambda)$ and $b_b(\lambda) = b_{bw}(\lambda) + b_{bp}(\lambda)$, respectively, where subscripts w, ϕ, g, d, and p refer to pure water, phytoplankton, gelbstoff (i.e. CDOM), detritus, and particles, respectively. The absorption for CDOM and detritus are combined as one single component due to their spectral similarity. The three IOP components are further modeled as follows

$$a_\phi(\lambda) = A_c(\lambda)\mathrm{Chl}^{Bc(\lambda)} \tag{3.6}$$

$$a_{gd}(\lambda) = a_{gd}(440)\exp(-S(\lambda-440)) \tag{3.7}$$

$$b_{bp}(\lambda) = b_{bp}(555)\,(555/\lambda)^{Y} \tag{3.8}$$

Eqs.(3.6-3.8) are based on the IOP submodels proposed by Bricaud et al (1995), Carder et al. (1991), and Lee et al. (1994), respectively. In this forward model setup, the model parameter vector is $\Theta(\lambda) = [A_c(\lambda), B_c(\lambda), S, Y]$ that fully defines the IOP submodels. The constituent concentration vector $\boldsymbol{C}$ to be inverted is [Chl, $a_{gd}(440)$, $b_{bp}(555)$], where the optical properties, $a_{gd}(440)$ and $b_{bp}(555)$, act as surrogates for concentrations.

Model parameterization

A bio-optical database of *in situ* measurements from 1367 stations was compiled for the model parameterization. The measurements were made globally and collected from different sources (Moore et al. 2001). The database includes remote sensing reflectance spectra $R_{rs}(\lambda)$, total, CDOM and phytoplankton absorption coefficient spectra, and chlorophyll concentration [Chl].

In order to generate model-simulated datasets that represent distinct optical water types, a cluster classification algorithm (Moore et al., 2001) was first applied to the 1367 measured $R_{rs}(\lambda)$ spectra, consequently leading to six optically-distinct water types. For each optical water type, IOP submodels formulated according to Eqs.(3.6-3.8) were parameterized using corresponding *in situ* measured data, each with its own model parameter vector $\Theta(\lambda)$ (Dowell et al. 2000). For simplification, we are presenting the results from four of the six optical waters in this paper (Figure 3.1). They may be described as oligotrophic (type1), eutrophic (type 2), absorption-dominated (type 3) and scattering-dominated (type 4). In effect, the cluster classification resulted in a sorting of in-water constituent concentrations. The derived model parameters of these four optical water types are given in Table 3.1, and statistics calculated from the *in situ* measurements, ranges, means, standard deviations, correlation matrixes of the three constituents ([Chl, $b_{bp}(555)$, $a_{gd}(440)$]) in a 10-base logarithmic scale and a linear scale are given in Table 3.2a and Table 3.2b, respectively.

Inversion techniques by semi-analytical ocean color model

A description for the three inversion algorithms is detailed in the Appendix. A fundamental distinction of the NLO technique from the PCA and ANN techniques is that NLO is not dependent directly on model-simulated dataset to find a statistical inversion function f^{-1}. NLO algorithms complete their inversions on each ocean color spectrum by an iterative procedure such that the forward modeled spectrum matches the observed spectrum given a minimization criterion to retrieve optically-active concentrations. In this sense, the NLO inversion algorithm can be considered more analytical (physically-based)

than the two other inversion techniques. By contrast, PCA and ANN techniques find statistical inversion functions f^1 based on a model-simulated training dataset and then complete their inversions using the estimated inversion function f^1. The procedure for finding the inversion function f^1 is called "training" or "learning." In this sense, PCA and ANN are more empirical (data-based).

In this work, three steps were taken for completing the PCA and ANN inversions: Step 1: generate two independent simulated datasets, called *training* and *testing* datasets, by running the forward model $f(\Theta(\lambda), \boldsymbol{C})$. Step 2: complete a PCA/ANN training to determine weights and offsets defined in Eq. (A2) for PCA and weights and biases defined in Eq. (A3) for ANN. Step 3: complete the inversions using a *testing* dataset and evaluate performance. For the NLO inversions, only Steps 1 and 3 are taken with the *testing* dataset. The same *testing* datasets were used for all three methods, and the same *training* sets were used for the PCA and ANN methods.

Simulations

The inversion functions f^1 to be found for the PCA and ANN methods are dependent upon simulated *training* datasets whose statistical properties might have some influence on the functions of f^1. It is common practice to assume uniform or normally distributed variables and independent constituent concentrations in the vector $\boldsymbol{C}$ used for running forward model simulations. In this study, a concerted effort was made to simulate constituent input datasets that are as realistic as possible in terms of their individual distributions, and the covariance among constituents.

Campbell (1995) has shown that many bio-optical variables in the marine environment can be described as log-normally distributed. We assumed that the constituent vector $\boldsymbol{C}$ follows a three-dimensional lognormal distribution with a mean vector and covariance matrix calculated from *in situ* measurements for each optical water type (Tables 3.2a-b). Specifically, an ensemble of N vectors of log-transformed constituents $\boldsymbol{c}$ = {log(Chl), log(b_{bp}(555)), log(a_{gd}(440))} was simulated by the following calculation (Dowell et al. 2000):

$$\boldsymbol{c}_i = \boldsymbol{m}_c + \gamma_{1i}\boldsymbol{U}_1 + \gamma_{2i}\boldsymbol{U}_2 + \gamma_{3i}\boldsymbol{U}_3 \qquad i = 1,\ldots,N \tag{3.9}$$

where $\boldsymbol{m}_c$ is the mean vector, and $\{\boldsymbol{U}_1, \boldsymbol{U}_2, \boldsymbol{U}_3\}$ are the three eigenvectors of the covariance matrix calculated from *in situ* log-transformed constituent data for each optical type; $\{\gamma_{1i}, \gamma_{2i}, \gamma_{3i}\}$ are three independent normally distributed random variables with zero mean and standard deviation equal to 1 realized by a computerized pseudo-random number generator.

The correlations among the constituents have been included in these simulations to avoid combinations that are highly unlikely to occur in a realistic marine environment. In preliminary work, not reported here, we did run simulations with uncorrelated input variables, but the performance results were much worse for all three methods compared with the results shown here. We believe that it is necessary for semi-analytical inverse modeling practices to include realistic covariance structures among optically-active constituents so that true assessments of performance can be made.

For each optical water type described above, a set of simulated vectors $\boldsymbol{C}$ = [Chl, a_{gd}(440), b_{bp}(555)] with the ensemble size of N=10,000 was first generated and then used to obtain simulated ocean color signals, i.e. $L_{wn}(\lambda)$, by running the forward model

through Eqs. (3.3-3.7). To consider the effect of noise on inversions, noise-contained $L'_{wn}(\lambda)$ signals were generated by adding 5% spectrally-independent random errors to noise-free signals $L_{wn}(\lambda)$ to simulate noisy ocean color signals. In addition, we generated a second independent dataset of 10,000 samples which was used for training the PCA and ANN methods. Both the noise-free and noise-contained simulated ocean color spectra were then inverted by the three inversion techniques under consideration to obtain retrieved vectors $\hat{\boldsymbol{C}}$ that were then compared with the "true" $\boldsymbol{C}$ vectors for inversion performance assessments.

Statistical measures of inversion performance

To compare the inversion performance of the three methods, three error measures were adopted. They are the root mean square error (RMSE) defined by

$$\text{RMSE} = \sqrt{\frac{1}{N}\sum_j \{\log_{10}[\hat{C}_j] - \log_{10}[C_j]\}^2}\ , \tag{3.10}$$

the mean error (bias) defined by

$$\text{Bias} = \sqrt{\frac{1}{N}\sum_j \{\log_{10}[\hat{C}_j] - \log_{10}[C_j]\}}\ , \tag{3.11}$$

and one minus the squared correlation coefficient $(1 - r^2)$ where $\hat{C}_j$ and C_j refer to the j^{th} retrieved and "true" constituent, respectively.

3.3 Results

3.3.1 Simulated and real constituent distributions

The means of the three constituent-related terms generally increase from type 1 to type 4 (Figure 3.2, Tables 3.2a-b). The exception is that the mean of $a_{gd}(440)$ for type 3, the absorption-dominated Case 2 water type, is slightly higher than that of type 4. The variances of the three constituent terms for types 2 and 3 are much higher than the others. The *in situ* measurements clearly show that there exist co-variation among the three components, but the degree of correlation is type-specific. It has been well accepted that the correlation among the three optically active constituents can be regarded as a significant indicator of the bio-optical complexity of the waters. As expected, the correlation levels among the constituents are generally higher in water types 1 and 2 (Case 1 waters) than those for types 3 and 4. There is almost no correlation between chlorophyll concentration and $b_{bp}(555)$ for type 4, strongly suggesting there is a significantly independent non-algal particulate component contributing to the particle backscattering. Likewise, chlorophyll and $a_{gd}(440)$ for type 4 are nearly uncorrelated, indicating the origins of absorbing agents (CDOM or detritus) are different from the phytoplankton.

The simulated log-normal constituent concentration distributions of [Chl], $[b_{bp}(555)]$, and $[a_{gd}(440)]$ are shown in Figure 3.3, where they are compared with the distributions in the *in situ* data. The correlations among the three simulated variables are demonstrated in Figure 3.4. The means, variances and covariances of the simulated constituent concentrations mimic those of the *in situ* measurements, although their ranges are slightly different (Figures 3.3 and 3.4).

3.3.2 Inversion performance comparison

The statistical results of inversion performance measures are shown graphically in Figures 3.5 and 3.6. Table 3.3 gives the details of the statistical measures of inversion performance.

Inversion performance for noise-free signals

The inversion performance with respect to noise-free ocean color signals (blue bars in Figure 3.5) measures the *inherent* ability of the three inversion methods to solve the complex nonlinear bio-optical inverse problem with which we are dealing. The NLO inversion method had arbitrarily small retrieval errors for the three constituent retrievals for all four water types. The ANN method had nearly the same result, clearly indicating that both inversion methods are capable of retrieving the constituent concentrations from noise-free ocean color signals and are inherently "perfect" for modeling the inverse problem of the semi-analytical bio-optical model. In contrast, the concentration retrievals by the PCA method had large errors, and thus are inherently unable to solve the inverse problem even for noise-free ocean color signals. Thus for the PCA inversion algorithm, the underlying assumption of a linear relationship between the ocean color signals and the log-transformed concentrations is inherently incorrect.

Inversion performance for signals containing noise

The inversion performance diminished significantly for the NLO and ANN methods when a 5% noise was added to the signal (red bars in Figure 3.5). In the presence of noise, these two methods were not much better (and sometimes worse) than

the PCA method. The ANN inversion performed better than the other two methods in nearly every situation.

The effect of water type on inversion performance

In general, the inversion performance for all three methods is best for type 1, and degrades towards type 4 which had the worst inversion performance. This is more apparent in the $1-r^2$ criterion than in RMSE measures (Figure 4.6). The inversion performance for the PCA method apparently depends more upon the range of the optically-active constituent concentrations to be retrieved than upon the actual level. For instance, PCA inversions perform very well for type 1 in which the ranges of the three concentrations are small and least energetic. For this water type, its performance is comparable with those of the other two methods, and actually gives a better retrieval accuracy than NLO. For types 2 and 3, the PCA inversion performance was significantly worse than the others. Presumably this is because type 2 and type 3 exhibit much wider concentration ranges, indicating the inability of the linear PCA inversion to deal with such a large range of concentrations.

For type 4, all three inversion methods apparently found difficulty in solving the inverse problem to retrieve the constituent concentrations with a good performance. This point is most noticeable from the $1-r^2$ values seen in Figure 3.6. The values of r^2 are significantly lower in type 4 waters compared with those of the other three types.

Information content (signal) vs. noise

Even for the best skilled inversion method, performance will depend largely on the presence and level of the signals of optically-active constituents contained in ocean color data. For realistic (noisy) ocean color data, noise apparently masks the signals and

thus affects inversion performances. In fact, the effect of noise contamination differs in the three constituent retrievals. Among the three optically-active constituents to be retrieved, [Chl, $b_{bp}(555)$, $a_{gd}(440)$], our simulations consistently show that the best performance is for the retrieved $b_{bp}(555)$, and the worst is for the retrieved [Chl]. The simulated signals representing chlorophyll concentration are relatively weak and thus are most significantly affected by noise, while signals from $b_{bp}(555)$ are strong and least affected.

3.4 Discussion and Conclusion

In the present study, we evaluated the ability of three fundamentally-distinct inverse methods (NLO, PCA, and ANN) to retrieve optically active constituents from simulated ocean color data. A complex non-linear bio-optical system was simulated by semi-analytical ocean color models with three-component IOPs related to three optically-active constituents. A simulation scheme was implemented to simulate waters of different bio-optical complexities and to see how differently the inversion methods perform with respect to optical water type. Independent datasets were generated to train the PCA and ANN algorithms. We then applied the three inverse methods to simulated *testing* datasets to objectively compare their inversion performance. Among the three inversion methods, this study shows that they have distinct weaknesses and strengths.

The advantage of the NLO inversion method is that it directly seeks a match between an observed ocean color spectrum and a forward-modeled spectrum (based on underlying physical principles). Once a solution is found successfully, we can say that the forward model being used is able to interpret the measured ocean color. Our simulations show that the NLO method itself is "perfect" in interpreting noise-free data. In addition,

its implementation is relatively easy. Ongoing improvements or modifications of the forward model can be implemented and easily tested since no training is necessary. Therefore, the NLO method is a good tool for validating a forward model from an inverse point of view. However, finding the "true" solution is not easy in practice because there are various errors contained in the ocean color data (noisy data). Our simulation shows that NLO inversions are very sensitive to noise, particularly for highly complex water types where the bio-optical property signal is low relative to the noise. The minimized cost function in Eq.(A1) represents just a minimum error spectrum between a forward modeled $f((\lambda), \boldsymbol{C})$ and measured $L(\lambda)$ spectra. If noise contained in $L(\lambda)$ significantly contaminates the signals representing $\boldsymbol{C}$ to be retrieved, then (1) a non-convergent failure may occur, or (2) a solution may converge to a local minimum "noise-contaminated" solution that is quite different from the true solution. Therefore, the NLO method faces a serious issue that its inverse solution is not stable. Table 3.4 gives the number of non-convergent cases and the CPU time for inverting 10,000 simulated spectra for all the types. With the increasing complexity of the bio-optical environment, NLO required more time for completing its inversion (busy in searching) and leads to more non-convergent failures. A better selection of initial values might improve this situation. In this study, we simply selected the type-specific mean of $\boldsymbol{C}$ as an initial guess. In practice, other smarter selections have been proposed, such as using empirical algorithms to create the first guess to improve its inversion performance. Another major weakness for NLO is that its computational load is substantially high (Table 3.4), and thus it becomes unrealistic as an operational algorithm. We admit that more advanced NLO-like algorithms such as the genetic algorithm (Zhan et al., 2003) may overcome some of the

weaknesses mentioned. The GA claims itself superior to conventional NLO algorithms in the sense of finding global minima, but the topic is beyond this study. At any rate, more efficient inversion algorithms, such as PCA and ANN methods, are needed in terms of improving both computation speed and solution stability.

As shown in this simulation study, the most significant weakness for the PCA inversion method is its assumption of an underlying linear relationship between optically-active constituents in $\boldsymbol{C}$ and the ocean color spectral signals. This assumption is inherently false, although a logarithmic transformation applied to the elements of $\boldsymbol{C}$ likely has accounted for some nonlinear behavior. However, for cases with a limited range of variability and lower values of the optically-active constituents, the linear assumption is an excellent approximation. This was demonstrated with the type 1 results in which PCA inversions gave a comparable performance with the other two, and was even superior to the NLO method. A notable advantage of the PCA method is that its inversions are much less sensitive to noise. The reason may lie in the PCA's ability to suppress the effect of noise by neglecting some principal components with low information content. In addition, the PCA inversion has no convergence issues as exist with the NLO method, and its computation load is very low in both training and its applications.

In this simulation study, the ANN inversion method exhibited its powerfulness in dealing with the complex nonlinear ocean color inversion problem to retrieve the three in-water constituents. Among the three inversion methods under scrutiny, it should be the first option for solving ocean color inverse problem in many respects. As shown, the ANN inversion method overcomes most of the weaknesses and disadvantages which the other two methods possess, but possesses advantages the other do not have. ANN is

inherently capable of inverting noise-free ocean color signals to retrieve concentrations as perfectly as NLO. It is less sensitive to noise than NLO. Its inversion solution is very stable and fast. Some attention must be paid to the ANN inversion method during its implementation and applications. It is important to remember that the ANN inversion algorithm is data-dependent (quite empirical) although the usage of semi-analytical forward models for simulations makes it hold more direct physical meaning in comparison to an ANN algorithm trained strictly with measured data.

Acknowledgments for Chapter 3

This research was supported partially by NASA through a MODIS Instrument Team Contract (NAS5-96063, J. Campbell, P.I.). H. Feng also acknowledges a partial support from a GEST/NASA-GSFC through D. Vandemark (P.I.).

Appendix: A brief description of the three inversion algorithms

A.1. Non-Linear Optimization (NLO)

Given a measured ocean color spectrum $L(\lambda_j)$ at a set of discrete wavelengths as well as a parameterized forward model $f(\mathbf{C},\Theta(\lambda_j))$, minimize a so-called cost function:

$$O(\boldsymbol{C}) = \sum_{j}^{M}[L(\lambda_j) - f(\boldsymbol{C},\Theta(\lambda_j)]^2 \qquad (A.1)$$

by adjusting the inversed constituent concentration vector $\mathbf{C}$ iteratively to a convergent value $\mathbf{C}_c$ so that the forward-modeled ocean color spectrum $f(\mathbf{C}_c,\Theta(\lambda))$ represents the measured color $L(\lambda)$ with an overall minimum error spectrum where j=1..M(number of spectral bands) for this case. The Gauss-Newton NLO algorithm was selected in this work (Garver and Seigel, 1997; Feng et al., 1998; Moore et al., 2001).

A.2. Principal Component Analysis (PCA)

The fundamental assumption for the PCA inversion algorithm by Krawczyk et al.(1997, 1999) is that any constituent concentration to be inverted is represented by a linear combination of the spectral signals of an ocean color measurement, that is

$$\log_{10}(\hat{C}_i) = \sum_{j=1}^{M} K_{ij} L_j + \Gamma_i \qquad (A.2)$$

where $\hat{C}_i$ is the estimate of the i^{th} (=1,2,3 for this study) constituent concentration; K_{ij} is the weight of the j^{th} (=1..M where M=5 for this study) spectral band for the i^{th} concentration; L_j is ocean color signal at the j^{th} band; Γ_i is the offset for the i^{th} concentration. Note that in this algorithm a log-transformed $\log_{10}(\boldsymbol{C})$, rather than original $\boldsymbol{C}$, was applied to concentration component to account for the "notorious" non-linear

behaviors between the optically-active constituents and the ocean color spectral signals. Eq. (A.2) is essentially a multiple linear regression model. In applying a simulated (or measured) bio-optical dataset to Eq.(A.2), the weights and offsets for each constituent can be obtained in terms of the least square principle along with PCA essence, including to compute the dimensionality of the spectral data and to suppress noise in the spectral signals by ignoring some principle components with low signal contents.

A.3. Artificial Neural Network (ANN)

The most commonly-used neural network architecture, called feed-forward multiplayer perceptron (MPL), was chosen for this study. The neural network consists of a system of fully-interconnected nodes under an architecture that is organized by layers with an input layer, an output layer and one or more hidden layers between input and output layers (Krasnopolsky, 1995 and Nabney, 2001). Each layer consists of a number of nodes. The input layer has as many nodes as the number of inputs (=M) and brings ocean color signals to be processed into a NN system. The output layer has as many nodes as the number of outputs (=number of constituents to be inverted). The number of hidden layers and the number of nodes in hidden layer(s) needs to be given in advance to construct an ANN architecture. In the layers (except the first input layer), each node is composed of two parts: a linear summation function and a nonlinear function. The linear portion of a node is a weighted combination of its inputs. If a node has N inputs L_k (k=1....N), the linear part is to transform input L_k to a linear combination Y_i at node i as the form of

$$Y_i = \sum_{k=1}^{N} W_{ki} L_k + B_i \qquad \text{(A3)}$$

where W_{ki} is the weight which associates input node k with node i, B_i is the bias associated with node i. In the hidden layer that right follows the input layer, N = M(# of spectral bands). In any following layer, N is # of nodes of its parent layer. Once Y_i is formed in a layer, a nonlinear so-called activation function g is applied to generate an output C_i at node i, given by $C_i = g(Y_i)$. The hyperbolic tangent sigmoid function was selected for transfer function g. In the output layer, C_i is the concentration to be inverted (i=1...3).

The Levenberg-Marquardt optimization algorithm was applied for a so-called back-propagation training. An ANN training actually is to minimize mean square error between the data used for the training and ANN outputs by iteratively adjusting the weights and biases. To properly select an architecture of the ANN used, there has been no theory that shows the best architecture. For this application, an empirical testing was completed by using six two-hidden-layer architectures with the noise-contained data of Type 1 to evaluate their performance (Figure A1). The architecture #3 (bold) was finally selected. The chosen AAN consists the input layer with 5 nodes (number of spectral bands), two hidden layers with 7 nodes in the first and 5 nodes in the second, and the output layer contained 3 nodes (number of constituent concentrations to be inverted). The Neural Network algorithm available in MATLAB (Mathworks, 1998) was adopted for the implementation of the proposed NN inversion.

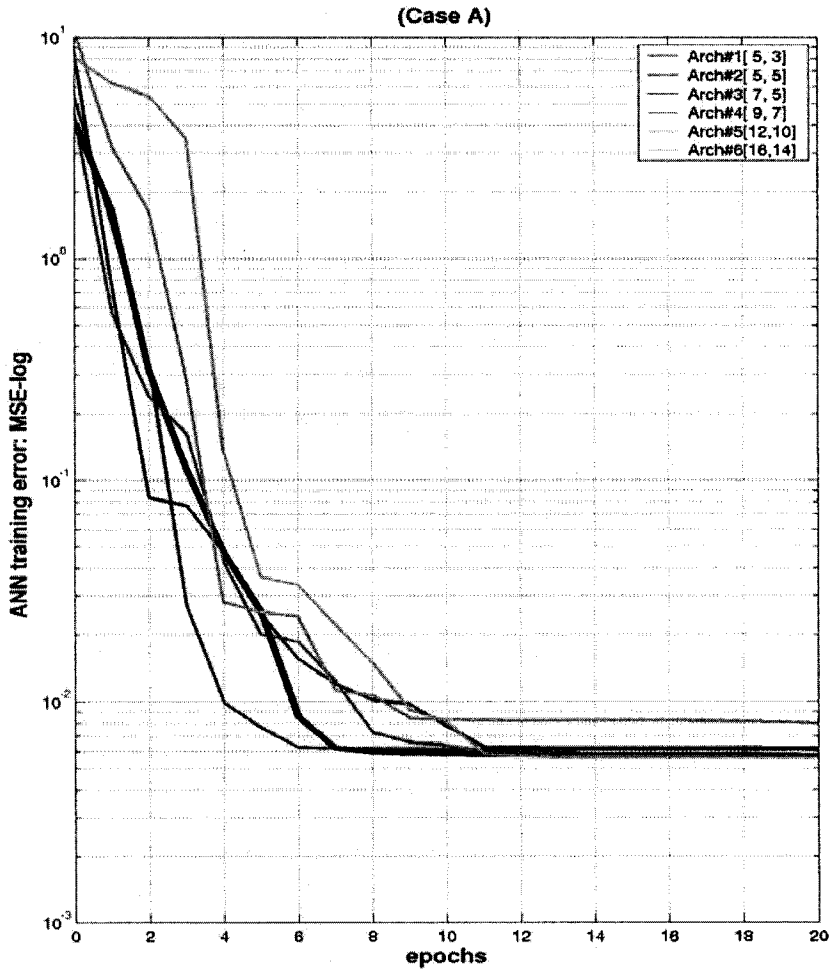

Figure A.1. The overall training errors against epochs for testing ANN performance using six two-hidden-layer architectures with the noise-contained data for the optical type 1. The numbers of neurons in the first and second hidden layers for the 6 tested architectures are shown in the legend. The architecture #3 (bold) was finally selected.

References

Bricaud, A., Babin, M., Morel, A. and Claustre, H., 1995. Variability in the chlorophyll-specific coefficients of natural phytoplankton: analysis and parameterization, Journal of Geophysical Research, 100(C7),13,321-13,332.

Bukata, R.P., Bruton, J.E. and Jerome, J.H., 1985. Application of direct measurements of optical parameters to the estimation of lake water quality indicators. Environment, Canada IWD Scientific Series No.140.

Bukada, R.P., Jerome, J.H., Kondratyev, J.E., Ya, K. and Pozdnyakov, D.V., 1991. Estimation of organic and inorganic matter in inland waters: Optical cross sections of Lakes Ontario and Ladoga, Journal of Great Lakes Research, 17, 461-469.

Bukada, R.P., Jerome, J.H., Kondratyev, J.E. and Pozdnyakov, D.V., 1995. Optical properties and remote sensing of inland and coastal water, CRC Press.

Campbell, J.W., 1995. The lognormal distribution as a model for bio-optical variability in the sea, Journal of Geophysical Research, 100(C7), 13237-13254.

Carder, K.L., Hawes, S.K., Baker, K.A., Smith, R.C., Steward, R.G. and Mitchell, B.G., 1991. Reflectance model for quantifying chlorophyll a in the presence of productivity degradation products, Journal of Geophysical Research, 96, 20599-20611.

Doerffer, R. and Fischer, J., 1994. Concentrations of chlorophyll, suspended matter, and gelbstoff in case II waters derived from satellite coastal zone color scanner data with inverse modeling methods, Journal of Geophysical Research, 99(C4), 7457-7466.

Doerffer, R. and Schiller, H.,1999. First test of a two-step neural network inverse modeling technique using MOS data, The 2nd International Workshop on MOS-IRS and Ocean Colour, Berlin, June 1-12, 1999.

Dowell, M. D., Moore, T.S., Campbell, J.W. and Hoepffner, N., 2000. Universally Tailored Optical Parameter Inversion Algorithm (UTOPIA) II: Class Parameterization, OOXV, Monaco, SPIE Proc.

Feng, H., Campbell, J. W. and Moore, T.S., 1998. Uncertainty analysis for retrieval of chlorophyll concentration from ocean color: a simulation study, Journal of Advanced Marine Science and Technology Society, 4(2), 265-274.

Frette, O., Stamnes, J.J. and Stamnes, K., 1998. Optical remote sensing of marine constituents in coastal waters: a feasibility study, Applied Optics, 37(36), 8318-8326.

Fisher, J., Doerffer, R. and Grass, H., 1986. Factor analysis of multispectral radiances over coastal and open ocean waters based on radiative transfer calculations, Applied Optics, 25(3), 448-456.

Garver, S.A. and Siegel, D.A., 1997. Inherent optical property inversion of ocean color spectra and its biogeochemical interpretation 1. Time series from the Sargasso Sea, Journal of Geophysical Research, 102(C8), 18607-18625.

Gordon, H.R., Brown, O.B., Evans, R.H., Brown, J.W., Smith, R.C., Baker, K.S. and Clark, D., 1988. A semi-analytical radiance model of ocean color, Journal of Geophysical Research, 93, 10909-10924.

Gower, J.F.R., Lin, S.R. and Borstad, G.A., 1984. The information content of different optical spectral ranges for remote chlorophyll, International Journal of Remote Sensing, 5(2), 346-364.

Grew, W.G, 1977. Characteristic vector analysis as a technique for signature extraction of remote ocean color data, Symposium at the 6th Annual Remote Sensing of Environment, Tullahoma, Tennessee.

Gross, L., Thiria S, Frouin, R. and Mitchell, B.G., 2000. Artificial neural networks for modeling the transfer function between marine reflectance and phytoplankton pigment concentration, Journal of Geophysical Research, 105(C2), 3483-3495.

IOCCG Report Number 3: Remote Sensing of Ocean Colour in Coastal, and Other Optically-Complex, Waters (2000), in S. Sathyendranath (Ed.), Dartmouth, Canada.

Jain, S.C. and Miller, J.R., 1976. Subsurface water parameters: Optimization approach to their determination from remotely sensed water color data. Applied Optics, 15, 4886-4890.

Hetscher, M., Krawczyk, H., Neumann, A. and Zimmermann, G., 2004. Four years of ocean colour remote sensing with MOS-IRS An updated version of a paper originally presented at Oceans from Space 'Venice 2000' Symposium , Venice, Italy, 9-13 October 2000, International Journal of Remote Sensing, 25, 7/8, 1415.

Keiher, L.E. and Brown, C.W., 1999. Estimating oceanic chlorophyll concentration with neural networks, International Journal of Remote Sensing, 20, 1,189-194.

Krasnopolsky, V.M., Breaker, L.C. and Gemmill, W.H., 1995. A neural network as a nonlinear transfer function model for retrieving surface wind speeds from the special sensor microwave imager, Journal of Geophysical Research, 100, C6, 11033-11045.

Krawczyk, H., Neumann, A. and Walzel, T., 1995. A Complex approach to quantitative interpretation of spectral high resolution imagery, The Third Thematic Conference on Remote Sensing for Marine and Coastal Environments, September, Seattle, USA, pp. II-57-68.

Krawczyk, H., Neumann, A. and Hetscher, M., 1999. Mathmatical and physical backgraound of principal componet inversion, In Proceedings of the 3rd International Workshop on MOS-IRS and Ocean Color. 83-92.

Lee, Z.P., Carder, K.L., Hawes, S.K., Steward, R.G., Peacock, T.G. and Davis, C.O., 1994. Model for the interpretation of hyperspectral remote-sensing reflectance, Applied Optics, 33, 5721-5732.

Morel, A. and Prieur, L., 1977. Analysis of variations in ocean color, Limnology and Oceanography, 22, 709-722.

Moore, T.S., Campbell, J.W. and Feng, H., 2001. A fuzzy logic classification scheme for selecting and bending satelliete ocean color algorithms, IEEE Transactions on Geoscience and Remote Sensing, 39(8), 1764-1776.

Mueller, J.L., 1976. Ocean color spectra measured off the Oregon coast: characteristic vectors, Applied Optics, 15, 2394-2402.

Nabney, I.T., 2001. NETLAB: Algorithms for Pattern Recognition. Springer-Verlag UK.

Roesler, C.S. and Perry, M.J., 1995. In situ phytoplankton absorption, fluorescence emission, and particular backscattering spectra determined from reflectance, Journal of Geophysical Research,100, 13279-13294.

Sathyendranath, S., Prieur, L. and Morel, A., 1989. A three-component model of ocean color and its application of phytoplankton pigments in coastal waters, International Journal of Remote Sensing, 10, 81373-81794.

Schiller, H. and Doerffer, R., 1999. Neural network for emulation of an inverse model---operational derivation of Case II water properties from MERIS data, International Journal of Remote Sensing, 20, 9, 1735-1746.

Zhan, H., Leee,Z., Shi,P., Chen,C. and Carder, K.L., 2003. Retrieval of water optical properties for optically deep waters using genetic algorithms. IEEE Transactions on Geoscience and Remote Sensing, 41, 5, 1123-1128.

Zhang, T., Fell, F., Liu, Z., Preusker R., Fischer J. and He, M., 2003. Evaluating the performance of artificial neural network techniques for pigment retrieval from ocean color in Case I waters, Journal of Geophysical Research, 108, 2,1-12.

Table 3.1. Parameters of IOP submodels in Eqs. (6-8) for the four optical water types. Parameters are listed in column 1, units in column 2, and values for each spectral band in columns 3-8.

Parameters	**Units**		**412nm**	**443nm**	**490nm**	**510nm**	**555nm**
RQ(λ)	None		1.92	1.92	1.92	1.92	1.92
M(λ)	None		0.5375	0.5373	0.5398	0.5390	0.5390
Fo(λ)	$Mw/cm^2/\mu m$		171.7	189.2	194.4	187.5	185.9
		Type 1					
Ac(λ)	m^{-1}		0.0313	0.0393	0.0274	0.0180	0.0071
Bc(λ)	None		0.717	0.6599	0.639	0.740	0.966
Y	m^{-1}	2					
S	nm^{-1}	0.018					
		Type 2					
Ac(λ)	m^{-1}		0.0272	0.0385	0.036	0.0109	0.0036
Bc(λ)	None		0.699	0.608	0.518	0.818	0.952
Y	m^{-1}	2					
S	nm^{-1}	0.016					
		Type 3					
Ac(λ)	m^{-1}		0.023	0.0464	0.035	0.0104	0.0047
Bc(λ)	None		0.7442	0.558	0.543	0.831	0.963
Y	m^{-1}	1					
S	nm^{-1}	0.014					
		Type 4					
Ac(λ)	m^{-1}		0.0256	0.0433	0.033	0.01168	0.00452
Bc(λ)	None		0.718	0.567	0.569	0.800	0.97118
Y	m^{-1}	0.5					
S	nm^{-1}	0.011					

Table 3.2a. The type-specific statistics (ranges(min,max), means, standard deviations, correlation matrixes) of the three constituent concentrations [Chl, $b_{bp}(555)$,$a_{gd}(440)$] in a 10-base logarithmic scale for the four water types in terms of the insitu measurements.

	Chl	$b_{bp}(555)$	$a_{gd}(440)$	Chl	$b_{bp}(555)$	$a_{gd}(440)$
	Type 1			Type 2		
Min	-1.4202	-2.8233	-2.4020	-1.2596	-2.8032	-1.9771
Max	-0.2757	-1.9995	-1.1295	1.6871	-1.4646	-0.2899
Mean	-0.8797	-2.4766	-1.6838	0.0088	-2.1218	-0.9678
Std	0.1994	0.1215	0.1900	0.5137	0.3095	0.3386
Correlation matrix						
Chl	1	0.6799	0.5517	1	0.8009	0.6927
$b_{bp}(555)$		1	0.9086		1	0.9386
$a_{gd}(440)$			1			1
	Type 3			Type 4		
Min	-1.2441	-2.8920	-1.9009	-0.4277	-1.8413	-0.9973
Max	1.5873	-1.4205	0.1542	1.5495	-1.0364	-0.1428
Mean	0.3765	-2.0888	-0.6579	0.6960	-1.4594	-0.5982
Std	0.5322	0.3014	0.3778	0.5051	0.1631	0.1832
Correlation matrix						
Chl	1	0.7665	0.5847	1	0.3999	-0.0221
$b_{bp}(555)$		1	0.8933		1	0.7046
$a_{gd}(440)$			1			1

Table 3.2b. The type-specific statistics (ranges(min,max), means, standard deviations, correlation matrixes) of the three constituent concentrations [Chl, $b_{bp}(555)$,$a_{gd}(440)$] in a linear scale for the four water types in terms of the *in situ* measurements.

	Chl	$b_{bp}(555)$	$a_{gd}(440)$	Chl	$b_{bp}(555)$	$a_{gd}(440)$
	Type 1			Type 2		
Min	0.0380	0.0015	0.0040	0.0550	0.0016	0.0105
Max	0.5300	0.0010	0.0742	48.65	0.0343	0.5130
Mean	0.1459	0.0035	0.0228	2.1139	0.0096	0.1400
Std	0.0670	0.0010	0.0105	4.0294	0.0071	0.0998
Correlation matrix						
Chl	1	0.7057	0.5866	1	0.5571	0.3149
$b_{bp}(555)$		1	0.9255		1	0.9224
$a_{gd}(440)$			1			1
	Type 3			Type 4		
Min	0.0570	0.0013	0.0126	0.3735	0.0144	0.1006
Max	38.66	0.0380	1.4263	35.44	0.0920	0.7198
Mean	4.7809	0.0102	0.3119	8.6579	0.0371	0.2762
Std	6.4796	0.0069	0.2762	8.6617	0.0136	0.1278
Correlation matrix						
Chl	1	0.4671	0.1618	1	0.1942	-0.1991
$b_{bp}(555)$		1	0.8301		1	0.7390
$a_{gd}(440)$			1			1

Table 3.3. Statistical performance measures of the three inversion methods for the four water types. Units are decodes of logarithm.

	RMSE	Bias	r^2	RMSE	Bias	r^2
Type 1	**noise-free**			**noise-contained**		
NLO Chl:	0.000	0.000	1.00	0.282	-0.041	0.34
bbp555:	0.000	0.000	1.00	0.035	0.000	0.92
agd440:	0.000	0.000	1.00	0.053	-0.004	0.93
PCA Chl:	0.089	0.000	0.80	0.133	0.002	0.55
bbp555:	0.013	0.000	0.99	0.029	0.000	0.94
agd440:	0.022	0.001	0.99	0.043	0.000	0.95
ANN Chl:	0.001	0.000	1.00	0.123	0.004	0.62
bbp555:	0.010	0.000	0.99	0.023	0.000	0.96
agd440:	0.006	0.000	1.00	0.038	-0.001	0.96
Type 2						
NLO Chl:	0.000	0.000	1.00	0.258	-0.017	0.80
bbp555:	0.000	0.000	1.00	0.096	0.005	0.92
agd440:	0.000	0.000	1.00	0.088	0.006	0.94
PCA Chl:	0.167	0.003	0.89	0.270	0.003	0.72
bbp555:	0.109	0.003	0.88	0.129	0.003	0.83
agd440:	0.118	0.004	0.89	0.130	0.004	0.86
ANN Chl:	0.005	0.000	1.00	0.203	-0.000	0.84
bbp555:	0.003	0.000	1.00	0.082	-0.001	0.93
agd440:	0.004	0.000	1.00	0.077	-0.001	0.95
Type 3						
NLO Chl:	0.000	0.000	1.00	0.221	-0.002	0.83
bbp555:	0.000	0.000	1.00	0.115	-0.003	0.85
agd440:	0.000	0.000	1.00	0.106	-0.002	0.92
PCA Chl:	0.246	0.005	0.79	0.281	0.005	0.78
bbp555:	0.177	0.000	0.66	0.186	0.000	0.63
agd440:	0.183	0.002	0.77	0.188	-0.003	0.76
ANN Chl:	0.011	0.000	1.00	0.175	-0.002	0.89
bbp555:	0.006	0.000	1.00	0.104	0.000	0.88
agd440:	0.008	0.000	1.00	0.097	0.000	0.94
Type 4						
NLO Chl:	0.000	0.000	1.00	0.250	-0.002	0.77
bbp555:	0.000	0.000	1.00	0.150	0.011	0.52
agd440:	0.000	0.000	1.00	0.163	0.011	0.55
PCA Chl:	0.208	0.002	0.83	0.238	0.002	0.78
bbp555:	0.010	0.000	0.63	0.125	0.000	0.42
agd440:	0.008	0.000	0.83	0.125	0.001	0.54
ANN Chl:	0.004	0.000	1.00	0.162	-0.001	0.90
bbp555:	0.003	0.000	1.00	0.099	0.000	0.63
agd440:	0.004	0.000	1.00	0.109	0.000	0.64

Table 3.4. Number of convergence and CPU time for inverting 10,000 simulated spectra using the Gauss-Newton NLO algorithm.

	Number of convergences		CPU time in seconds	
	Case A	Case B	Case A	Case B
Type 1	9905	9789	85.7	92.0
Type 2	9639	9456	120.6	216.6
Type 3	9332	8866	224.0	279.3
Type 4	9256	9186	208.4	118.3

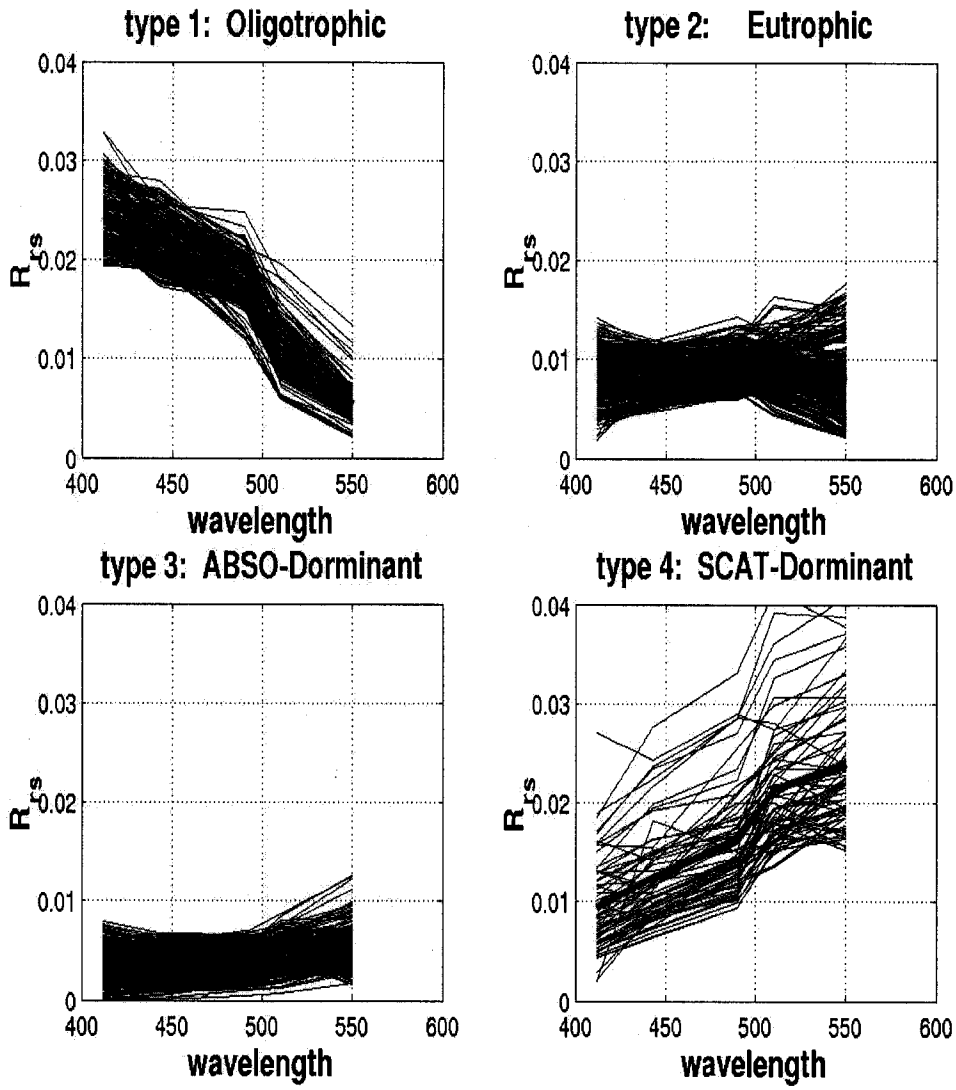

Figure 3.1. The type-specific mean remote sensing reflectance spectra along with the corresponding measured spectra for the four water types.

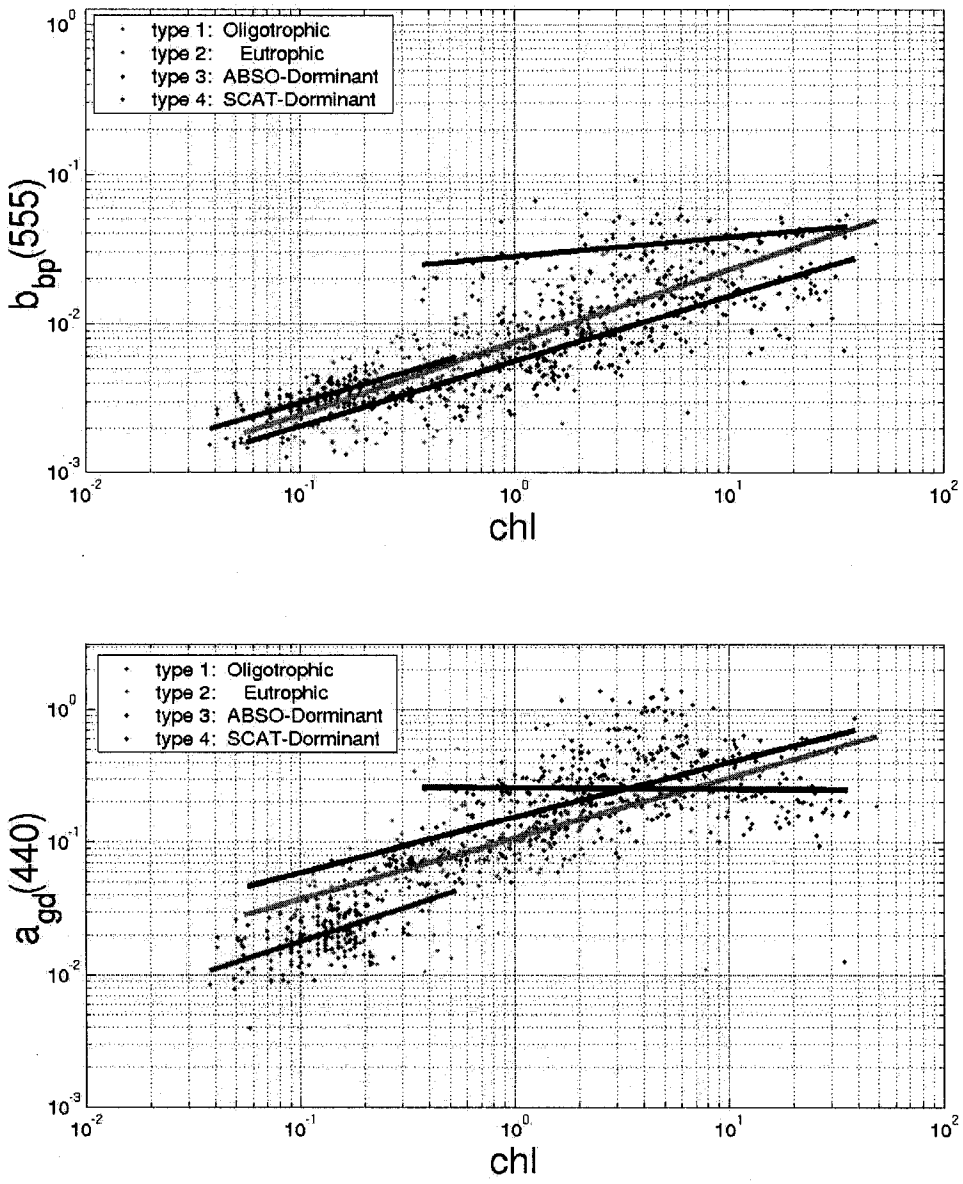

Figure 3.2. Scatter plots of [Chl] vs. [$b_{bp}(555)$] (top panel) and [Chl] vs. [$a_{gd}(440)$] (lower panel) for four optical water types using in-situ optically-active constituent concentrations. The regression lines are also shown.

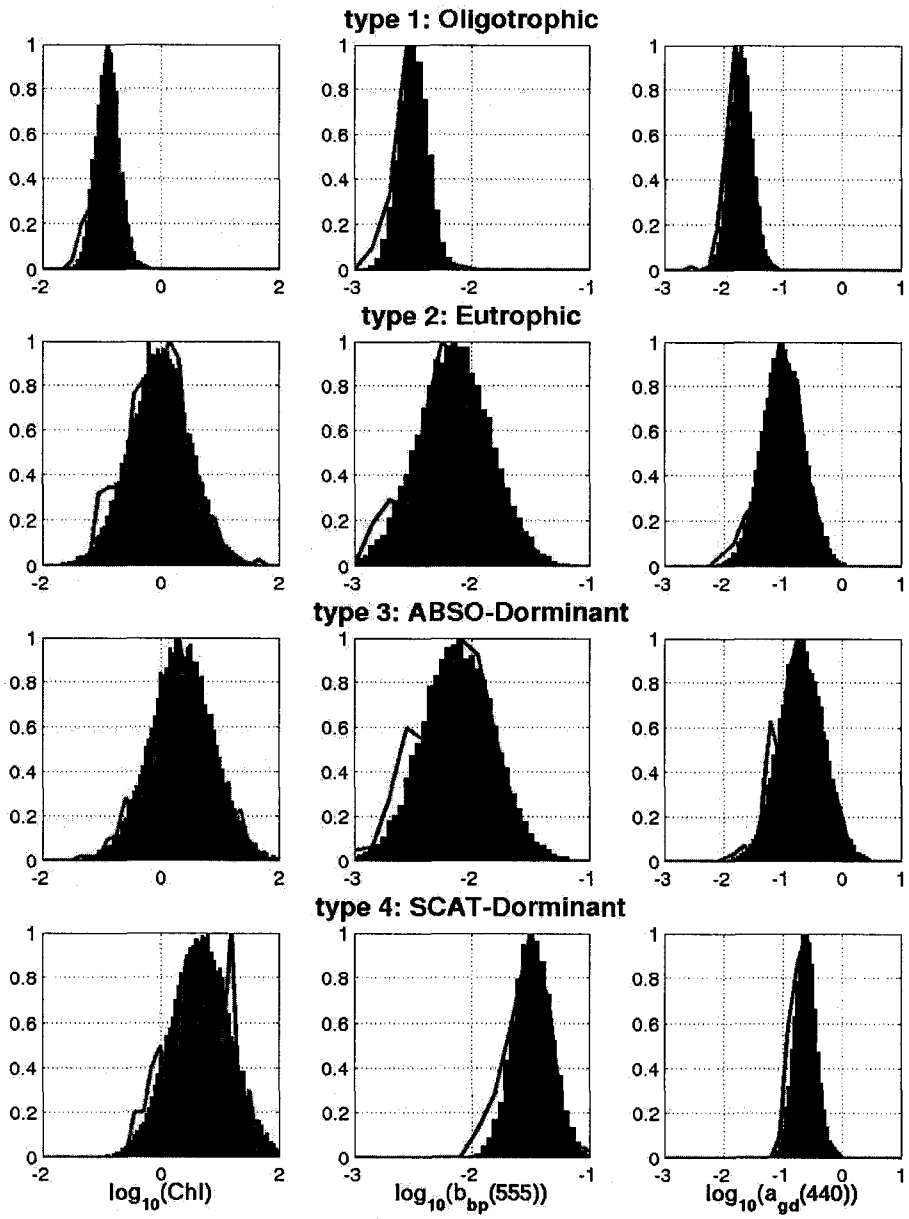

Figure 3.3. Simulated optically-active constituent distributions (3D lognormal assumption) for the four optical water types. The red lines overlaid represents the corresponding distributions of the in-situ datasets.

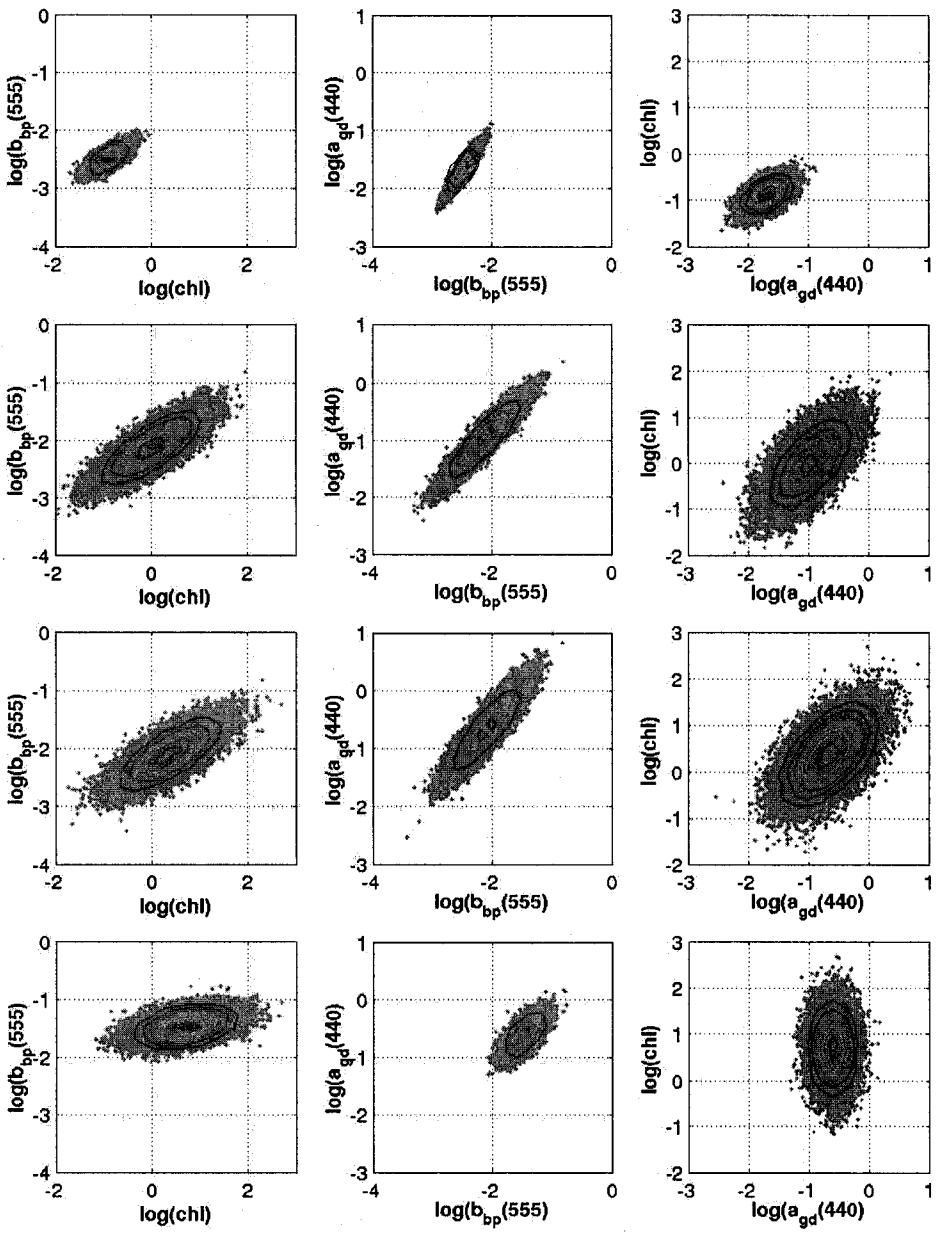

Figure 3.4. Scatter/density plots of the simulated in-water constituent concentrations used for forward model simulations for Case A for the four optical water types, showing the correlation levels among the three constituent concentrations [Chl, $b_{bp}(555)$, and $a_{gd}(440)$].

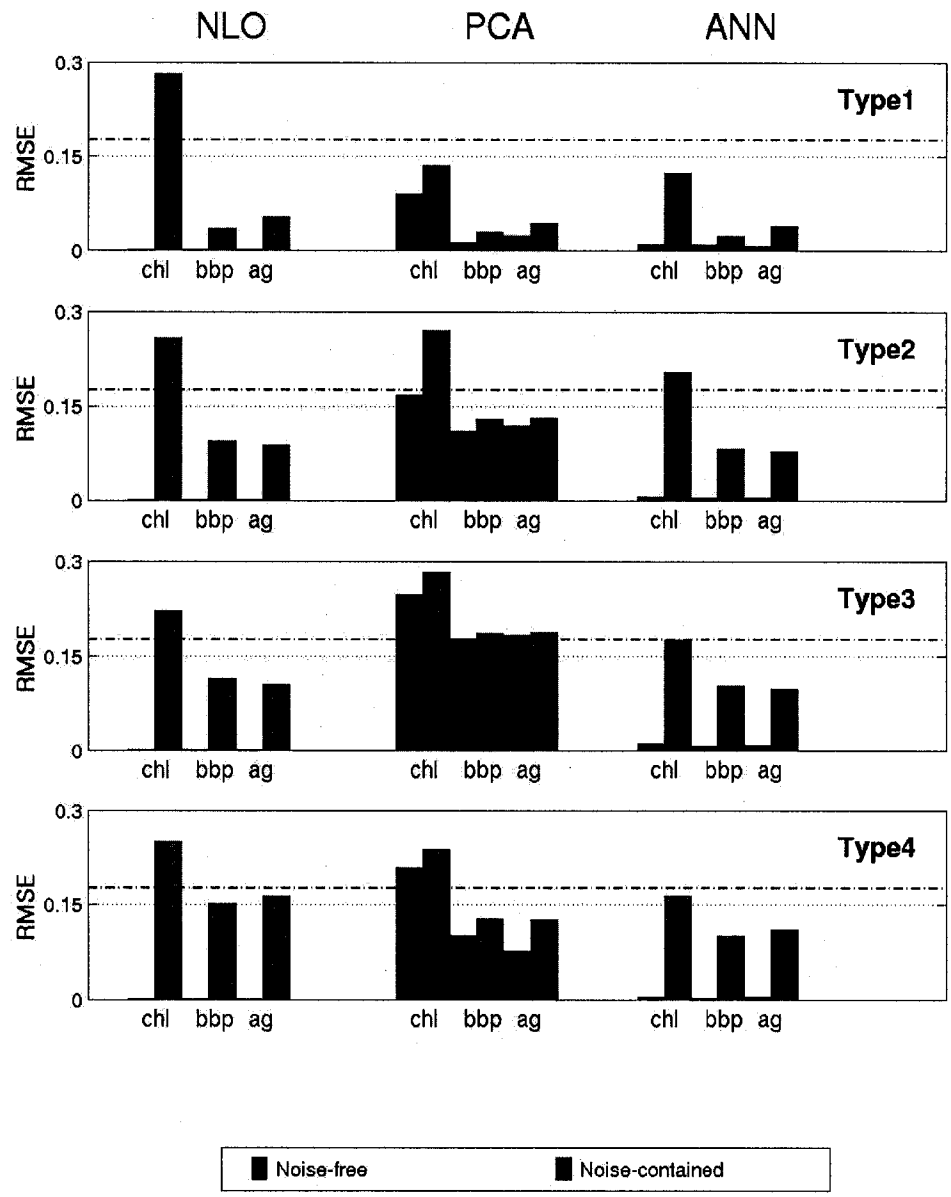

Figure 3.5. Inversion performance plots of root mean square error (RMSE) for all the four optical water types and three inversion methods. The horizontal dash line represents the 50% relative error level.

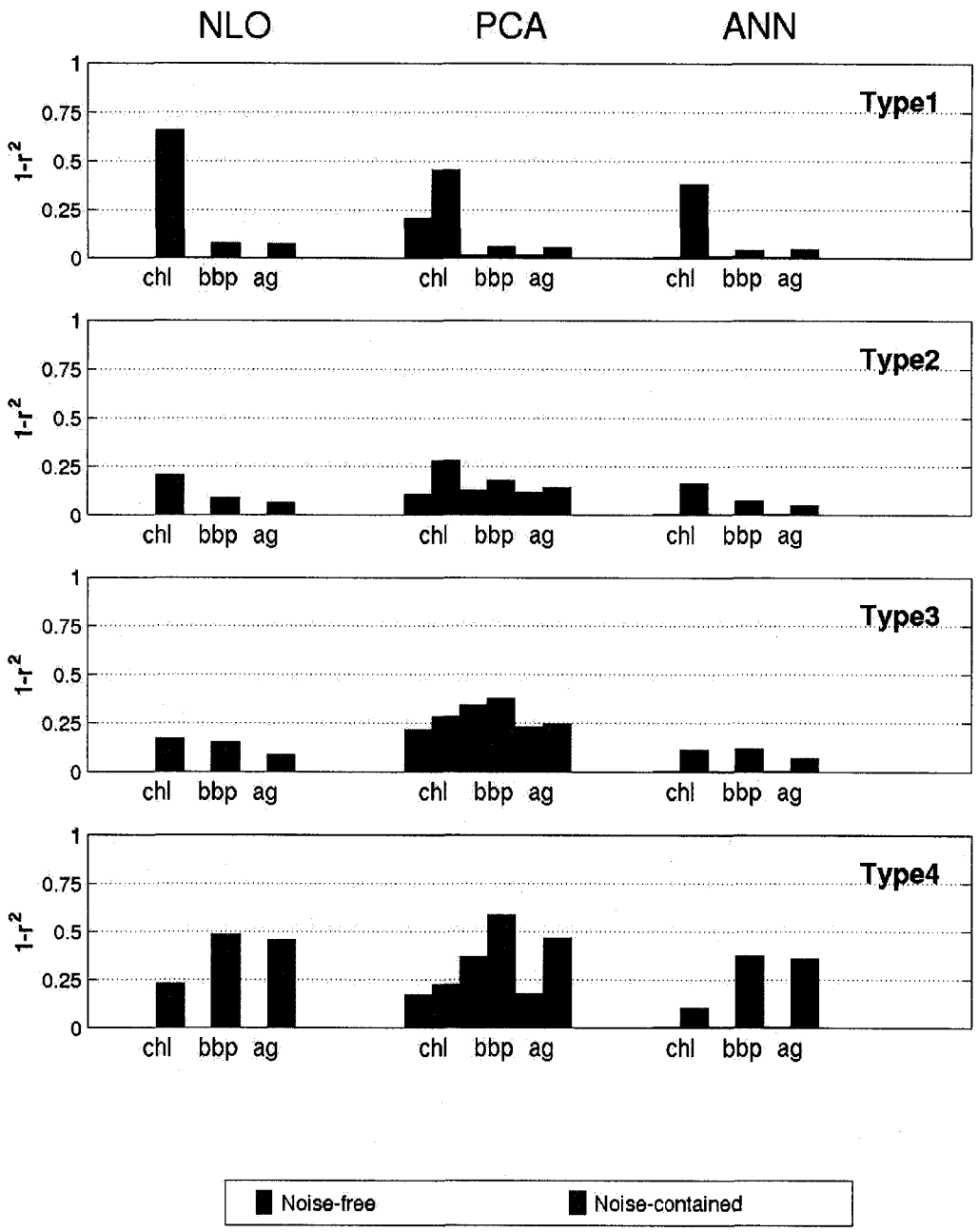

Figure 3.6. Inversion performance plots of ($1-r^2$) for all the four optical water types and three inversions where r^2 is correlation coefficient square.

Chapter 4 Modeling spectral reflectance of optically complex waters using *in situ* bio-optical measurements in Tokyo bay (to be submitted to Remote Sensing of Environment by Hui Feng, Janet W. Campbell, Mark Dowell and Timothy S. Moore)

Abstract

This study presents an approach for optimally parameterizing a reflectance model. A parameterization scheme is realized based on a comprehensive bio-optical data set, including subsurface downwelling and upwelling irradiance spectra, absorption spectra of particle and dissolved substances, as well as chlorophyll and total suspended matter concentrations at 45 stations near Tokyo Bay between 1982 and 1984. The irradiance reflectance model is implemented with three-component inherent optical property (IOP) submodels.

In this parameterization scheme, an unsupervised classification was applied in the hyper-spectral space of reflectance, leading to three spectrally-distinct optical water types. The reflectance model was parameterized for the entire dataset, and then parameterized for each of the water types. The three sets of type-specific model parameters, which define corresponding IOP submodels, are believed to accommodate differences in the optical properties of the in-water constituents. The parameterized reflectance model was evaluated by both reconstructing measured reflectance spectra and solving for the non-linear inverse problem to retrieve in-water constituent concentrations. The model accuracy was significantly improved in the forward direction for classified waters over that of non-classified waters, but no significant improvement was achieved in the retrieval accuracy (inverse direction). A larger dataset with greater resolution of constituent IOPs would likely improve the modeling results.

4.1 Introduction

Optically active constituents in the upper ocean significantly affect an ocean color spectrum (radiance or reflectance) measured at the surface of the water. How do we interpret an ocean color spectrum quantitatively to derive the concentrations of these constituents? Techniques for constituent retrieval have evolved from empirical (data-based) towards analytical (model-based) algorithms over the last decade. Today's semi-analytical algorithms (Lee *et al.*, 1994; Roesler and Perry, 1995; Garver and Seigel, 1997; Maritorena *et al.*, 2002; Chomko *et al.*, 2003; Chami and Robiliard, 2002) are based on well-established relationships between apparent optical properties (e.g., radiance or reflectance) and inherent optical properties (absorption and scattering). The relationships between the IOPs and the constituent concentrations are empirically derived, and thus these algorithms are said to be "semi-analytical."

Empirical algorithms (Gordon and Morel, 1983) often focus only on retrieving a single constituent concentration, whereas semi-analytical algorithms are capable of retrieving three or more in-water constituents simultaneously. For semi-analytical algorithms, an inversion technique is usually applied to a parameterized ocean color model whose parameters have been predetermined from *in situ* bio-optical measurements. Precise radiative transfer calculations (Gordon *et al.*, 1975 and 1988; Kirk, 1984) have provided a solid physical and analytical basis for quantitatively interpreting a measured ocean color spectrum as a function of the IOPs, that is, absorption and backscattering coefficients. The constituent-specific IOPs can be related to constituent concentrations through corresponding IOP submodels.

Morel and Prieur (1977) pointed out that a successful reconstruction of reflectance spectra (direct problem) is a necessary condition for solving the corresponding inverse problem. In other words, only if a parameterized reflectance model can reconstruct measured reflectance spectra to a satisfactory accuracy will it be possible to invert it precisely for retrieving in-water constituents. However, this condition is necessary but not sufficient. An ideal ocean color model must be optimal for both direct (describing the light environment in terms of in-water constituent concentrations) and inverse (retrieving constituents from an ocean color spectrum) solutions.

For the past decade, considerable progress has been made towards understanding the relationship between absorption coefficients and chlorophyll concentration (Garver *et al.*, 1994; Bricaud *et al.*, 1995 and 1998; Reynolds *et al.*, 2001). In these studies, the absorption of living phytoplankton and total particulate matter are modeled with a chlorophyll-dependent parameterization scheme that accounts for the non-linearity of absorption with chlorophyll. However, the residual errors in modeling phytoplankton and particulate absorption are large when a single model is applied to the global dataset (Bricaud *et al.* 1998). It is suggested that more detailed models may be needed to describe spatial and temporal variations in the size and structure of phytoplankton species and other particulate matter.

In coastal and estuarine waters, in-water constituents, such as suspended inorganic particles and colored dissolved organic matter (CDOM), become optically significant along with phytoplankton in affecting the optical properties. For the CDOM absorption spectrum, a spectral "slope" parameter, S, is often used to describe the spectral shape of the CDOM absorption coefficient. It has been reported that S varies within a very large

range from about 0.004 to 0.032m^{-1} in surface waters (Bricaud *et al.*, 1981; Carder *et al.*, 1989; Vodacek *et al.*, 1997; Kowalczuk, 1999; Salisbury *et al.*, 2004). These studies have shown that S varies spatially and sometimes temporally, also suggesting that a single spectral model of CDOM absorption may not be adequate to describe its variability if applied to a large geographical domain. Compared with absorption measurements, backscattering measurements of suspended particulate matter have been much less studied mainly due to the limitation of commercial instrumentation. Until recently, few measurements of backscattering by suspended matter have been reported (Whitlock *et al.* 1980; Galie and Murtha, 1992; Bukada *et al.*, 1995; Maffione and Dana, 1997). For backscattering measurements from different oceanic, coastal and inland waters, Bukata *et al.* (1995) indicated that backscattering has significant locality and seasonality.

Optical properties vary for two primary reasons: variations in the concentrations of constituents in the water, and variations in the materials themselves, e.g., variations in the size and refractive index of particles. An ocean color model parameterized for one set of optically active constituents should be able to describe optical variability due to varying concentrations of those constituents. Such a model could then be inverted successfully to retrieve the concentrations. But the same model might prove unsuccessful if applied to an ocean color spectrum from waters having different constituents.

In all, special consideration must be given to develop a modeling strategy to apply a parameterized ocean color models properly to different water environments. In this work, we demonstrate an optimal approach to model spectral reflectance based on an *in situ* bio-optical dataset measured near Tokyo Bay from different seasons. The performance of the parameterization scheme was evaluated by both reconstructing

reflectance spectra and solving the inverse problem to retrieve in-water component concentrations.

4.2 Methods

4.2.1 Data

The bio-optical dataset used for this study was obtained from 45 stations in Tokyo Bay and nearby regions from 5 cruise surveys in different seasons between 1982 and 1984 (Kishino *et al.* 1984; Kishino, 1994). The measurement sites ranged in depth from 1000m in clear open-ocean waters to less than 5m deep in very turbid coastal waters. The Secchi disk depth records, compared with corresponding physical depths, indicate that bottom reflection effects need not be considered in the ocean color modeling.

The dataset used consisted of

- subsurface irradiance reflectance spectra calculated as the ratio of upwelling to downwelling irradiance measured just below the surface,
- total absorption and CDOM absorption coefficients, and
- total suspended matter [TSM] and chlorophyll-a [CHL] concentrations.

Absorption measurements were made between 350 nm and 750nm at a 5-nm spectral resolution. Underwater upwelling and downwelling irradiances (and hence irradiance reflectance) were measured between 362nm and 762nm with a 2-nm resolution, and subsequently converted to a 5nm spectral resolution by linear interpolation. This work focused only on the spectral range between 400nm and 700nm. The CDOM absorption coefficient at 375nm, a_{y375}, was used as a surrogate for CDOM concentration.

4.2.2 Models

Reflectance model

An irradiance reflectance model by Gordon *et al.* (1975) for deep waters

$$R(\lambda, j) = \sum_{k=0}^{2} \gamma_k \left[\frac{b_b(\lambda, j)}{a(\lambda, j) + b_b(\lambda, j)} \right]^k \tag{4.1}$$

was used where $R(\lambda,j)$, $b_b(\lambda,j)$ and $a(\lambda,j)$ are irradiance reflectance just beneath the surface, backscattering and absorption coefficients, respectively, measured at wavelength λ and at site j; γ_k is a set of expansion coefficients where for solar angle <=~20° (referred to as sun case), γ_0 =0.0001, γ_1 =0.3244, and γ_2 =0.1425; and for solar angle =>~30° (referred to as sky case), γ_0=0.0003, γ_1=0.3687, and γ_2=0.1802;

In-water bio-optical models

In general, IOPs can be expressed by

$$a(\lambda, j) = a_w(\lambda) + \sum_i a_i(\lambda, j) \tag{4.2a}$$

$$b_b(\lambda, j) = b_{bw}(\lambda) + \sum_i b_{bi}(\lambda, j) \tag{4.2b}$$

where $a_w(\lambda,j)$ and $b_{bw}(\lambda,j)$ are absorption and backscattering coefficients for seawater; and $a_i(\lambda,j)$ and $b_{bi}(\lambda,j)$ are the absorption and backscattering coefficients for the *ith* optically-active constituent.

After various trial plots were made of constituent-dependent $a(\lambda,j)$ and $b_b(\lambda,j)$ against constituent concentrations, the spectral absorption and backscattering coefficients in Eqs.(4.2a) and (4.2b) were finally modeled as

$$a(\lambda, j) = a_w(\lambda) + a_p^*(\lambda)[CHL] + a_{y375} \exp[-S(\lambda - 375)] \quad (4.3a)$$

$$b_b(\lambda, j) = b_{bw}(\lambda) + b_{bp}^*(\lambda)[TSM] \quad (4.3b)$$

where the values of $a_w(\lambda)$ and $b_{bw}(\lambda)$ were taken from Pope *et al.* (1997), and $a_p^*(\lambda)$ and $b_{bp}^*(\lambda)$ are the constituent-specific absorption and backscattering coefficients defined for particles and total suspended matter by:

$$a_p^*(\lambda) = A_c(\lambda)[CHL]^{B_c(\lambda)} \quad (4.4)$$

$$b_{bp}^*(\lambda) = A_b(\lambda)[TSM]^{B_b(\lambda)} \quad (4.5)$$

The third term in Eq(4.3a) is the CDOM absorption coefficient. The spectral shape parameter, S(j), was determined from each measured CDOM absorption spectrum, and the average S was used as the model parameter. The second term is the absorption for all particles, including phytoplankton, detritus, and all other particles, fitted using a logarithmic regression at each wavelength □ (Bricaud *et al.*, 1995, 1998) between the particle absorption (obtained by subtracting the absorption contributions from CDOM and sea water from the total absorption) and the chlorophyll concentration [CHL].

The second term in Eq. (4.3b) is the backscattering coefficient for the total particles, $b_{bp}(\lambda)$. Given measured $a(\lambda,j)$ and $R(\lambda,j)$, the total backscattering coefficient spectrum, $b_b(\lambda,j)$, was calculated by solving Eq.(4.1) for this term (Gordon *et al.* 1975), and then the water backscattering, $b_{bw}(\lambda)$, was subtracted to obtain the "measured" $b_{bp}(\lambda)$ spectrum. The $b_{bp}(\lambda)$ model was then parameterized as a function of [TSM] using a logarithmic regression at each wavelength λ.

4.2.3 Parameterization and evaluation

A set of model parameters was first derived from all the measurements, and then an unsupervised classification was completed in the spectral space of measured irradiance reflectance, leading to three spectrally distinct water types. The IOP parameterization procedure was then repeated for each of the three water types. The first model parameterization using all the stations will be referred to as the "non-classified" model, and the three type-specific model parameterizations as the "classified model."

To evaluate model performance, two different aspects were considered. For the direct problem, a parameterized model should be capable of reconstructing measured reflectance to a satisfactory accuracy. For the inverse problem, the model needs to be inverted to retrieve in-water constituent concentrations well. Normally, a model is parameterized with a subset of available data, and later tested using an independent subset of the data. Due to the limited number of measurements (only 45 sites) in this work, there was no independent test dataset available. An alternative method, called the Leave-One-Out Method (LOOM) (Fukurage, 1990) was adopted for validation.

The LOOM is described here briefly. For an ensemble with N samples, one sample is excluded, and the remaining N-1 samples (called parameterization dataset) are used for model parameterization. The parameterized model is then tested using the excluded sample. This operation is repeated N times to test all N samples. Test statistics are based on a sample of size N consisting of the N observations and the N model-predictions parameterized with the remaining N-1 samples. Because each sample in the testing dataset is excluded from the dataset used for the parameterization procedure, the parameterization dataset is independent of the testing dataset. This method utilizes a

limited dataset effectively so that all N samples are tested and N-1 samples are used for the parameterization.

This method was used in both direct and inverse directions to evaluate the models' performance. For the direct problem, N sets of the model parameters were calculated using N parameterization datasets, each with N-1 samples. For each excluded station, the spectra of $a(\lambda)$, $b_b(\lambda)$ and $R(\lambda)$ were reconstructed using the measured in-water constituent concentrations for that station, and these were then compared with corresponding measured spectra. For the inverse problem, a nonlinear optimization algorithm, the Gauss-Newton method (Garver and Siegel, 1997; Feng *et al.* 1998), was applied to each excluded reflectance spectrum to derive estimates of the constituent concentrations. The nonlinear optimization minimizes the residual error between the measured $R(\lambda)$ and modeled $R(\lambda)$ with the model parameters derived from the corresponding parameterization dataset. The derived constituent concentrations were be compared with the measured ones to evaluate the performance of the inverse model.

4.2.4 Error analysis: performance measures

At site j and wavelength λ, let

$$D_j(\lambda) = \hat{x}_j(\lambda) - x_j(\lambda) \tag{4.6}$$

denote the difference between a modeled variable $\hat{x}_j(\lambda)$ and measured variable $x_j(\lambda)$. The following statistical measures were used for evaluating model performance. The mean error (or bias) defined by

$$M(\lambda) = \frac{1}{N}\sum_j D_j(\lambda) \ , \tag{4.7}$$

the standard deviation of the error defined by

$$S(\lambda) = \sqrt{\frac{1}{N}\sum_{j}(D_j(\lambda) - M(\lambda))^2}\ , \tag{4.8}$$

and the root-mean-square error defined by

$$RMSE(\lambda) = \sqrt{S^2(\lambda) + M^2(\lambda)}\ . \tag{4.9}$$

In addition, the correlation coefficient between measured and modeled variables was also used to reveal the degree of correspondence of the two.

4.3 Results

4.3.1 Constituent concentrations

Tokyo Bay may be considered moderately eutrophic according to the criteria of eutrophic status in an aquatic ecosystem (Bukata *et al.*, 1995). Its chlorophyll concentrations [CHL] are high, showing considerably large variations with a mean value of about 5 mg/m^3 and a standard deviation of 6.3 mg/m^3. Most of the observations are below 10 mg/m^3, but an extreme value of 35 mg/m^3 was measured. Concentrations of CDOM were very high with high variations as well. The absorption coefficient for CDOMs at 375nm, a_{y375}, varied between 0.2 and 0.5 m^{-1}. The total suspended matter concentrations [TSM] were relatively low with a mean of 1.6 g/m^3 and a standard deviation value of 1.25 g/m^3 (Table 4.1).

All three optically-active components (i.e. [CHL], [TSM], and a_{y375}) covary moderately with positive correlation. In particular, the covariance between [TSM] and [CHL] suggests that biologically-generated particles are a significant component of the total suspended matter.

4.3.2 Non-classified waters

Originally, all 45 measurements were used to parameterize the reflectance model and then reflectance spectra were reconstructed using the measured constituents and the derived model parameters. The correlation coefficient spectra between measured and reconstructed absorption, backscattering and reflectance are shown in Figure 4.1(a). Both modeled backscattering and absorption coefficients were correlated quite well with corresponding measured ones. The former was higher than 0.6, and the latter was higher than 0.8 at all wavelengths. However, the correlation between measured and modeled reflectances was not satisfactory, particularly in the middle spectral region. The error plots for the modeled $a(\lambda)$, $b_{bp}(\lambda)$ and $R(\lambda)$ (Figure 4.1(b)-(d)) showed that the spectral shape of the $R(\lambda)$ errors mimics that of $b_{bp}(\lambda)$ with the highest RMSE errors in the middle spectral region. The estimates of $R(\lambda)$ were also somewhat biased in the middle spectral region. This result suggested that the variability in backscattering was not described well by a single model of $b_{bp}(\lambda)$.

4.3.3 Classified waters

An unsupervised classification algorithm (Moore *et al.*, 2001) was then applied to the spectral space of reflectance to classify the waters. This resulted in the identification of three optical water types. The concentration ranges for the three water types (Figure 4.2) indicate that water types 1, 2 and 3 correspond, respectively, to moderate, high, and low concentrations of all three in-water concentrations. In essence, the classification led to a sorting of the stations relative to the concentrations of optically-active constituents. The measured $R(\lambda)$, $a(\lambda)$, $b_{bp}(\lambda)$ for the three types are shown in Figures (4.3), (4.4) and (4.5), respectively.

For type 1, the irradiance reflectance peaks around 500-580nm with a relatively wide spectral domain (Figure 4.3). A second maximum appears at 685 nm where the chlorophyll fluorescence emission occurs. The values of [CHL], [TSM] and a_{y375} are all moderate. This water type exhibits the highest reflectance values among the three types. For type 2, the reflectance amplitudes are generally lower than those of type 1 (Figure 4.3), with the peaks shifting towards 560-580nm. The corresponding absorption plots (Figure 4.4) indicate that strong absorption from CDOM and phytoplankton in this water type significantly affect the spectral characteristics of reflectance in the spectral region below 530nm. Above 530nm, the effect of absorption agents diminishes, and particle backscattering (Figure 4.5) along with water absorption takes more responsibility for the reflectance properties. For type 3, the overall reflectance levels (Figure 4.3) are considerably lower than those of the other two types. The exception is that its reflectance spectra are relatively higher in the range below 480nm where CDOM and chlorophyll absorptions usually play a significant role. Due to the low concentrations of CDOM and chlorophyll in this water type, the reflectance spectra are affected mainly by sea water and detritus, and are thus relatively high in the spectral region below 480nm.

4.3.4 Modeled IOP spectra

For the three water types, three sets of IOP model parameters i.e. $A_c(\lambda)$, $B_c(\lambda)$, $A_b(\lambda)$, $B_b(\lambda)$, and S, were estimated. All the IOP spectra can be predicted using these parameters in accordance with equations (4.3-4.5). In this section, a comparison of these parameters and predicted IOP spectra among different types is presented.

CDOM absorption spectra

The mean and standard deviation of the spectral shape factor S for CDOM absorption were 0.0147 and 0.0024, respectively, based on the 45 stations. There was no significant difference of S factors among the three water types.

Particle backscattering spectra

The specific backscattering coefficient for particles was modeled as a nonlinear power-law function of the total suspended matter [TSM] given by equation (4.5). The $A_b(\lambda)$ parameter spectrum describes the amplitude, and $B_b(\lambda) \neq 0$ indicates a nonlinear relationship between particle backscattering and [TSM]. This implies that the particle-specific backscattering coefficient changes at different [TSM] concentrations. $B_b(\lambda) = 0$ would mean that the amount of backscattering per unit [TSM] is constant. Results are shown in Figure 4.6(a-b).

$A_b(\lambda)$ spectra are significantly different in the three water types over most of the spectral range. The values in $A_b(\lambda)$ decrease in order from type 1 to 3 at all wavelengths in Figure 4.6(a). For types 1 and 2, $A_b(\lambda)$ peaks in the spectral region between 480nm and 580nm, consistent with those in reflectance. For type 3, $A_b(\lambda)$ values generally decrease with increasing wavelength.

Negative values in $B_b(\lambda)$ for all three water types indicate that an increase in [TSM] leads to a decrease in $b_{bp}^*(\lambda)$. Below about 600nm, no significant differences in $B_b(\lambda)$ can be seen in Figure 4.6(b), whereas above 600nm, the distinction can be seen among the three water types. A general spectral pattern is that $B_b(\lambda)$ increases from 450nm to 600m for all three water types, and then above 600nm, type 3 remains the "most nonlinear" (i.e., is more negative) while the type 2 $B_b(\lambda)$ gets close to zero.

The $b_{bp}^*(\lambda)$ and $b_{bp}(\lambda)$ spectra derived using the mean [TSM] values of the three water types are plotted in Figure 4.7. The spectral patterns of backscattering for types 1 and 2 are very similar, having the same spectral pattern as those of chlorophyll-bearing particles (Bukata *et al.*, 1995). Backscattering per unit [TSM] (i.e. $b_{bp}^*(\lambda)$) is higher for type 1 than for type 2 even though the mean [TSM] for type 2 is higher. This may be due to the fact phytoplankton-associated particles are the dominant component in the total suspended matter [TSM]. The spectral pattern of backscattering for type 3 resembles that for inorganic particles which is commonly modeled with a power-law decay with wavelength (Galie and Murtha, 1992; Bukada *et al.*, 1995).

A possible explanation for the non-linear change of b_{bp} with [TSM] is that the particle size distribution or the index of refraction of particles changed with concentrations. According to Mie scattering theory, both of them would influence backscattering properties significantly.

Particle absorption spectra

The particle-specific absorption coefficient spectrum was modeled in accordance with equation (4.4). Like the backscattering model, the wavelength-dependent parameters $A_c(\lambda)$ and $B_c(\lambda)$ describe the amplitude and nonlinear relationship between $a_p^*(\lambda)$ and [CHL], respectively. A general spectral pattern of $A_c(\lambda)$ for the three types (Figure 4.6(c)) is that a spectral increase is observed particularly from 600nm to 400nm, due to the contribution of the absorption from phytoplankton and organic particles, such as detritus. The difference in the amplitude value $A_c(\lambda)$ between types 1 and 2 is probably not significant, whereas the amplitude for type 3 is lower than those of the other two models. The difference within the red absorption band is slight among the three types. Negative

values in $B_c(\lambda)$ for all the three types indicate a general trend of the $a_p^*(\lambda)$ values decreasing with increasing [CHL]. The general spectral patterns of $B_c(\lambda)$ parameters are very similar for all three types (Figure 4.6(d)).

The spectra of $a_p^*(\lambda)$ and $a_p(\lambda)$ estimated using mean [CHL] values of the three types are shown in Figure 4.7. The spectral patterns of all the water types are similar, generally in agreement with previously published work (Bricaud *et al.* 1998). Again due to the absorption contribution from detritus and other organic particles, the spectral increase in absorption below 550nm is noted. For types 1 and 3, the amount of absorption per unit [CHL] is of the same magnitude although they have different mean [CHL] levels of 2.96 and 1.22 mg/m^3, respectively. For type 2 waters, with the highest chlorophyll concentrations, the specific $a_p^*(\lambda)$ spectrum is more like that of large, highly packaged phytoplankton (Bricaud *et al.*, 1995) with lower amplitudes than the other two.

4.3.5 Modeling performance

Forward direction

Using the type-dependent model parameters, the reflectance spectra were reconstructed for all 45 measurement stations. A composite plot comparing the reconstructed reflectance spectra with measured reflectance spectra for all the stations is shown in Figure 4.8. For most of the stations, there was good agreement between reconstructed (modeled) and measured reflectance. In some of the stations, however, errors were still high.

The modeling performance was quantitatively evaluated using both the correlation coefficients and error spectra between modeled and measured $R(\lambda)$, $a(\lambda)$, and $b_{bp}(\lambda)$. Compared with Figure 4.1(a) (from non-classified waters), Figure 4.9(a) (classified waters) shows that the correlation coefficient levels in modeling $R(\lambda)$ for this parameterization scheme are above 0.6 at all wavelengths, and thus significantly improved after the classification. Figure 4.7(b-d) show that the overall improvement in accuracy of modeling reflectance $R(\lambda)$ is mainly attributed to the improvement in modeling $b_{bp}(\lambda)$ by classifying the waters. The estimates of $R(\lambda$, $a(\lambda)$, and $b_{bp}(\lambda)$ are almost unbiased in all the spectral regions (Figure 4.9(b-d)).

Inverse direction

The nonlinear optimization algorithm was applied to the reflectance spectrum from each station, and the derived concentrations were then compared with the measured concentrations to assess the performance of the inverse model. Table 2 gives the overall evaluation statistics for the inverse problem, where the bold font indicates an improvement after classification. According to Table 2, the accuracy was the highest in predicting total suspended matter concentrations, but there was no improvement in the predictive capability of [TSM] by using classified-water models. The CDOM absorption (i.e., a_{y375}) was predicted with the worst success among the three concentrations. Using classified-water models, the RMS and bias errors were significantly lowered, indicating an improved capability in predicting a_{y375} using classified-water models. The chlorophyll concentrations were predicted with a moderate accuracy. Using the classified-water models, the chlorophyll retrievals were slightly improved over the non-classified-water models.

On another aspect, without using classified-water models six negative values of a_{y375} were retrieved, all belonging to water type 3. Such negative values are physically meaningless (and were not included in the error analysis). After using the classified-water models, only four negative values were predicted. In this sense, the classification of waters resulted in an improvement for the inverse model.

4.4 Discussion

The poor performance of the model parameterization in the forward direction using all 45 stations suggested the requirement to improve the accuracy of the IOP submodels. To achieve improved accuracy in modeling reflectance spectra, one way would be to resolve more constituents. For instance, the particulate backscattering coefficient might be modeled with two (or more) components to account for scattering by organic and inorganic suspended matter, instead of using only the one-component model we used in this work. Particulate absorption could also be modeled with more component submodels. Two-component (organic and inorganic) IOP submodels should be able to describe optical variability more precisely and thus improve the model accuracy. But this requires a more comprehensive bio-optical dataset in which the concentrations of organic and inorganic particles are measured separately. Due to the limitations of the dataset being used, an optical classification of waters was adopted in an effort to improve the accuracy of the model parameterization. The results from using type-related models indicated an improvement in the forward modeling of IOPs and reflectance (Figures 4.1 and 4.9).

In our opinion, the classification strategy is objective and practical for remote sensing applications because it needs only reflectance (or radiance) spectral information without the need of any *in situ* information, such as IOPs and concentrations. Reflectance or radiance spectra are derived directly from ocean color remote sensing measurements after atmosphere correction. In a real application, we are able to use remotely sensed reflectance spectra to identify which water type a pixel in an image belongs to based on some statistical recognition method, and then look up a proper bio-optical algorithm available for that water type from a multiple-algorithm database. Such a database may include a variety of optical-type-specific (spectrally-distinct) models that have been pre-parameterized with *in situ* bio-optical measurements taken over a region or globally. In a recent paper, Moore *et al.* (2001) demonstrated a robust fuzzy logic approach to select and blend water-type specific bio-optical algorithms.

The classified-water model parameterization scheme did achieve an improvement in reflectance model accuracy, particularly in the forward direction, but there were significant errors remaining for the inverse problem. A close look at a station with significant underestimation in [CHL] helps explain this result. Three different reflectance spectra are plotted in Figure 4.10. The measured spectrum (red-solid) is dramatically different from the forward-predicted spectrum (black-dash-dot) that was derived using measured constituent concentrations in the model. The "NLO-inversed" spectrum (blue dash) shows the "best fit" spectrum derived from the non-linear optimization algorithm. This algorithm was applied to the measured reflectance spectrum to obtain the "retrieved" concentrations shown on this figure. If the NLO routine were applied to the forward-predicted spectrum, it would retrieve the measured values exactly. But due to inaccuracy

in the forward model, a high uncertainty exists in the concentration retrievals. It is evident that the uncertainty in parameterizing IOP submodels (the forward reflectance model) can propagate to concentration retrievals with a high uncertainty. In other words, the uncertainty in forward modeling results in the inverse model (algorithm) having very large errors.

4.5 Conclusions

In this work, an approach is presented to parameterize an irradiance reflectance model in terms of IOP submodels that are non-linear functions of associated constituent concentrations. An unsupervised classification applied to the spectral space of reflectance resulted in three spectrally-distinct water types with distinct constituent concentrations. Three type-dependent models were parameterized on the basis of different constituent-dependent IOP submodels. The parameterization scheme was evaluated by both reconstructing measured reflectance spectra and by solving the non-linear inverse problem to retrieve constituent concentrations. The modeling performance in reconstructing reflectance spectra (forward problem) was higher for classified-water models than for non-classified water models. However, there was no improvement in the inverse problem of retrieving constituent concentrations from an observed reflectance spectrum.

It is believed that the approach of first classifying waters based on reflectance spectra and then parameterizing models for the different optical water types is still a valid strategy. This allows one to use relatively simple models (as described in section 4.2.2) to describe optical variability within a homogeneous water type. Differences between

water types may be due to differences in the nature of the materials in the water, which would call for a different parameterization. For example, the water types may differ with respect to phytoplankton populations, the source of the CDOM and hence differences in the spectral slope parameter, and different mineral particles or suspended sediments. The disappointing results from this study are in part due to the lack of information about the constituents in the water, and the small sample size. A more thorough evaluation of this parameterization scheme would require a large comprehensive bio-optical database with detailed information about the nature of the particles and dissolved materials affecting the water color.

References

Bricaud, A., Morel, A. and Prieur, L., 1981. Absorption by dissolved organic matter of the sea (yellow substance) in the UV and visible domains, Limnol. And Oceanogr. 26,1, 43-53.

Bricaud, A., Babin, M., Morel, A., and Claustre, H., 1995. Variability in the chlorophyll-specific coefficients of natural phytoplankton: analysis and parameterization, Journal of Geophysical Research, 100(C7),13,321-13,332.

Bricaud, A., Morel,A., Babin, M. and Claustre, H., 1998. Variations of light absorption by suspended particles with chlorophyll concentration in oceanic (case 1) waters: analysis and implications for bio-optical models, J.Geophys. Res. **103**, C13, 31,033-31,044.

Bukada, R.P., Jerome, J.H. Kondratyev, J.E., Ya, K. and Pozdnyakov, D.V., 1991. Estimation of organic and inorganic matter in inland waters: Optical cross sections of Lakes Ontario and Ladoga, Journal of Great Lakes Research, 17, 461-469.

Bukada, R.P., Jerome, J.H. Kondratyev, J.E. and Pozdnyakov, D.V., 1995. Optical properties and remote sensing of inland and coastal water , CRC Press.

Carder, K.L., Steward R.G., Harvey, G.R. and Ortner, P. B., 1989. Marine humic and fulvic acids: their effects on remote sensing of ocean chlorophyll, Limnology and Oceanography, 3,68-81.

Chami, M. and Robiliard, D., 2002. Inversion of oceanic constituents in case I and II waters with generic programming algorithms, Applied Optics, **41**, 6260-6275.

Chomko, R.M., Gordon, H.R., Maritorena, S. and Siegel, D.A., 2003. Simultaneous retrieval of oceanic and atmospheric parameters for ocean color imagery by spectral optimization: a validation," Rem. Sens. Environ. **84**, 208-220.

Feng, H., Campbell, J. W. and Moore, T.S., 1998. Uncertainty analysis for retrieval of chlorophyll concentration from ocean color: a simulation study, Journal of Advanced Marine Science and Technology Society, 4(2), 265-274.

Galie, E.A. and Murtha, P.A., 1992. Specific absorption and backscattering spectra for suspended minerals and chlorophyll a in Chiko Lake, British Columbia, Rem. Sens.Environ. 39, 103-118.

Garver, S.A., Siegel, D.A. and Mitchel, B.G., 1994. Variability in near-surface particulate absorption spectra: what can a satelite ocean color imager see?, Limnol. And Oceanogr. 39,6, 1349-1367.

Garver, S.A. and Siegel, D.A., 1997. Inherent optical property inversion of ocean color spectra and its biogeochemical interpretation 1,Time series from the Sargasso Sea,. J.Geophys. Res., 102, C8, 18,607-18,625.

Gordon, H.R., Brown, O. B. and Jacobs, M.M., 1975. Computed relationship between the inherent and apparent optical properties of a flat homogeneous ocean, Appl.Opt., 14,417-427.

Gordon, H.R. and Morel, A.Y., 1983. Remote assessment of ocean color for interpretation of satellite visible imagery, A review. New York,: Springer.

Gordon, H.R., O.B. Brown, R.H. Evans, J.W. Brown, R.C. Smith, K.S. Baker, and D.K. Clark, 1988. A semi-analytical radiance model of ocean color, J. Geophys. Res., 93, 10,909-10,924.

Kirk, J.T.O., 1984. Dependence of relationship between inherent and apparent optical properties of water on solar altitudes, Limnology and Oceanography, 29, 350-356.

Kishino, M. Okami, N.and Ichimura, S., 1985. Estimation of the spectral absorption coefficients of phytoplankton in the sea, Bul. Mar.Sci. 37, 634-642.

Kishino, M., 1994. Interrelationships between light and phytoplankton in the sea, in Ocean Optics, R.W. Spinrad, K.L. Carder, and M.J. Perry, eds. (Oxford, University Press, New York,).

Kowalczuk, P., 1999. Seasonal variability of yelow substance absorption in the surface layer of the Baltic Sea, J. Geophys. Res., 104,C12, 30 047-30 058 .

Fukurage, K., 1990. Introduction to statistical pattern recognization, Academic Press, Inc..

Lee, Z.P., Carder, K.L., Hawes, S.K., Steward, R.G.,. Peacock, T.G. and Davis, C.O., 1994. Model for the interpretation of hyperspectral remote-sensing reflectance, Applied Optics, **33**, 5721-5732.

Maffione, R.A and Dana, D.R., 1997. Instruments and methods for measuring the backward-scattering coefficient of ocean waters. Applied Optics, 36, 6057-6067.

Maritorena, S. Siegel, D.A. and Peterson, A.R., 2002. Optimization of a semianalytical ocean color model for global-scale applications, Applied Optics, **41**, 2705-2714.

Morel, A. and Prieur,L., 1977. Analysis of variations in ocean color, Limnology and Oceanography, 22, 709-722.

Moore, T.S., Campbell, J.W. and Feng, H., 2001. A fuzzy logic classification scheme for selecting and bending satelliete ocean color algorithms. IEEE Transactions on Geoscience and Remote Sensing, 39(8), 1764-1776.

Pope, R.M. and Fry, E.E., 1997. Absorption spectrum (380-700nm) of pure water: II. Integrating cavity measurements, Applied Optics, 6, 8710-8723.

Reynolds,R. A., Stramski, D. and Mitchel, B.G., 2001. A chlorophyl-dependent semianalytical reflectance model derived from field measurements of absoption and backscattering coefficients within the Southern Ocean, J.Geophys. Res. 106, C4, 7,125-7,138.

Roesler, C.S. and Perry, M.J., 1995. *In situ* phytoplankton absorption, fluorescence emission, and particular backscattering spectra determined from reflectance, J. Geophys. Res. 100,13279-13294.

Salisbury, J.E., Campbell, J.W., Linder, L.D., Meeker, D., Muller-Karger, F.E. and Vörösmarty, C.J., 2004. Spatio-temporal studies of the Mississippi Plume using satellite ocean color, wind discharge data, Deep Sea Research (in press).

Vodacek, A., DeGrandpre, M.D., Peltzer, E.T., Nelson, R.K. and. Blough, N.V., 1997. Seasonal variation of CDOM and DOC in the Middle Atlantic Bight: Terrestrial inputs and photooxidation, Limnol. Oceanogr. 42:674-686.

Whitlock, C.H., Poole, L.R., Usry, J.W., Houghton, W.M. , Witte, W.G., Morris, W.D. and Gurganus, E.G., 1980. Comparison of reflectance with backscatter and absorption parameters for turbid waters, Applied Opt. 20, 517-522.

Table 4.1. Basic statistics of in-water constituent concentrations in Tokyo Bay, including chlorophyll *a* ([CHL] in mg/m^3), total suspended matter ([TSM] in g/m^3), and colored dissolved organic matter (CDOM) absorption at 375nm (a_{y375} in m^{-1}).

	max	min	mean	std
Tokyo Bay (total 45 stations)				
[CHL]	34.480	0.2500	5.0982	6.2971
[TSM]	6.4000	0.1000	1.6142	1.2480
a_{y375}	1.0229	0.0553	0.3545	0.2179
Type 1 (16 stations)				
[CHL]	7.3800	1.0600	2.9588	1.9523
[TSM]	2.8000	0.2900	1.4694	0.7869
a_{y375}	0.7084	0.1568	0.3216	0.1457
Type 2 (18 stations)				
[CHL]	34.480	1.5300	9.3694	8.0906
[TSM]	6.4000	0.6700	2.3939	1.4296
a_{y375}	1.0229	0.2218	0.5104	0.2184
Type 3 (11 stations)				
[CHL]	2.9600	0.2500	1.2209	0.8842
[TSM]	1.0000	0.1000	0.5491	0.2727
a_{y375}	0.2246	0.0553	0.1471	0.0576

Table 4.2. Statistics of retrieval errors for constituent concentrations [CHL] (mg/m^3), [TSM] (mg/l) and a_{y375} (in m^{-1}). The leave-one-out method (LOOM) was used so that the data being retrieved are independent from the data used to parameterize the models. Bold font indicates an improvement of the classified-water model over the non-classified model.

For classified waters				
	M	S	RMSE	r
[CHL]	**-1.0553**	4.6760	**4.7936**	0.7137
[TSM]	0.0377	0.8315	0.8324	**0.8187**
a_{y375}	**0.2469**	**0.7600**	**0.7991**	0.6838
For non-classified waters				
	M	S	RMSE	r
[CHL]	-1.7169	4.5852	4.8961	0.7543
[TSM]	0.0133	0.7736	0.7737	0.7914
a_{y375}	0.4558	1.0583	1.1522	0.7063

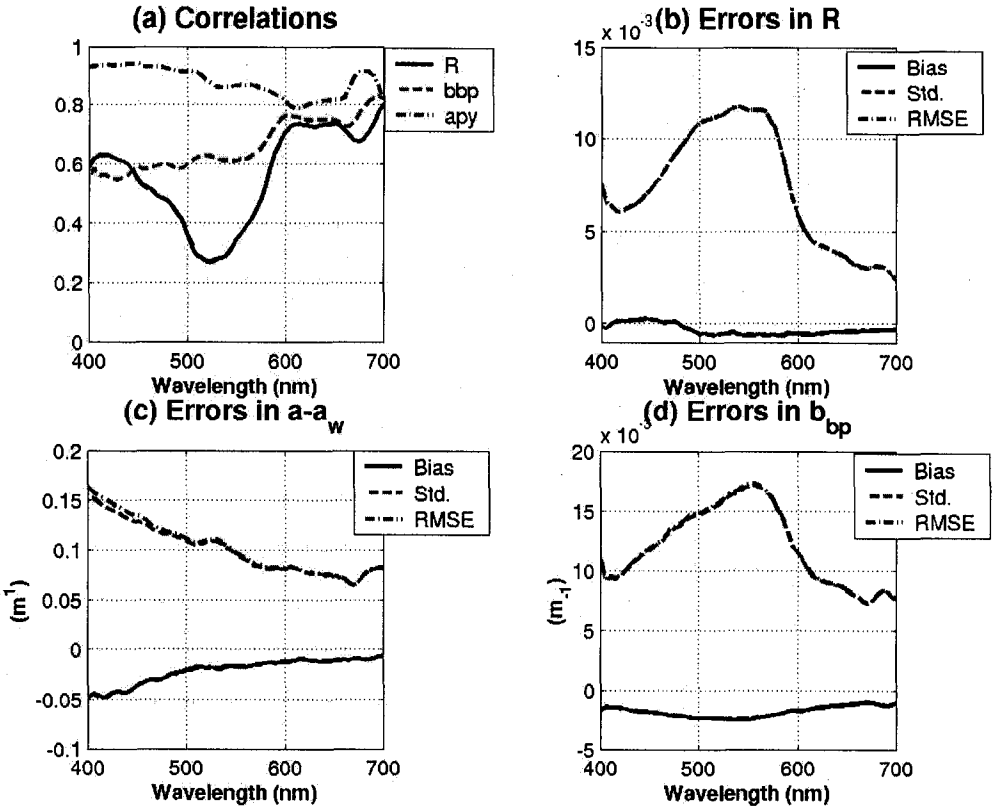

Figure 4.1. Performance measures for the model parameterized with all the data. **(a)** Correlation coefficient spectra between modeled and measured reflectance (solid line), non-water absorption ($a\text{-}a_w = a_{py}$, dashdot line), and backscattering (dashed line). Bias, Std, and RMSE errors for modeled **(b)** $R(\lambda)$, **(c)** $a(\lambda)$, and **(d)** $b_{bp}(\lambda)$.

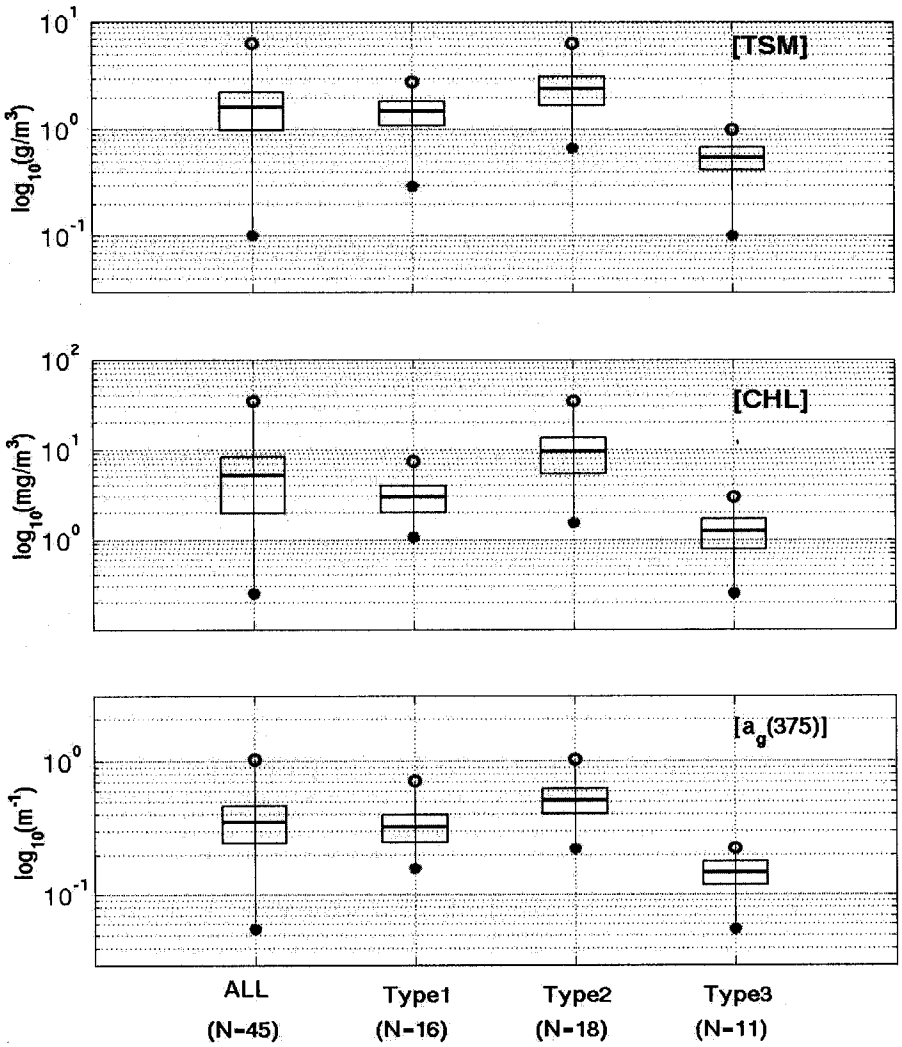

Figure 4.2. Box plots of the detailed concentration ranges of chlorophyll [CHL] (Upper), total suspended matter [TSM] (middle), and CDOM absorption coefficient at 375nm, ay_{375} (lower) for all 45 stations, and for type 1, type 2, and type 3 stations. Open circles and star signs are for maximum and minimum, respectively. The boxes indicate the variation ranges defined by one standard deviation, and lines in the boxes indicates the mean values.

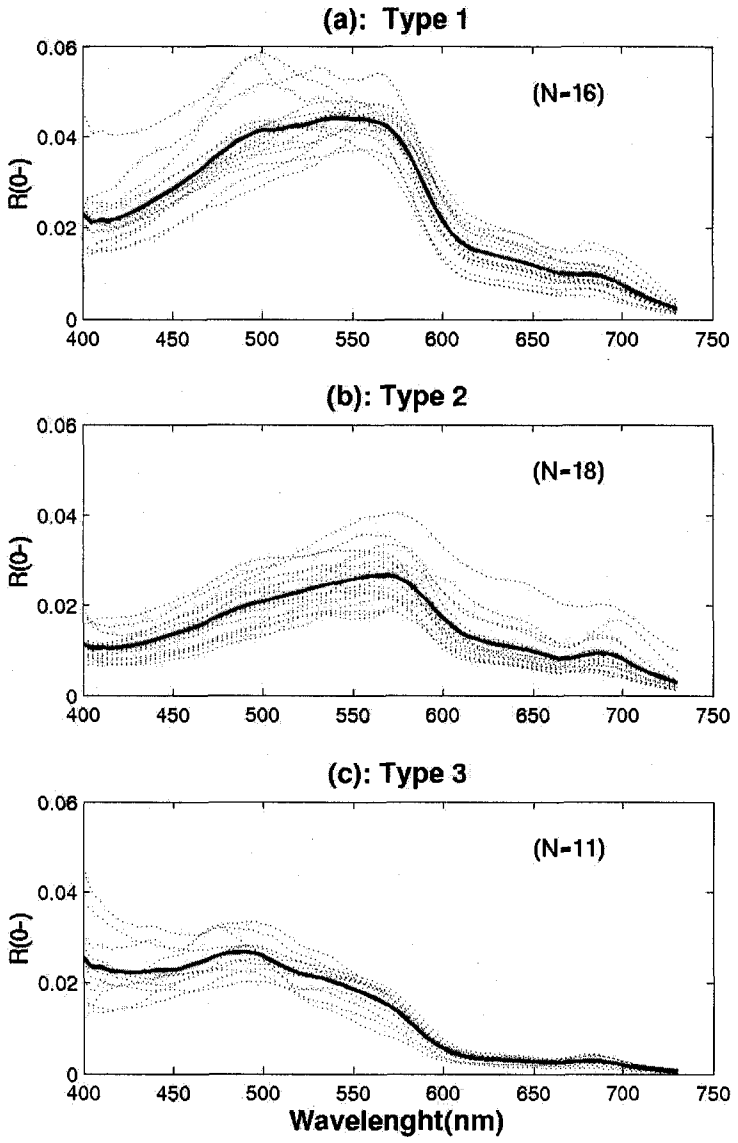

Figure 4.3. Measured irradiance reflectance spectra for the three water types as indicated. Dash lines are the *in situ* observations, and bolded solid red lines are the mean spectra.

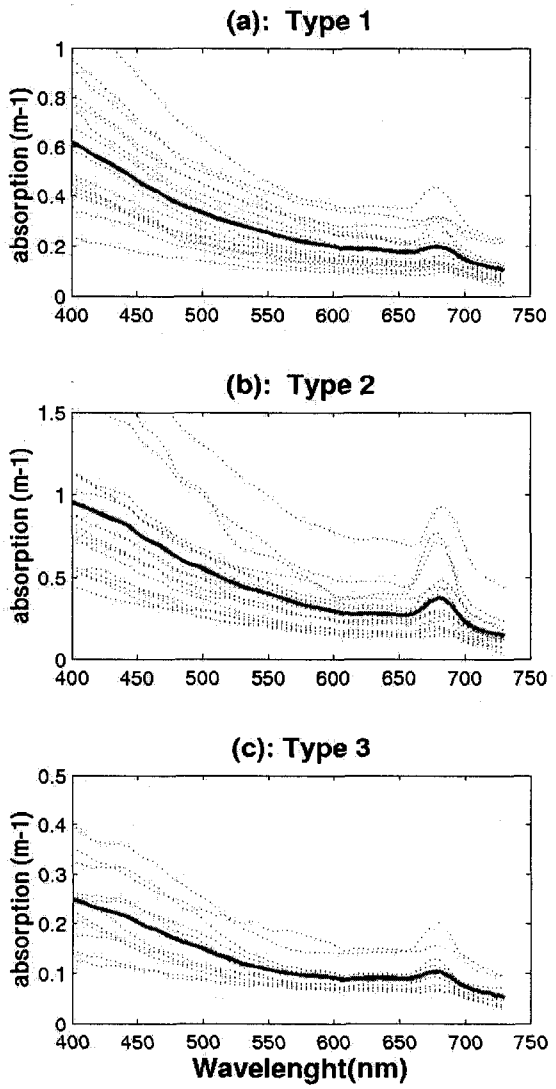

Figure 4.4. Measured absorption spectra for the three water types as indicated. Dash lines are the *in situ* observations, and bolded solid red lines are the mean spectra. Note that different vertical scales are used in the individual panels.

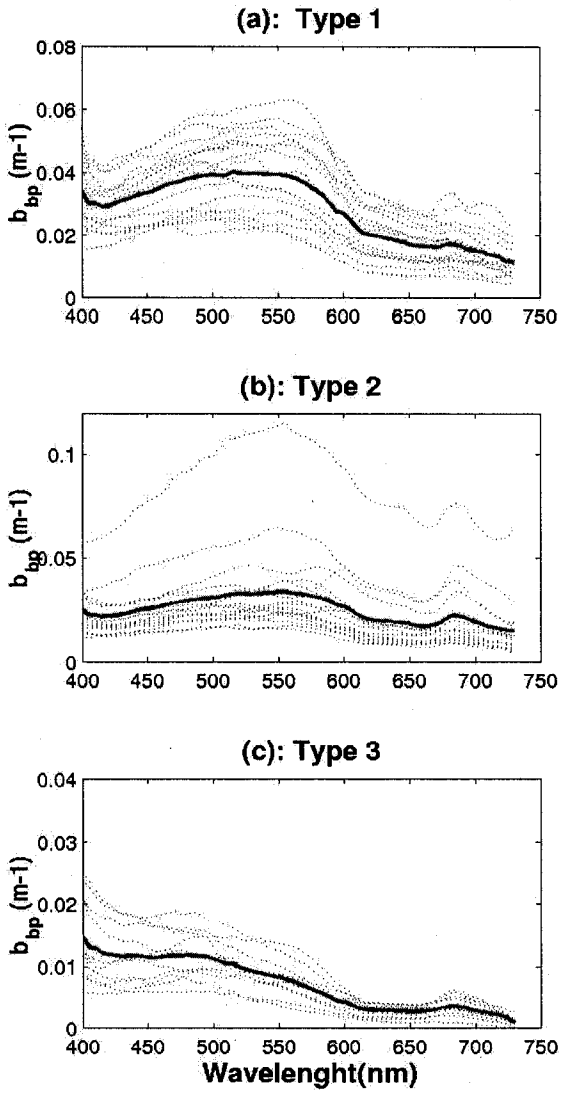

Figure 4.5. "Measured" backscattering spectra for the three water types derived by solving equation 4.1 for the backscattering coefficient. Dash lines are the *in situ* observations, and bolded solid red lines are the mean spectra. Note that different vertical scales are used in the individual panels.

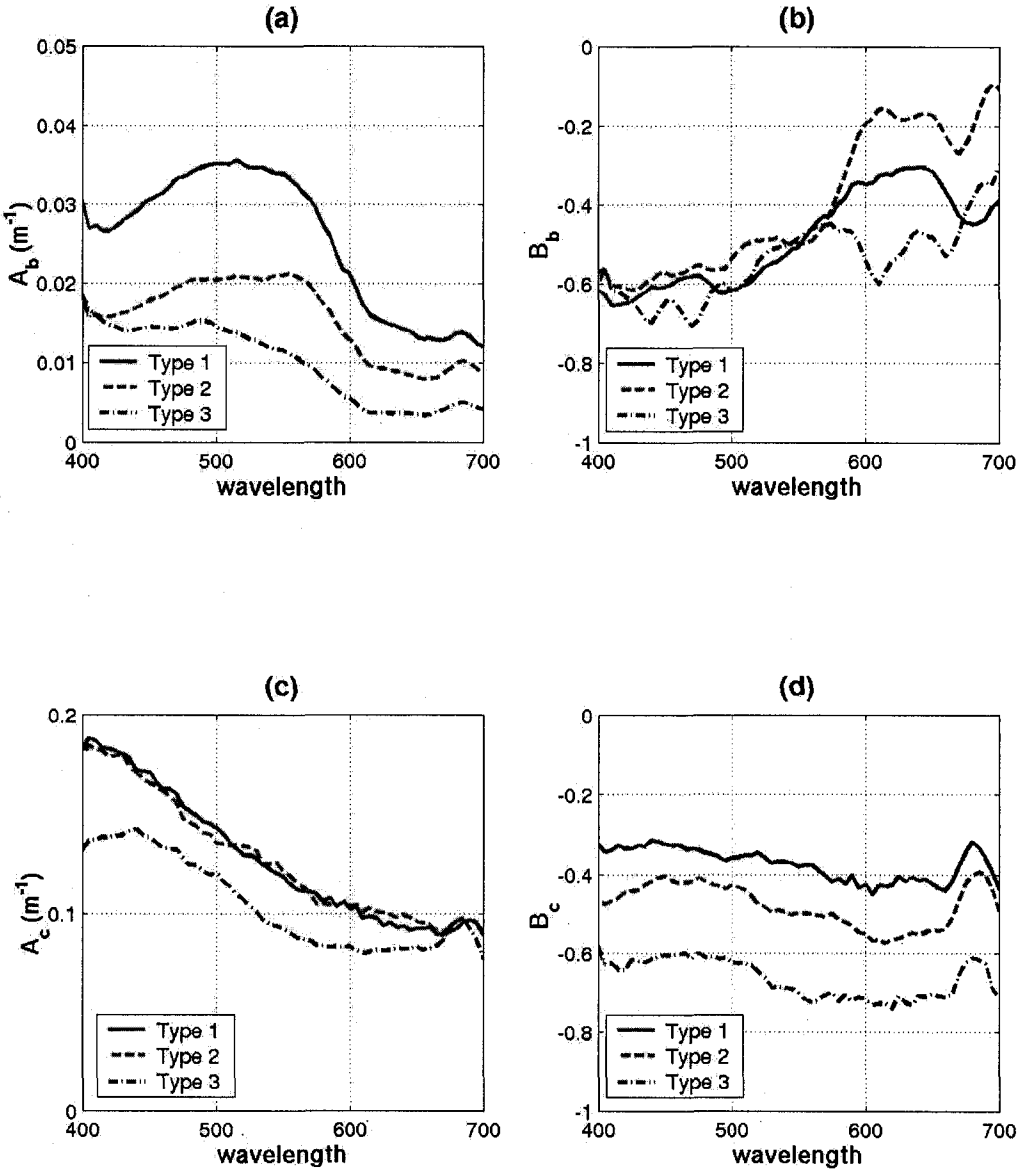

Figure 4.6. Averages of the parameter spectra: **(a)** $A_b(\lambda)$, **(b)** $B_b(\lambda)$, **(c)** $A_c(\lambda)$, and **(d)** $B_c(\lambda)$ for three water types. Solid lines stand for type 1; dotted lines stand for type 2; dash dotted lines stand for type 3). Note that these are the average spectra derived from the N parameter sets by leaving one station out (see LOOM method in text).

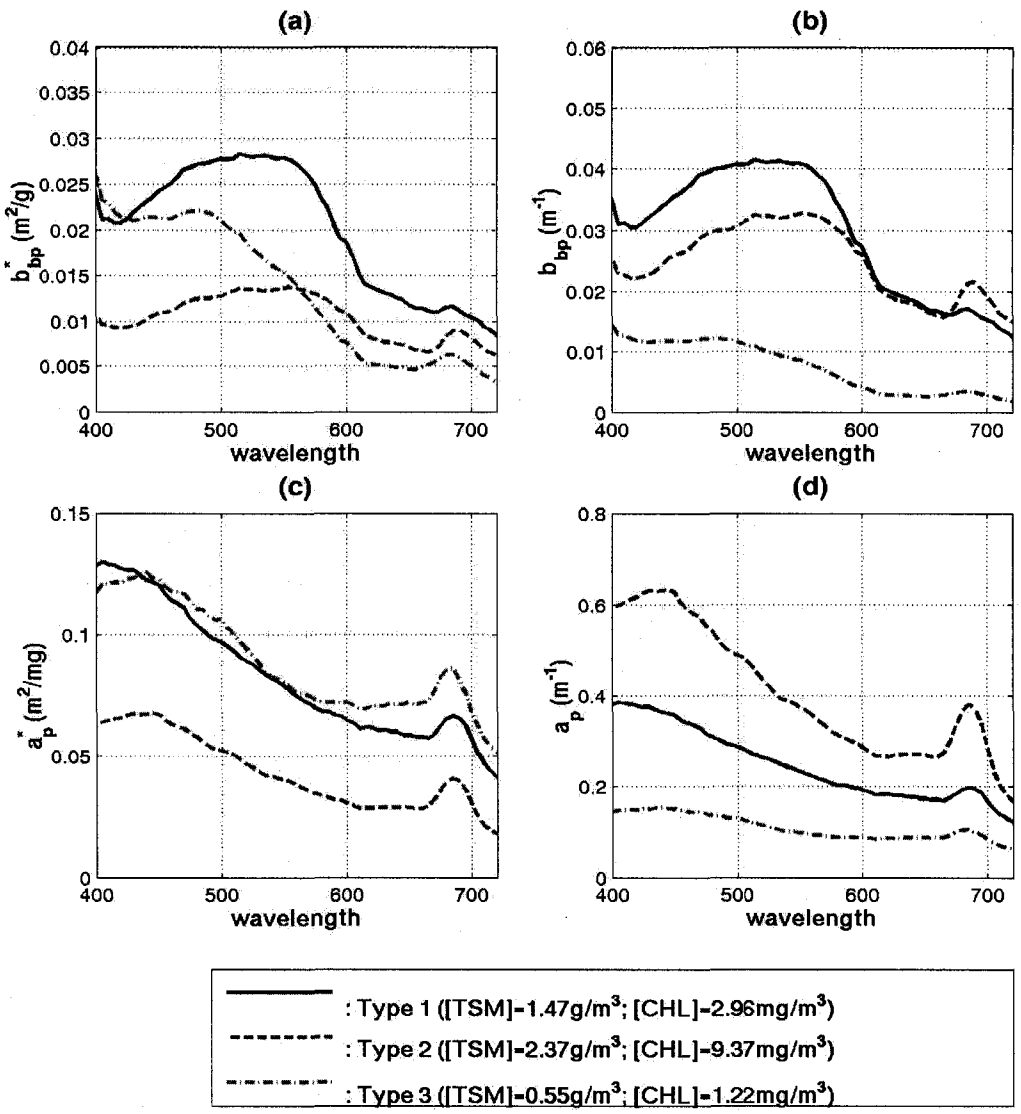

Figure 4.7. Examples of IOP spectra calculated from the means of [TSM] and [CHL] for each type: **(a)** Particle-specific backscattering spectra, **(b)** particle backscattering spectra, **(c)** particle-specific absorption spectra, and **(d)** particle absorption spectra.

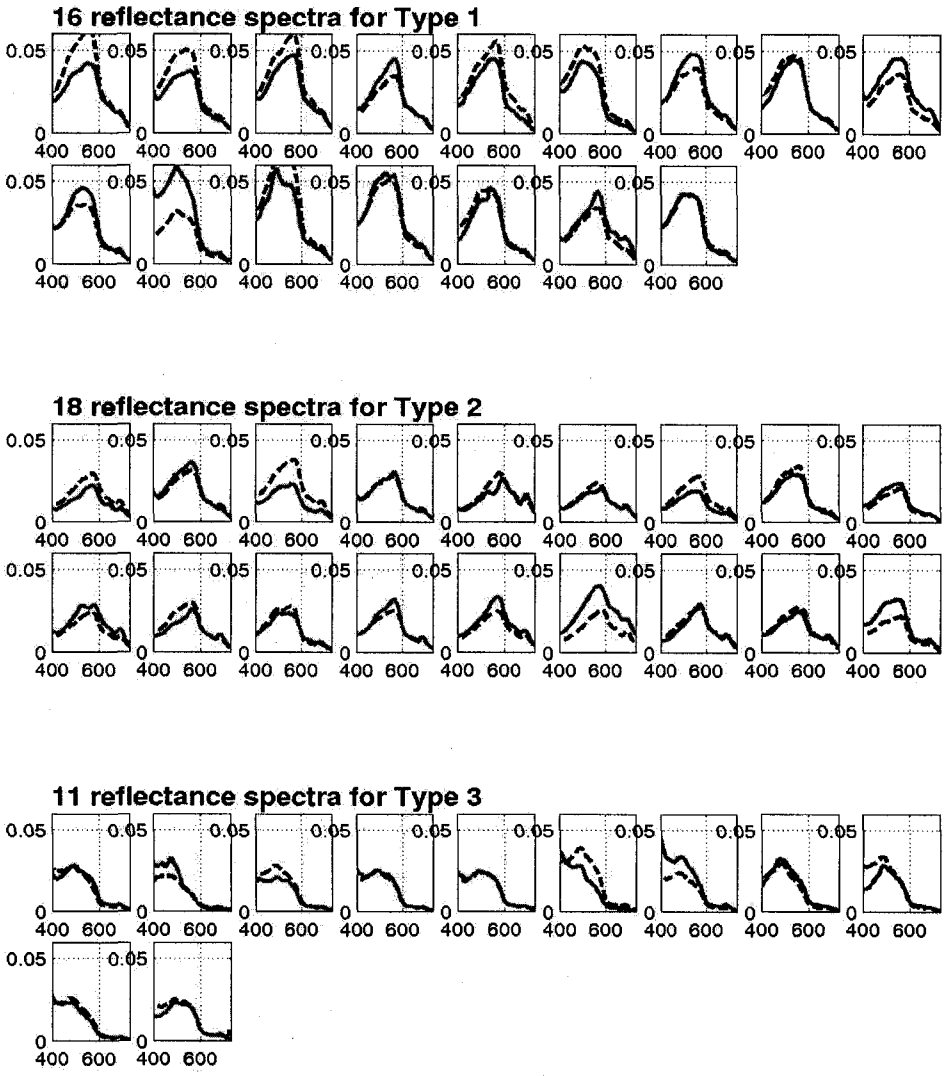

Figure 4.8. Comparison of measured reflectance spectra (solid curves) with reconstructed spectra (dashed curves) for stations in all three water types.

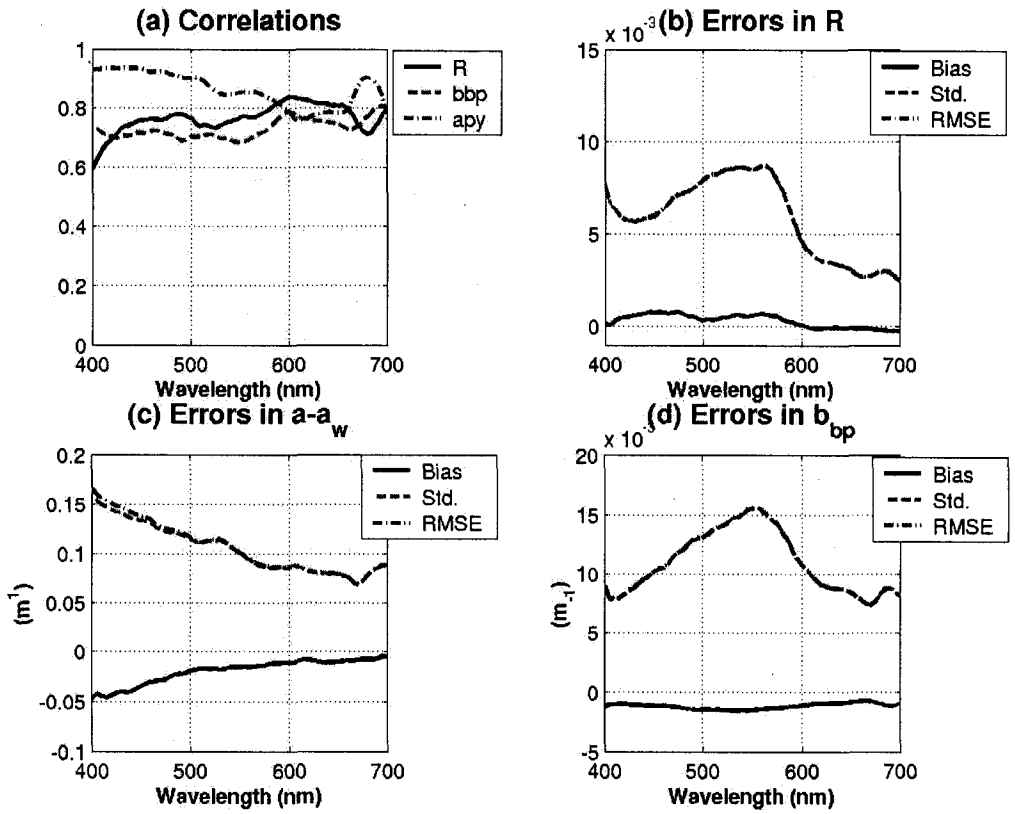

Figure 4.9. Performance measures for the models parameterized after classifying the stations into 3 water types. **(a)** Correlation coefficient spectra between modeled and measured reflectance (solid line), non-water absorption ($a\text{-}a_w$ = apy, dashdot line), and backscattering (dashed line). Bias, Std, and RMSE errors for modeled **(b)** $R(\lambda)$, **(c)** $a(\lambda)$, and **(d)** $b_{bp}(\lambda)$.

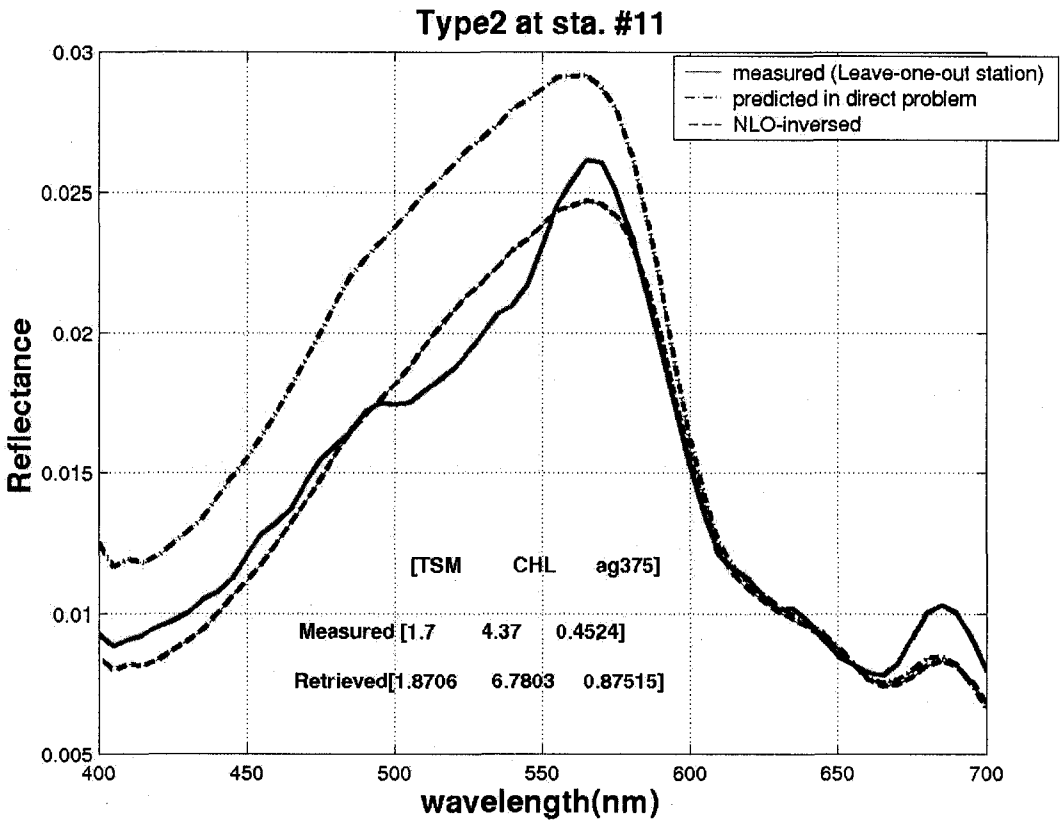

Figure 4.10. Comparison of the measured (red-solid) reflectance spectrum for a type-2 water station with the forward-predicted spectrum (black-dash-dot), and the "best fit" (blue-dash) irradiance reflectance corresponding to the retrieved constituent concentrations. The measured and retrieved concentrations are also listed. The forward-predicted spectrum was obtained by using the measured concentrations in the type-2 model.

Chapter 5 Summary, significance and future research

5.1 Thesis summary

For almost three decades, ocean color remote sensing has entered in a stage aiming to model more bio-optically complex coastal or Case 2 waters from simple open oceanic or Case 1 water. It is not just because the quantitative interpretation of Case 1 waters has been in a mature operational phase so that more attentions have shifted to Case 2 waters, but there also have existed scientific desires to grasp more synoptic marine bio-geo-chemical products from space for various applications in the oceanographic, environmental and ecological researches. Ocean color modeling efforts are centering on to precisely estimate three major optically-active constituents from ocean color measurements. Many challenges are being faced in this arena. This dissertation generally addresses some critical issues to be studied in view of the inverse problem.

In chapter two, a general simulation approach was proposed to demonstrate how to quantitatively characterize in-water optically-active constituent retrieval errors induced by uncertainties in individual parameterized IOP submodels. Significant finding in this part of study is that precise knowledge of spectral shapes of IOP submodels configured in a semi-analytical forward model is critical for precise constituent concentration retrievals, pointing to one of the potential avenues of improvement for the next generation ocean color inverse algorithms.

Having recognizing the "notorious" non-linearity of the ocean color forward model, various statistical inversion techniques have been proposed and applied for solving the ocean color inverse problem to retrieve optically-active constituents. In

chapter three, three functionally-distinct inversion techniques including nonlinear optimization (NLO), principal component analysis (PCA) and artificial neural network (ANN) were compared to test their math skills and to assess their inversion performance to retrieve optically-active constituents for a complex non-linear bio-optical system simulated by a semi-analytical ocean color model. In order to simulate different bio-optical complexities of waters from Case 1 to Case 2, a well-designed simulation scheme was implemented, and then the three inversion methods were applied to these simulated datasets for performance evaluation. The advantage of NLO is that its inversion lies directly on a forward ocean color model, and holds a "clear" physical meaning. On the side of disadvantage, its inverse solution is not stable and its computational load is high. The PCA inversion algorithm is based on the assumption that the linear combination between constituent components (logarithm-transformed) and ocean color spectral signals. Within a limited ranges and with lower values of optically-active constituents, our simulations show that such the linear assumption is an excellent approximation to the nonlinear problem, giving a comparable inversion performance with the other two methods. In addition, PCA possesses the capacity of suppressing the effect of noise on inversions. ANN exhibits its powerfulness in solving the complex nonlinear ocean color inverse problem. ANN generally overcomes most of the weaknesses and disadvantages the other two methods possess.

Finally (chapter four), an approach is presented for optimally parameterizing an irradiance reflectance model configured with a three-component IOP submodels by using a dataset of bio-optical measurements made at 45 stations in the Tokyo Bay and nearby regions in different seasons between 1982 and 1984. The measured irradiance reflectance

spectra show they are seasonally and spatially highly variable in their spectral pattern. An initial parameterization attempt based on all the 45 measurements to find a single parameterized model showed a quite poor performance in reconstructing reflectance spectra (forward problem), suggesting that a single parameterized forward model cannot represent the highly varying bio-optical environment. Therefore, we proposed a new parameterization scheme by which an unsupervised classification was first applied to the spectral space of irradiance reflectance, leading to three spectrally-distinct water types that clearly vary from Case 1 to Case 2. In effect, the application of this classification to reflectance spectra leads to a sorting of in-water concentrations arranged in order of the mean values and variations of in-water optically-active constituents. The reflectance model was then parameterized for individual classified optical water types. As a result, three sets of the type-specific model IOP parameters were derived, showing that they are significantly type-specific. The model validation exhibits that the accuracy was significantly improved in parameterizing the reflectance model for classified (type-specific) waters over for non classified waters for the forward problem (i.e. reconstructing the measured reflectance spectra), but the accuracy improvement for constituent retrieval (inverse problem) was not significant.

5.2. Significance and future research

For the newly proposed parameterization scheme, we intend to hypothesize that parameterizing classified type-specific models can acquire a better performance than parameterizing a single model in sense of both forward and inverse problems. A more scientific significance implied in the hypothesis is that spectrally-distinct optical water

types identified by ocean color (radiance or reflectance) measurements are associated very likely with distinct marine bio-optical environments.

In fact, this hypothesis possesses its observational evidence and theoretical basis. For bio-optically complex Case 2 waters, their inherent optical properties and hence forward models vary spatially and temporally because properties in optically-active constituents, such as physical and chemical properties of phytoplankton species and inorganic particulate substances (composition and size distribution), vary regionally and seasonally. To directly classify ocean color measurements (radiance or reflectance) is expected in effect to identify IOPs variations to some degree so that a type-specific forward model is adequately used to the IOPs for that type. Our experiment by using the Tokyo Bay bio-optical dataset for this newly-proposed parameterization has shown its significant success in the forward problem, i.e. reconstruction of the measured reflectance spectra although no significant improvement in the corresponding inverse problem solved by a NLO algorithm was slightly discouraging. One possible reason is due to be the NLO inversion method itself as shown in chapter three that NLO inversion performance is very sensitive to noise. Second, the limited dataset may not reach statistically significant conclusion for the inverse problem yet.

We believe that this parameterization scheme is very promising. As known, the challenge for Case 2 waters lies in no universal forward model available for solving their inverse problem. Consequently, one has to depend on various local algorithms. Many applications by using locally developed algorithms have been reported, but most of them focus only on a very local or limited region as a demonstration for algorithm development validation. Even if many local algorithms have been developed and ready

for use, a "proper" or "objective" algorithm selection is still a difficulty, for instance, for a real global application. What is the criterion for an algorithm switch?

Our proposed parameterization scheme attempts to jump the hurdle. It first identifies spectrally-distinct water types based on in-situ measured reflectance spectra, and then parameterizes them to derive type-specific forward models. Once optically type-specific algorithms are developed, a robust fuzzy logic method (Moore et al., 2001) can be used to objectively select proper algorithms and statistically blend algorithm-retrieved in-water concentrations by comparing the similarity of a remotely-sensed reflectance spectrum to the type-specific reflectance spectra on which the forward models are based. However, more work is really required to test the new parameterization scheme. Particularly, we need a large bio-optical database for a solid validation.

BIBLO GRAPHY

Bricaud, A., Morel, A. and Prieur, A., 1981. Absorption by dissolved organic matter of the sea (yellow substance) in the UV and visible domains, Limonology and oceanography, 26,1, 43-55.

Bricaud, A. and Morel, A. 1986. Light attenuation and scattering by phytoplanktonic cells: A theoretical modeling, Applied Optics, 25, 571-580.

Bricaud, A., Morel, A., Babin, M. and Claustre, H., 1988. Variations of light absorption by suspended particles with chlorophyll concentration in oceanic (case 1) waters: analysis and implications for bio-optical models. Journal of Geophysical Research-Oceans, 103, C13, 31033-31044

Bricaud, A., Babin, M., Morel, A., and Claustre, H., 1995. Variability in the chlorophyll-specific coefficients of natural phytoplankton: analysis and parameterization, Journal of Geophysical Research-Oceans, 100, C7,13321-13332.

Bricaud, A., Morel, A., Babin, M., and Claustre, H. 1998. Variations of light absorption by suspended particles with chlorophyll concentration in oceanic (case 1) waters: analysis and implications for bio-optical models, 103, C13, 31033-31044.

Bukada, R.P., Jerome, J.H., Kondratyev, J.E., Ya, K. and Pozdnyakov, D.V., 1991. Estimation of organic and inorganic matter in inland waters: Optical cross sections of Lakes Ontario and Ladoga, Journal of Great Lakes Research, 17,461-469.

Bukata, R.P, Jerome, J.H., Kindratyev, K.Y., and Pozdnyakov, D.V., 1995. Optical properties and remote sensing of inland and coastal water, New York, CRC Press, pp362.

Campbell, J.W., 1995. The lognormal distribution as a model for bio-optical variability in the sea, Journal of Geophysical Research-Oceans, 100, C7. 13237-13254.

Campbell, J.W., Moore, S.T. and Feng, H., 1997. Phytoplankton backscattering properties derived from satellite ocean color data (Abstract), ASLO97, Santa Fe, NM.

Carder, K.L., Steward R.G., Harvey, G.R. and Ortner, P. B., 1989. Marine humic and fulvic acids: their effects on remote sensing of ocean chlorophyll. Limnology and Oceanography, 3, 68-81.

Carder, K.L., Hawes, S.K., Baker, K.A., Smith, R.C., Steward, R.G. and Mitchell, B.G., 1991. Reflectance model for quantifying chlorophyll a in the presence of productivity degradation products, Journal of Geophysical Research-Oceans, 96, 20, 20599-20611.

Chami, M. and Robiliard, D., 2002. Inversion of oceanic constituents in case I and II waters with generic programming algorithms, Applied Optics, 41,6260-6275.

Chomko, R.M., Gordon, H.R., Maritorena, S. and Siegel, D.A., 2003. Simultaneous retrieval of oceanic and atmospheric parameters for ocean color imagery by spectral optimization: a validation, Remote Sensing of Environment, 84, 208-220.

Doerffer, R. and Fischer, J., Year: 1994. Concentrations of Chlorophyll, suspended matter, and gelbstoff in Case II waters derived from satellite coastal zone color scanner data with inverse modeling methods, Journal of Geophysical Research-Oceans, 99, 7457-7466.

Doerffer, R.; and Schiller, H., 1999. First test of a two-step neural network inverse modeling technique using MOS data, The 2nd International Workshop on MOS-IRS and Ocean Colour,, Berlin, June 1-12.

Dowell, M.D. and Hoepffner, N., 1997. Reflectance model in Case II waters: contamination of the elastic signal by CDOM fluorescence, The 1st International Workshopp on MOS-IRS and Ocean Colour, Berlin, April 28-30.

Dowell, M.D., Moore, T.S., Campbell, J.W. and Hoepffner, N.,2000. Universally Tailored Optical Parameter Inversion Algorithm (UTOPIA) II: Class Parameterization.,Ocean Optics XV,SPIE Proc., Monaco, France.

Feng, H., Campbell, J. W., and Moore, T.S. 1998. Uncertainty analysis for retrieval of chlorophyll concentration from ocean color: a simulation study, Journal of Advanced Marine Science and Technology Society, 4, 2, 265-274.

Fisher, J., Doerffer, R. and Grass, H., 1986. Factor analysis of multispectral radiances over coastal and open ocean waters based on radiative transfer calculations, Applied Optics, 25, 3, 448-456

Frette, O., Stamnes, J.J. and Stamnes, K., 1998. Optical remote sensing of marine constituents in coastal waters: a feasibility study, Applied Optics, 37, 36, 8318-8326.

Fukurage, K., 1990. Introduction to statistical pattern recognization, New York, Academic Press.

Galie, E.A. and Murtha, P.A., 1992. Specific absorption and backscattering spectra for suspended minerals and chlorophyll a in Chiko Lake, British Columbia, Remote Sensing of Environment, 39, 103-118.

Garver, S.A., Siegel, D.A. and Mitchel, B.G., 1994. Variability in near-surface particulate absorption spectra: what can a satelite ocean color imager see? Limnology and Oceanography, 39,6, 1349-1367.

Garver, S.A. and Siegel, D.A., 1997. Inherent optical property inversion of ocean color spectra and its biogeochemical interpretation 1. Time series from the Sargasso Sea, Journal of Geophysical Research-Oceans, 102, C8, 18607-18625.

Gordon, H.R., Brown, O. B. and Jacobs, M.M., 1975. Computed relationship between the inherent and apparent optical properties of a flat homogeneous ocean, Applied Optics, 14, 417-427.

Gordon, H.R. and Morel, A.Y., 1983. Remote assessment of ocean color for interpretation of satellite visible imagery, A review, New York, Springer.

Gordon, H.R., Brown, O.B., Evans, R.H., Brown, J.W., Smith, R.C., Baker, K.S. and Clark, D.K., 1988. A semi-analytical radiance model of ocean color, Journal of Geophysical Research, 93, 10909-10924.

Gower, J.F.R., Lin, S.R. and Borstad, G.A., 1984. The information content of different optical spectral ranges for remote chlorophyll, International Journal of Remote Sensing, 5,2,346-364.

Gregg, W.W. and Carder, K.L., 1990. A simple spectral solar irradiance model for cloudless maritime atmospheres, Limnology and Oceanography, 35, 1657-1675.

Grew, W.G., 1977. Characteristic vector analysis as a technique for signature extraction of remote ocean color data, The 6th Annual Remote Sensing of Environment, Tullahoma, Tennessee.

Gross, L., Thiria,S., Frouin, R. and Mitchell, B.G., 2000. Artificial neural networks for modeling the transfer function between marine reflectance and phytoplankton pigment concentration, Journal of Geophysical Research-Oceans, 105, C2, 3483-3495.

Hetscher, M., Krawczyk, H., Neumann, A. and Zimmermann, G., 2004. Four years of ocean colour remote sensing with MOS-IRS An updated version of a paper

originally presented at Oceans from Space 'Venice 2000' Symposium, International Journal of Remote Sensing, 25, 7/8, 1415-1419.

Hoge, F. E. and Lyon, P.E., 1996. Satellite retrieval of inherent optical properties by linear matrix inversion of oceanic radiance model: an analysis of model and radiance measurement error, Journal of Geophysical Research-Oceans, 100, C7, 16631-16648.

Jain, S.C. and Miller, J.R., 1976. Subsurface water parameters: Optimization approach to their determination from remotely sensed water color data, Applied Optics, 15, 4886-4890.

Jerome, J.H., Bukata, R. P. and Bruton, J.E., 1988. Utilizing the components of vector irradiance to estimate the scalar irradiance in natural waters, Applied Optics, 27, 4012-4018.

Jin, Z. and Stamnes, K., 1994. Radiative transfer in nonuniformly refracting layered media: atmosphere-ocean system, Applied Optics, 33 431-442.

Keiher, L.E. and Brown, C.W., 1999. Estimating oceanic chlorophyll concentration with neural networks, Journal: International Journal of Remote Sensing, 20, 1, 189-194.

Kirk, J.T.O., 1981. A Monte Carlo study of the nature of the underwater light field in, and the relationships between optical properties of turbid yellow waters, Journal: Aust. J. Mar. Freshwater Res., 32, 517-532.

Kirk, J.T.O., 1984. Dependence of relationship between inherent and apparent optical properties of water on solar altitudes, Limnology and Oceanography, 29, 350-356.

Kishino, K.M., Okami, N. and Ichimura, S., 1985. Estimation of the spectral absorption coefficients of phytoplankton in the sea, Bullitin. Marine Science, 37, 634-642.

Kishino, M., 1994. Interrelationships between light and phytoplankton in the sea, in Ocean Optics, (eds. Spinrad, R.W., Carder, K.L. and Perry, M.J.), New York, Oxford University Press.

Klemas, V., Bartlett, D., Philpot, W., Rogers, R. and Reed, L., 1974. Coastal and estuarine studies with ERTS-1 and Skylab, Remote Sensing of Environment, 3, 153-174.

Kowalczuk, P., 1999. Seasonal variability of yelow substance absorption in the surface layer of the Baltic Sea, Journal of Geophysical Research-Oceans, 104, C12, 30047-30058.

Krasnopolsky, V.M., Breaker, L.C. and Gemmill, W.H., 1995. A neural network as a nonlinear transfer function model for retrieving surface wind speeds from the special sensor microwave imager, Journal of Geophysical Research-Oceans, 100, C6, 11033-11045.

Krawczyk, H., Neumann, A. and Walzel, T., 1995. A Complex approach to quantitative interpretation of spectral high resolution imagery, The Third Thematic Conference on Remote Sensing for Marine and Coastal Environments, Seattle, USA , II-57-68.

Krawczyk, H. and Hetscher, M., 1997. Principal Component inversion algorithm for the retrieval of water constituents and its application, the 1st International Workshop on MOS-IRS and Ocean Color, Berlin.

Krawczyk, H., Neumann, A. and Hetscher, M., 1999. Mathmatical and physical backgraound of principal componet inversion, the 3rd International Workshop on MOS-IRS and Ocean Color, Berlin, 83-92.

Lee, Z.P., Carder, K.L., Hawes, S.K., Steward, R.G., Peacock, T.G. and Davis, C.O., 1994. Model for the interpretation of hyperspectral remote-sensing reflectance, Applied Optics, 33, 5721-5732.

Maffione, R.A. and Dana, D.R., 1996. Recent measurements of the spectral backward-scattering coefficient in coastal waters, Ocean Optics XIII, SPIE 2963, Halifax, Canada.

Maffione, R.A. and Dana, D.R., 1997. Instruments and methods for measuring the backward-scattering coefficient of ocean waters, Applied Optics, 36, 6057-6067.

Maritorena, S., Siegel, D.A. and Peterson, A.R. 2002. Optimization of a semianalytical ocean color model for global-scale applications, Applied Optics, 41, 2705-2714.

Mobley, C.D., Gentili, B., Gordon, H.R., Jin, Z., Kattawar, G.W ., Morel, A., Reinersman, P., Stamnes, K. and Stavn, R.H., 1993. Comparison of Numerical Models for Computing Underwater Light Fields, Applied Optics, 32, 7484-7504.

Mobley, C. D., 1994. Light in water; Radiative transfer in natural waters. San Diego, Academic Press, Inc.

Moore, T.S., Campbell, J.W. and Feng, H., 2001. A fuzzy logic classification scheme for selecting and bending satellite ocean color algorithms, IEEE Transaction Geoscience and Remote Sensing, 39,8, 1764-1776.

Morel, A. and Prieur, L., 1977. Analysis of variations in ocean color, Limnology and Oceanography, 22, 709-722.

Morel, A. and Bricaud, A., 1981. Some theoretical results concerning optics of phytoplankton with spectral reference to remote sensing, in Oceanography from Space (ed., Gower, J.F.R), New York, Plenum Press, 313-317.

Mueller, J.L., 1976. Ocean color spectra measured off the Oregon coast: characteristic vectors, Applied Optics, 15,2394-2402.

Nabney, I.T., 2001, NETLAB: Algorithms for Pattern Recognition, London, Springer-Verlag UK.

Pope, R.M. and Fry, E.S., 1997. Absorption spectrum (380-700nm) of pure water: II. Integrating cavity measurements, Applied Optics, 6, 8710-8723.

Preisendorfer, R.W.H., 1961. Application of radiative transfer theory to light measurements in the sea, Internataional Union of Geodesy and Geophysics Monograp (Symposium on Radiant energy in the Sea), 10, 11-30.

Press, W.H., Tuekolsy, S.A.,Vettering, W.T. and Flannery, B.P., 1992. Numerical Recipes in C: the Art of Scientific Computing, Cambridge Press, 2nd edition, 1,pp994.

Roesler, C.S., Perry, M.J. and Carder, K.L ., 1989. Modeling in situ phytoplankton absorption from total absorption spectra in productive inland marine waters, Limnology and Oceanography, 34, 1510-1523.

Roesler, C.S. and Perry, M.J., 1995. In situ phytoplankton absorption, fluorescence emission, and particular backscattering spectra determined from reflectance, Journal of Geophysical Research, 100, 13279-13294.

Salisbury, J.E., Campbell, J.W. , Linder, L.D., Meeker, D., Muller-Karger, F.E. and Vörösmarty, C.J., 2004. Spatio-temporal studies of the Mississippi Plume using satellite ocean color, wind discharge data, Deep Sea Research (in press).

Sathyendranath, S., Prieur, . and Morel, A., 1989. A three-component model of ocean color and its application of phytoplankton pigments in coastal waters, International Journal of Remote Sensing, 10,8, 1373-1794.

Sathyendranath, S.(Ed.), 2000. IOCCG Report Number 3: Remote Sensing of Ocean Colour in Coastal, and Other Optically-Complex, Waters (2000), Dartmouth, Canada.